Experimentele studie van het hydrodynamische gedrag
van een natuurvriendelijke oeverbescherming belast door scheepsgolven
in een beperkte, niet-tijgebonden waterweg

Experimental Study of the Hydrodynamic Performance
of a Nature-Friendly Bank Protection Subject to Ship Waves
in a Confined, Non-Tidal Waterway

Sieglien De Roo

UNIVERSITEIT
GENT

Universiteit Gent
Faculteit Ingenieurswetenschappen en Architectuur
Vakgroep Civiele Techniek
Labo voor Hydraulica

Supervisor:

Prof. dr. ir. P. Troch

Research institute:

Ghent University
Faculty of Engineering and Architecture

Department of Civil Engineering
Hydraulics Laboratory
Sint-Pietersnieuwstraat 41
B-9000 Ghent, Belgium

Tel.:   +32-9-264.32.81
Fax.:   +32-9-264.35.95

*The most beautiful thing we can experience is the mysterious.*
It is the source of all true art and all science.
He to whom this emotion is a stranger,
who can no longer pause to wonder and stand rapt in awe,
is as good as dead: his eyes are closed.
[A. Einstein]

Acknowledgements
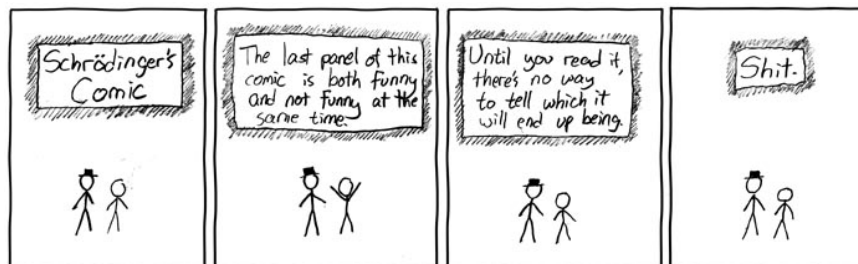
[Comic from the hand of Randall Monroe (xkcd.com)]

Hoewel Erwin Schrödingers queeste omtrent 'What is life?' veel diepgaander en filosofischer is, kunnen de voorbije 5 jaren ook wel gecatalogeerd worden als 'Sieglien's comic', gebundeld tot dit document. Hope you get the funny side (too).

Volgens de tweede wet van de thermodynamica, ofte de omzetting van warmte (enthousiasme, stress?) naar arbeid, neemt de entropie van een geïsoleerd systeem toe zolang dit niet in evenwicht is, en dit tot de maximale entropie voor dat systeem bereikt is. Gelukkig is Sieglien's 'life' geen geïsoleerd systeem... Volgende mensen verdienen 'een dikke merci!' voor hun bijdrage tot dit doctoraal proefschrift (en de reductie van mijn entropisch niveau):

Prof. Peter Troch, mijn promotor, die besliste, buiten de geijkte civieltechnische paden, een onderzoeksvoorstel te schrijven omtrent natuurvriendelijke oevers en dit toe te kennen aan een bio-ingenieur. De vrijheid, het vertrouwen en de mogelijkheden die je me gaf om dit onderzoek 'mijn' vorm en richting te geven waardeer ik ten zeerste.

Mijn examencommissie, bestaande uit prof. Taerwe, prof. De Mulder, prof. De Rouck, prof. De Schutter, prof. Temmerman en prof. Vantorre, voor hun wetenschappelijke inbreng en kritische visie op dit proefschrift. Een bijzonder dankjewel aan prof. De Mulder, wiens deur steeds openstond voor, oa. sedimentgerelateerde, discussies en geanimeerde gesprekken.

Waterwegen en Zeekanaal NV (WenZ), afdeling Bovenschelde, ben ik zeer erkentelijk voor de financiële en logistieke steun die geboden werd bij de installatie van beide meetopstellingen, alsook voor de toegang tot scheepsgerelateerde informatie van de sluis te Sint-Baafs-Vijve. In het bijzonder dank ik dr. ir. Charlotte Beels en ir. Johny Van Acker, mijn aanspreekpunten bij WenZ, voor hun open en vlotte communicatie.

'Experimental Study', ofte...(heel) veel werk in een interessant spectrum van (geestige en uitdagende) natuurelementen.

Enerzijds waren beide meetopstellingen nooit geworden wat ze nu zijn (pareltjes :-) zonder het enthousiasme, de technische kennis en de spitsvondigheid van Marcel Anteunis, Herman Van der Elst en Tom Versluys. Naast hen wil ik ook Dave De Rynck, Sam Meurez, Stefaan Bliki en Davy Haerens bedanken voor hun hulp (vaak met een lach) bij de opbouw en het onderhoud van de installaties, alsook voor het ophalen van de meetgegevens. Tom, ook dankjewel voor de introductie tot en hulp met LabView programmering. Herman, bovenal merci om het concept van wijste, grijste compadre met waardigheid en (de nodige) humor in te vullen!

Anderzijds waren de tweemaandelijkse opmetingen van oevererosie op verschillende locaties langs de Leie onmogelijk geweest zonder de (enthousiaste) medewerking van Kevin Delecluyse, Dieter Meire, Serge Tichko en Lisa Vanhaute. Merci voor jullie bereidwilligheid tot omzetting van jullie kostbare (werk)tijd in

'community service time'!

Een inspirerende werkplek leidt tot creativiteit, werkgoesting en amusante middagpauze-uitlopende conversaties. Merci om hiertoe bij te dragen AWW en LvH collega's: Anke, Annelies, Anny, Binod, Boud, Charlotte, Dieter V., Edawi, Ellen, Florent, Griet, Jan, Julien, Kathleen, Kevin, Koen, Lander, Laurent, Leen, Lien, Liesbet, Ludo, Manuella, Pieter M., Pieter R., Rebeca, Renaat, Ronny, Stephan, Serge, Tom D.M., Tomas, Vicky, Yvan, en Dieter M. Deze laatste Dieter, ofte mijn roomie, merci voor je no-nonsense being who you are in de (ont)spannende, (on)verwachte momenten. Ook uwen eindsprint is ingezet, nog efkes volhardend (getraind ;-) doortrekken...the end is near and our sheep is ready!

Uiteraard there's life besides work, en hierin zorg(d)en vrienden voor on-wijs sjieke, verrassende, mooie en gekoesterde momenten: M.E.R.C.I.! Voor de (meeste) watergerelateerde daarvan ben ik mn mede(under)waterlovers van 't GUD uiterst dankbaar. Verder een grote, warme merci aan solid-as-a-rock compañeros Karen, Kinnie, Bert en Bob. Jullie unieke eigenschappen werden (des te meer ;-) in de verf gezet when life was hard... Jullie zijn precious!

Moeke en vake, een oprechte dankjewel voor jullie zorg, steun en vertrouwen in mn niet-altijd-evidente keuzes (en reisbestemmingen). Birgit, zussemus, merci voor het stevig supporteren langs de zijlijn!!

De laatste merci gaat naar de persoon die (samen met) mij (in) alle kleuren van de regenboog heeft gezien. Maarten, merci, voor de geestafleidende manoeuvres, de nature beauty uitstappen,... maar bovenal, een dikste merci voor je liefde, je geduld en rust, en je onvoorwaardelijke steun (zeker in de lastige strijd-tegen-de-tijd momenten)!

Nu, zo net voor de deadline achteromziend, peis ik:

It always seems impossible, until it is done. [N. Mandela]

Sieglien
Gent, 27 september 2013

Table of Contents

Nomenclature

1 List of symbols

A_s	[m^2]	immersed midship cross sectional area
A_w	[m^2]	waterway cross sectional area
B	[m]	ship's beam
C	[-]	proportionality constant applied for the calculation of bed shear stress
$\overline{C}_{\sum,m,bed}(T_0)$	[g m^{-3}]	cumulative amount of (re)suspended bed sediments (over duration of ship-induced hydrodynamic disturbance T_0)
$\overline{C}_{m,bed}(t)$	[g m^{-3}]	average concentration of (re)suspended bed sediments over the water column at time t
$\overline{C}_{m,bed}$	[g m^{-3} s^{-1}]	time- and depth-averaged amount of (re)suspended bed sediments (over duration of ship-induced hydrodynamic disturbance T_0)
CA_{bank}	[m^2]	contributing bank area
CA_{bed}	[m^2]	contributing bed area
C_B	[-]	block coefficient
d	[μm]	particle diameter
d_{10}	[μm]	the particle sizes for which 10% by weight of the material is finer
d_{50}	[μm]	the particle sizes for which 50% by weight of the material is finer
d_{90}	[μm]	the particle sizes for which 90% by weight of the material is finer
d_{LP}	[m]	influence width of the 'primary' wave pattern
D	[m]	ship's actual draught
D_{design}	[m]	ship's design draught
E	[J m^{-2}]	wave energy
ED_{bank}	[m]	depth of the uniform stripped silty bank layer
ED_{bed}	[m]	depth of the uniform stripped sandy bed layer
f	[Hz]	frequency
$f_{W,LP}$	[-]	'primary' wave friction factor
$f_{W,SP}$	[-]	'secondary' wave friction factor

Fr_d	[-]	depth-based Froude number
$Fr_{d,cr}$	[-]	critical depth-based Froude number
g	[m s^{-2}]	acceleration of gravity
h	[m]	water depth
h_{ADV}	[m]	average daily water height at the ADV
h_m	[m]	average water depth
h_{PS1}	[m]	average daily water height at PS 1
h_{PS2}	[m]	average daily water height at PS 2
h_{SSPA}	[m]	average daily water height at SSP A
H_{bow}	[m]	bow wave
H_i	[m]	incident wave height
H_{in}	[m]	index wave height
H_t	[m]	transmitted wave height
H_{surge}	[m]	maximum water level rise after the maximum drawdown occurred
$H_{SP,max}$	[m]	maximum 'secondary' wave height
H_{stern}	[m]	transversal stern wave height
i	[-]	number of ship event
K_T	[%]	wave transmission coefficient
L	[m]	ship's length
m	[-]	blockage coefficient
N	[-]	number of analysed data
N_{pas}	[-]	number of passenger boats
N_{tug}	[-]	number of tug boats
p	[Pa]	pressure
$q_{m,bed}(t)$	[g m^{-2} s^{-1}]	crosswise suspended sediment mass flux of bed sediments at time t
$q_{s,bed}(t)$	[m^3 s^{-1}]	suspended sediment volume transport of bed sediments at time t
$Q_{\sum,m,bed}(T_0)$	[g m^{-1}]	cumulative suspended sediment mass transport of bed sediments per unit alongstream width [m]
$Q_{\sum,s,bed}(T_0)$	[m^{-3}]	cumulative suspended sediment volume transport of bed sediments
R^2	[-]	coefficient of determination
$Rouse\,\#$	[-]	Rouse number
s	[-]	'primary' wave steepness
S	[-]	sorting coefficient
SSC_{silt}	[g m^{-3}]	added suspended sediment (silt) concentration in the control volume V_C
$SSC(z,t)$	[g m^{-3}]	suspended sediment concentration at height z and time t
t	[s]	time
$t_{\Delta h_{max}}$	[s]	occurrence time of Δh_{max}
$t_{H_{bow}}$	[s]	occurrence time of the bow wave
$t_{H_{surge}}$	[s]	occurrence time of H_{surge}

T_0	[s]	duration of an individual ship's hydrodynamic disturbance
T	[s]	wave period
T_{LP}	[s]	'primary' wave period
T_{SP}	[s]	'secondary' wave period
$T_{suction}$	[s]	drawdown duration until the maximum drawdown is reached
T_{surge}	[s]	duration of refilling of the maximum drawdown
u_r	[m s^{-1}]	return current
$u_{r,max}$	[m s^{-1}]	maximum return current
u_*	[m s^{-1}]	bed shear velocity
u_{*cr}	[m s^{-1}]	critical shear velocity
u'_X	[m s^{-1}]	fluctuating velocity components in horizontal streamwise (X) direction
$u_{X,LP}$	[m s^{-1}]	'primary' wave-induced velocity component in horizontal streamwise (X) direction
$u_{X,SP}$	[m s^{-1}]	'secondary' wave-induced velocity component in horizontal streamwise (X) direction
$u_{X,W}$	[m s^{-1}]	combined wave-induced velocity component in horizontal streamwise (X) direction
u'_Y	[m s^{-1}]	fluctuating velocity components in horizontal crosswise (Y) direction
$u_{Y,LP}$	[m s^{-1}]	'primary' wave-induced velocity component in horizontal crosswise (Y) direction
$u_{Y,SP}$	[m s^{-1}]	'secondary' wave-induced velocity component in horizontal crosswise (Y) direction
$u_{Y,W}$	[m s^{-1}]	combined wave-induced velocity component in horizontal crosswise (Y) direction
u'_Z	[m s^{-1}]	fluctuating velocity components in vertical (Z) direction
U_{LP}	[m s^{-1}]	resultant of the 'primary' wave-induced velocity components in horizontal direction
U_{SP}	[m s^{-1}]	resultant of the 'secondary' wave-induced velocity components in horizontal direction
U_W	[m s^{-1}]	resultant of the combined wave-induced velocity components in horizontal direction
$U_{W,bank}$	[m s^{-1}]	resultant of the combined bank-oriented wave-induced velocity components in horizontal direction
V_C	[m^3]	control volume
V_s	[m s^{-1}]	ship's sailing speed
V_l	[m s^{-1}]	ship's limit speed
w_s	[m s^{-1}]	particle settling velocity
W_{SWL}	[m]	width of the waterway on its still water level
y	[m]	sailing distance to off-bank timber piling

z	[m]	distance from the reference level
z_0	[m]	bed roughness length
α	[-]	parameter which accounts for the ratio of a ship's sailing speed V_s to its limit speed V_l
β	[-]	midship section coefficient
Δh	[m]	drawdown
Δh_{max}	[m]	maximum drawdown
Δ	[m^3]	ship's displacement
ϵ_i	[-]	random error term in a linear regression model
κ	[-]	Von Karman's constant
ν	[m^2 s^{-1}]	kinematic fluid viscosity
π	[-]	mathematical constant which is the ratio of a circle's circumference to its diameter
ρ	[kg m^{-3}]	fluid density, here: for water
ρ_s	[kg m^{-3}]	sediment density
ρ_{sand}	[g m^{-3}]	moist bulk density of sandy sediments
ρ_{silt}	[g m^{-3}]	moist bulk density of silty sediments
σ^2	[-]	variance of the normally distributed random error term ϵ_i
τ	[N m^{-2}]	bed shear stress
τ_{cr}	[N m^{-2}]	critical bed shear stress
τ_W	[N m^{-2}]	combined ship wave shear stress
$\tau_{W,LP}$	[N m^{-2}]	'primary' wave-induced shear stress
$\tau_{W,SP}$	[N m^{-2}]	'secondary' wave-induced shear stress
θ_{cr}	[-]	critical Shields parameter

2   List of acronyms

1-D	one-dimensional
3-D	three-dimensional
ADV	Acoustic Doppler velocimeter
ECMT	European Conference of Ministers of Transport
LD	Laser Distance meter
LP	Long period
OBS	Optical backscatter sensor
PS	Pressure sensor
SD	Standard deviation
SP	Short period
SP	Solar Panel
SSC	Suspended sediment concentration
SSP	Suspended solids profiler
SWL	Still water level
TAW	Tweede Algemene Waterpassing
TKE	Turbulent kinetic energy
USDA	United States Department of Agriculture

Nederlandse samenvatting
– Summary in Dutch

Goederentransport over de binnenwateren heeft de kleinste ecologische voetafdruk, in het bijzonder in vergelijking met goederentransport over de weg. Desondanks zet de binnenvaart ook druk op het fluviatiele milieu, door scheepsgeïnduceerde golven en stromingsveranderingen. Een varend schip veroorzaakt twee verschillende types golfpatronen. (i) Een 'primair' golfpatroon dat zich voortbeweegt rond de scheepsromp en samen met het schip, bestaande uit een kleine waterspiegelstijging ter hoogte van de boeg (de boeggolf), een waterspiegeldaling langsheen de scheepsromp, en wederom een waterspiegelstijging ter hoogte van het hek (de haalgolf). (ii) Een 'secundair' golfpatroon dat ontstaat ter hoogte van de boeg en het hek van het schip, bestaande uit transversale en divergerende golven die interferentiepieken vormen. Samen met deze golfpatronen treedt er een retourstroming op rond de scheepsromp, dewelke tegengesteld aan de vaarrichting van het schip is.

Deze impact van het hydrodynamische scheepsgolfgedrag dient geminimaliseerd te worden op een zo goed mogelijke manier, zonder evenwel het goederentransport via binnenwateren economisch onaantrekkelijk te maken.

In lijn met de Europese kaderrichtlijn water, waardoor het bewustzijn toeneemt ten aanzien van de milieuaspecten en -baten gerelateerd aan een waterweg, is er de uitdagende taak om hiertoe voordelige oplossingen te ontwikkelen, waarbij het ontwerp van een waterweg diens bouwtechnische, economische en milieunoden volledig integreert.

Dit in acht genomen is het een goed idee om natuurvriendelijke oeverbescherming te gebruiken ter voorkoming van oevererosie in plaats van een traditionele 'harde' oeverbekleding, zoals bijv. betonplaten of damplanken. De integratie van natuurlijke processen, zoals golfdemping door vegetatie in een oeverbeschermende structuur, is de beste manier om een optimaal ecologisch streefbeeld te bereiken, en dit met behoud van de technische functionaliteiten van een oeverbekleding. Bijgevolg, de gewenste 'win-win' situatie.

In een beperkte, niet-tijgebonden waterweg wordt het falen van oeverbekleding en/of dijken voornamelijk veroorzaakt door scheepsgolfbelasting. Een typisch natuurvriendelijk oeverontwerp voor deze waterwegen bestaat uit (i) een vooroeververdediging als eerste golfdempende constructie, die de golfbelasting reduceert tot een voor de achtergelegen plasberm aanvaardbaar niveau. Deze vooroeververdediging werkt tevens als een zandvang, en (ii) een achtergelegen plasberm, die een

graduele overgang vormt tussen de vaarweg en de oever, en dus tussen water- en landgebonden ecosystemen.

Echter, een gebrek aan gedetailleerde informatie omtrent ontwerp- en installatiecriteria voor natuurvriendelijke oeverbescherming leidt nog steeds herhaaldelijk tot een foutieve dimensionering of onbehoorlijke installatie van deze. In het algemeen blijft het een open vraag welke natuurvriendelijke oeverbescherming geschikt is, zeker in een energetisch scheepsgolfklimaat.

Ten gevolge van deze kennislacune heeft dit doctoraatsonderzoek tot algemene doelstelling **een bijdrage te leveren tot een verbeterd ontwerp voor natuurvriendelijke oeverbescherming op beperkte, niet-tijgebonden waterwegen belast met drukke scheepvaart**. Dit leidt tot de tweeledige specifieke doelstelling van dit onderzoek, nl. **de begroting van de (impact van) scheepsgolfbelasting op een bepaald type natuurvriendelijke oeverbescherming**. Dit type bestaat uit enerzijds, een gesloten houten palenrij als vlooroeververdediging en een achtergelegen plasberm, en anderzijds, een aangeplante rietkraag die het achterliggende talud bijkomend beschermt tegen golfbelasting. Er is dus geopteerd voor een dubbele golfdempende configuratie.

Aangezien beide scheepsgolfpatronen beïnvloed worden door het profiel van de waterweg, en dit profiel ten gevolge van de natuurvriendelijke oeverbescherming het scheepsgolfgedrag danig kan wijzigen, is geopteerd om het hydrodynamisch gedrag van deze natuurvriendelijke oeverbescherming te onderzoeken door **een experimentele studie**.

Hiertoe is de Leie, een Europese ECMT-IV waterweg, gekozen als studiegebied. De Leie is een drukke scheepvaartroute, waarlangs maandelijks gemiddeld 1600 schepen versluisd worden te Sint-Baafs-Vijve. Beneden deze sluis, in het meest stroomafwaarts gelegen deel van de Leie, zijn scheepspassages gemonitored met behulp van 2 terreinmeetopstellingen.

Een uitgebreide meetopstelling werd ontwikkeld en geïnstalleerd op een vaste locatie. Deze meetopstelling monitort accuraat de grootte van de scheepsgolfbelasting op, en de responsie van de natuurvriendelijke oeverbescherming. Onder andere de invallende scheepsgolven op de houten palenrij, hun interactie met deze golfdempende constructie, en hun ondiep water gedrag worden opgemeten.

Daarnaast werd ook een mobiele meetopstelling ontwikkeld. Deze opstelling dient specifiek voor het begroten van het hydrodynamische gedrag van de houten palenrij. Dankzij de modulaire, lichte structuur van deze meetopstelling kan deze gemakkelijk ingezet worden op verschillende locaties, waardoor verschillende configuraties van deze houten palenrij beoordeeld werden.

Ten eerste is het **scheepsgolfklimaat in de Leie gekarakteriseerd**. Een varend schip is begrensd door zijn limietsnelheid, dewelke bepaald wordt door de hydraulische randvoorwaarden voor scheepvaart op de Leie. Voor alle ongeladen schepen overschrijdt deze limietsnelheid de geldende snelheidsbeperking van $12\,\mathrm{km\,h^{-1}}$, en een kapitein tracht zo dicht mogelijk bij de limietsnelheid te varen.

De vaarsnelheid van een schip bepaalt de grootte van diens opgewekte golf-patronen. Bijkomend verhoogt het krappe vaarwegprofiel van de Leie de vaar-weerstand, en bijgevolg het 'primaire' golfpatroon. Dit domineert het globale scheepsgeïnduceerde golfpatroon.

Bovenstaande kenmerken leiden ertoe dat de grootste golfbelasting veroor-zaakt wordt door ongeladen ECMT-IV schepen, welke dichtbij of op hun limiet-snelheid varen. Deze verhouding van de werkelijke vaarsnelheid van een schip tot diens limietsnelheid is uitermate belangrijk. Indien een varend schip zijn li-mietsnelheid overschrijdt, wordt eveneens de toename van de ruimte die een schip inneemt in het dwarsprofiel van de waterweg, nl. de blockagecoëfficiënt, des te belangrijker.

De interactie van de scheepsgolven met de houten palenrij, alsook het gedrag van de scheepsgolven in ondiep water, zijn onderzocht voor verschillende configu-raties van de houten palenrij (een enkele of dubbele palenrij, aan- of afwezigheid van een dwarse palenrij,...). De grootte van het 'primaire' golfpatroon, i.e. de maximale waterspiegeldaling en de haalgolf, blijft behouden in de achtergelegen plasberm op voorwaarde dat er voldoende waterdiepte is. Er treedt bijgevolg een significante wateruitwisseling op tussen de vaargeul en de plasberm. Een rela-tieve demping van de (maatgevende) maximale 'secundaire' golfhoogte treedt wel op, en deze varieert van 20% tot 55%. Deze golfreductie is echter eerder locatie-afhankelijk dan wel het gevolg van 1 bepaalde configuratie van de houten palenrij.

Ten tweede is het **relatieve belang van de scheepsgolven tot sedimentdyna-miek in de plasberm bepaald**, en dit per scheepspassage. Hierbij is scheeps-geïnduceerd suspensietransport naar de vaarweg toe beschouwd als een indicatie voor bodem- en oevererosie.

Het bepalen van deze scheepsgeïnduceerde bijdrage tot sedimentdynamiek voor de bodem en de oever afzonderlijk wordt bemoeilijkt door de grote variabiliteit en gedeeltelijke overlap in beider korrelgroottes. Een onderscheid tussen beide is dan ook slechts (deels) gemaakt op basis van de verschillen in sedimentopwoelings -en transportkarakteristieken tussen verschillende korrelgroottes.

Het loskomen van lemig oeversediment gebeurt ten gevolge van een oever-georiënteerde, scheepsgeïnduceerde watersnelheid die groter is dan $0.4\,\mathrm{m\,s^{-1}}$. Dit impliceert onmiddellijk hun stroomafwaartse advectie. Voor het zandig bodemma-teriaal leidt (re)suspensie echter niet noodzakelijkerwijs tot netto sedimenttrans-port. Significant sedimenttransport (naar of van de oever weg) is enkel opgemeten ten gevolge van 6 ECMT-IV en Va scheepspassages. De afzettingsrichting voor dit in suspensie getransporteerd zandig sediment wordt bepaald door de verhouding tussen de waterspiegeldalingsgerelateerde verdringingsstroming naar de vaarweg toe en de haalgolfgerelateerde volgstroom naar de oever toe.

De gemeten grootte-ordes voor suspensietransport van zowel het lemig als zan-dig oever- en bodemsediment respectievelijk, wijzen erop dat de houten palenrij als vooroeververdeding geen afdoende bescherming biedt voor een gecontroleerde sediment dynamiek in de achtergelegen plasberm. Een reductie van de scheeps-golfgeïnduceerde watersnelheden tot minder dan $0.4\,\mathrm{m\,s^{-1}}$ zou het loskomen, de

(re)suspensie en het transport van zowel bodem- als oeversediment aanzienlijk verminderen.

Ten derde, en laatste, is in dit doctoraatsonderzoek geëvalueerd of **deze natuurvriendelijke oeverbescherming, welke een dubbele golfdempende configuratie heeft, een afdoende bescherming biedt tegen bodem- en oevererosie**. Hiertoe is opgemeten of er nog steeds geomorfologische wijzigingen optreden aan de natuurvriendelijk beschermde oever, en of deze significant verschillen tegenover deze die optreden aan natuurlijk eroderende oeverzones, en dit gedurende 1 vegetatiecyclus.

Uit deze opmetingen blijken er geen duidelijke verschillen te zijn in oevererosie tussen de beschermde en onbeschermde oeverzones. Er werd echter geen direct causaal verband tussen de belangrijkste hydrodynamische belastingen (was- en scheepsgolven) enerzijds, en de geërodeerde oevervolumes anderzijds, gevonden. Kwalitatief is wel afgeleid dat de scheepsgolfbelasting voldoende hoog is om oevererosie te bewerkstelligen.

Derhalve zou deze specifieke natuurvriendelijke oeverbescherming baat hebben bij een verbeterd ontwerp. Het is echter een waardevolle oplossing om een natuurvriendelijke oeverbescherming te vertalen in een dubbele golfdempende configuratie waarbij de eerste golfdempende constructie zich reeds in de waterweg bevindt. Een tweede, natuurlijke golfdemping door de rietkraag is een duurzame oplossing indien de groeicondities voor het riet verbeterd worden. Hiertoe is het noodzakelijk om de transmissie van de scheepsgolven doorheen de houten palenrij te verminderen.

English summary

Inland waterborne transport systems have the smallest ecological footprint, especially compared to road transport systems. Nevertheless, shipping traffic puts pressure on the fluvial environment, by producing waves and altering currents. A sailing ship causes two different types of wave patterns: (i) a 'primary' wave pattern around the ship's hull, which consists of a small water level rise, i.e. the bow wave, a drawdown along the ship's hull, and another surge, i.e. the transversal stern wave, and (ii) a 'secondary' wave pattern originating at the ship's bow and stern, which consist of transverse and diverging waves. Together with these wave patterns, a return current takes place in the opposite direction to the ship's sailing direction.

The impact of these ship-induced hydrodynamics must be minimized in the best possible way, without making inland waterborne transport economically unsustainable.

In line with the EU Water Framework Directive, which increased the awareness on the environmental aspects and assets of a waterway, the challenging task is to develop beneficial solutions, where the waterway design fully integrates the waterway's engineering, economic and environmental objectives.

On that account, it is good practice to obviate bank erosion by installing a nature-friendly bank protection instead of a traditional 'hard' revetment, such as concrete or riprap. Incorporating natural processes like wave attenuation by vegetation into a bank protecting structure is the way to achieve an optimal ecosystem context while preserving the technical functionalities of a revetment; hence, the desirable 'win-win' solution.

Failures of revetments, dikes or river banks are mainly caused by ship-induced hydrodynamics in confined, non-tidal waterways. For these waterways, a typical nature-friendly bank design features two main aspects: (i) an off-bank structure, which reduces the ship-induced hydrodynamic forcing to a lower level, and acts like a sediment trap, and (ii) a shallow water area behind the off-bank structure, which is subject to a controlled, manageable level of ship-induced hydrodynamics. This shallow water area creates a transitional zone between the fairway and the riverine area, i.e. between water- and land-based ecosystems.

However, a lack of detailed information regarding design and installation criteria still results in repetitive mistakes and inappropriate installation. In general, it remains an open question whether nature-friendly bank protection techniques are proven to be effective, especially in an energetic ship wave climate.

Hereto, the general objective of this PhD-research is to contribute to a deeper insight into an **optimized design for nature-friendly bank protections in non-tidal, confined waterways subject to heavy shipping traffic**. This fundamental research approach aims at **quantifying the (impact of) ship-induced hydrodynamics on a particular type of nature-friendly bank protection**. It consists of off-bank closed timber piling, which separates the fairway from the shallow water and riverine area behind, and a reed belt, planted at the base of the river bank. Hence, a **double wave attenuating configuration** is opted for: first, ship waves are reduced by the off-bank timber piling, and second, ship waves are attenuated through the reed belt.

Because ship-generated waves interact with topographic boundaries, and the **configuration** of a nature-friendly protected waterway might complicate the ship waves' behaviour, the hydrodynamic performance of a nature-friendly bank protection is investigated based on an **experimental field study**.

The Lys, a EU standard scale inland waterway (ECMT-Va, tonnage up to 3000 ton), is selected as study area. Shipping traffic is heavy; a monthly average of 1600 ships passes through the lock at Sint-Baafs-Vijve. Along the most downstream part of the Lys, two monitoring systems are applied to meet the twofold objective.

An extensive monitoring system is constructed and installed at a fixed location. This monitoring system accurately measures the magnitude of ship-induced hydrodynamic forcing on and the response of the nature-friendly bank protection. Among others, incident ship waves, their wave-structure interaction with the off-bank timber piling and their shallow water behaviour are monitored continuously.

To enhance the dynamic measurement possibilities, a flexible, mobile monitoring system is also developed. This monitoring system measures the ship wave-structure interaction with the off-bank timber piling. Because of its modular and lightweight setup, it can easily be installed at various locations and it is used to assess various configurations of off-bank timber piling.

First, **the ship wave climate is characterized** in the Lys. A sailing ship's speed is bounded to its limit speed, which, in turn, depends on the hydraulic boundary conditions for shipping traffic on the Lys. For all light draughted ships, this implies that the imposed speed limit $V_s = 12 \, \text{km h}^{-1}$ can easily be exceeded.

The ship's sailing speed dictates the amplitude of both ship wave patterns. The Lys' confined dimensions amplify however the ship's 'primary' wave pattern, which dominates the ship wave signature. The highest ship-induced hydrodynamics are caused by light draughted shipping traffic of ECMT-class IV (tonnage up to 1500 ton), sailing at a ratio of sailing speed to limit speed $V_s/V_l \geq 1$. The ratio of sailing speed to limit speed V_s/V_l appears to be of greatest importance; the higher the ratio V_s/V_l, the higher the ship-induced hydrodynamics. For $V_s/V_l \geq 1$, an increase of the space a ship occupies in the waterway's cross section, i.e. the blockage coefficient, additionally results in a more pronounced 'primary' ship wave pattern.

Ship wave-structure interaction with the off-bank timber piling and the ship waves' shallow water behaviour are examined for various configurations of off-bank timber piling (e.g. single or double row, varying length). The magnitude of the 'primary' wave pattern, i.e. the maximum drawdown and transversal stern wave, is preserved in the shallow water area on the condition that the water level is sufficiently high. The clear porosity effect of the timber piling yields a significant water exchange between the fairway and the shallow water area. Relative reduction of maximum 'secondary wave heights ranges from 20% to 55%, but is rather location-dependent than factor-dependent.

Second, the **relative importance of ship-induced hydrodynamics to sediment dynamics behind the off-bank timber piling** is investigated for individual ship passages. Suspended sediment transport towards the fairway is considered as a proxy for bed and bank erosion.

Quantification of sediment dynamics for the river bed and bank separately is hampered by the large variability and overlap in bed and bank grain sizes. Relying on the differences in sediment dislodge and transport characteristics for varying grain size (sand - silt), a partial distinction between both sediment sources is made.

Dislodgement of silty sediment might take place when the maximum bank-oriented combined wave-induced velocity $U_{W,bank,max}$ exceeds $0.4 \, \text{m s}^{-1}$, and directly implies their advection downstream. For the sandy bed sediments however, suspension does not necessarily lead to a net sediment transport. Significant (yet in absolute values relatively small) net crosswise sediment transport is observed due to the passage of 6 ECMT-IV and Va ships. The direction of crosswise sediment transport is determined by the ratio between the 'primary' wave-induced displacement flow (during the drawdown, and oriented towards the fairway) and its slope supply flow (during the transversal stern wave, and oriented towards the river bank).

The measured order-of-magnitude values of bed- and bank-related suspension transport suggest that the off-bank timber piling does not maintain a 'controlled' sediment dynamics in the shallow water area. A reduction of the combined wave-induced velocity to $U_W < 0.4 \, \text{m s}^{-1}$ behind the off-bank timber piling would lead to a significant decrease in sediment dislodgement,(re)suspension and transport for both sediment sources.

Third, it is evaluated whether **this particular type of nature-friendly bank protection, which has a double wave attenuating configuration, is technically sound to prevent river bed and bank erosion**, i.e. whether or not significant (long-term) morphological changes still occur along its riverine area, and whether or not these changes are significantly different from naturally eroding embayments. Since this particular type includes a reed belt as natural wave barrier, morphological changes are surveyed over one vegetation cycle.

The survey does not reveal clear differences in bank erosion rates (total and periodic areal losses) between the nature-friendly protected and naturally eroding embayments. Although the results do not demonstrate a direct cause and effect re-

lation between hydrodynamic forcing parameters (occasional flooding events and frequent ship wave action) and bank erosion, they qualitatively infer that ship-induced hydrodynamic forcing is sufficiently high to remove slumped bank material and to affect the bank-water contact zone.

Consequently, this nature-friendly bank protecting configuration would benefit from an improved design. It is however a valuable solution to translate a nature-friendly bank protection into a double wave attenuating configuration, of which the first structure is located in the waterway, especially when limited riverine area is available. A reed belt as second, natural wave barrier at the base of the river bank is a sustainable option in this waterway (given its ship-induced hydrodynamic forcing) on the condition that environmental growing conditions are more appropriately met. To this end, it is necessary to reduce the transmission of ship-induced hydrodynamic forcing through the first wave attenuating structure.

1

Problem statement

1.1 Framework

Inland waterborne transport systems are the most energy efficient means of transport compared to rail and road transport systems and they have the smallest ecological footprint, especially compared to road transport systems (PIANC, 2008). Nevertheless, shipping traffic puts pressure on the fluvial environment, by producing waves and altering currents. This must be minimized in the best possible way, without making inland waterborne transport economically unsustainable.

The establishment of the European Water Framework Directive (EU, 2000) altered the approach of waterway development and navigation facilitation, requiring more accountability with respect to the ecosystem. This increased(-ing) awareness of the environmental aspects and assets of a waterway creates the challenging task to develop beneficial solutions, where the waterway design fully integrates the waterway's engineering, economic and environmental objectives (PIANC, 2008).

In line with the European Water Framework Directive (EU, 2000), it is good practice to obviate bank erosion by installing a nature-friendly bank protection instead of a traditional, merely technology-based 'hard' revetment, such as concrete or sheet piles. Incorporating natural processes like wave attenuation by vegetation (Coops et al., 1996) into a bank protecting structure is the way to achieve an optimal ecosystem context while preserving the technical functionalities of a revetment; hence, the desirable 'win-win' solution.

Failures of revetments, dikes or river banks are mainly caused by currents, wa-

ter level variations (tidal and rainfall-driven), wind-generated and ship-generated waves. Inland canalized waterways (or canals) are generally not subject to tidal water level variations, and the fetch length for wind wave generation is limited. On that account, ship-induced hydrodynamics are the most frequent and important forcing towards the river bank.

For these waterways, a typical nature-friendly bank design features two main aspects: (i) an off-bank structure, which reduces the ship-induced hydrodynamic forcing to a lower level, and acts like a sediment trap, and (ii) a shallow water area behind the off-bank structure, which is subject to a controlled, manageable level of ship-induced hydrodynamics (Figure 1.1). This shallow water area creates a transitional zone between the fairway and the riverine area, i.e. between water- and land-based ecosystems (CUR, 1999). An ecologically sound layout is obtained when the dynamics in the shallow water area are controlled in such a way that water exchange with the fairway still takes place in order to maintain a good water quality and to allow a reduced (cyclic) bed erosion and accretion (CUR, 1999).
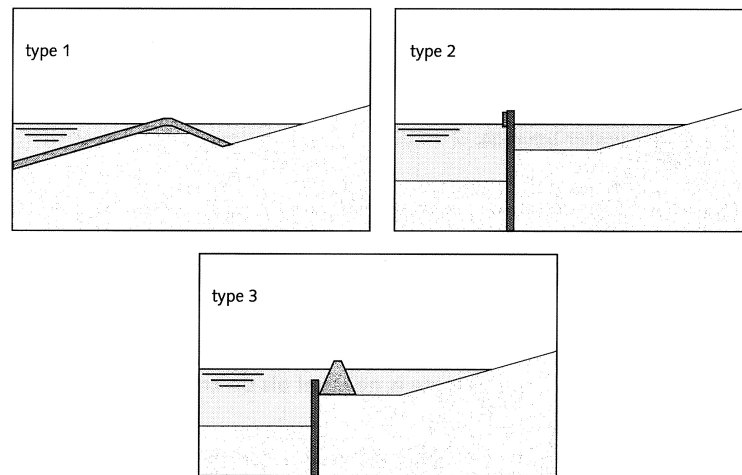
Figure 1.1: Different layouts of the type of nature-friendly bank protection, which consists of an off-bank structure and a shallow water area behind. This type is most frequently applied along inland waterways (source: CUR (1999))

As illustrated in Figure 1.1, this type of nature-friendly bank protection covers a variety of different layouts, which, in turn, can be realized in countless different ways. Figure 1.2(a) depicts a large nature-friendly bank protection along the North Sea Canal (alongstream length of 1.5 km). Its design is according to layout 1 in Figure 1.1. Figure 1.2(b) depicts a small nature-friendly bank protection along the Lys (alongstream length of 200 m). Its design is according to layout 2 in Figure 1.1.

(a)

(b)

Figure 1.2: (*a*) Large nature-friendly bank protection along the North Sea Canal, The Netherlands (> 100000 ship passages every year) (source: RWS) (according to variant 1 in Figure 1.1). (*b*) Small nature-friendly bank protection along the Lys, Belgium (> 19000 ship passages every year) (according to variant 2 in Figure 1.1).

Design guidelines for different layouts of this type of nature-friendly bank protection are formulated in CUR (1999). However, a lack of detailed information regarding design and installation criteria still results in repetitive mistakes and inappropriate installation. In general, it remains an open question whether these nature-friendly bank protection layouts are proven to be effective, especially in an energetic ship wave climate.

On that account, this PhD-research focusses on a particular design of this type of nature-friendly bank protection (Figure 1.1, type 2), installed in a confined, non-tidal waterway subject to heavy shipping traffic. This implies that maximum ship-induced hydrodynamic forcing acts on the bank protection. The nature-friendly bank protection under study consists of off-bank closed timber piling, which separates the fairway from the shallow water and riverine area behind, and a reed belt, planted at the base of the river bank (Figure 1.2(b)). Hence, a double wave attenuating configuration is opted for: first, ship wave action is reduced by the off-bank timber piling, and second, ship waves are further attenuated through the reed belt. No 'hard' bed or bank protecting materials are used in this design.

Ship-generated waves and their associated currents are considered to be the normative hydrodynamic forcings on the nature-friendly bank protection. The jet currents induced by a ship's propeller are not taken into consideration. They are mainly of importance when ships manoeuvre, e.g. near a berthing place, and this is outside the scope of this PhD-research.

To ensure an ecologically sound and technically effective nature-friendly bank protection, it is important to find a balance between the ship-induced hydrodynamic forcing on and the nature-friendly protection of the river bank. Hereupon, the objectives of this PhD-research are established.

1.2 Objectives

The general objective of this PhD-research is to contribute to a deeper insight into an optimized design for nature-friendly bank protections in confined, non-tidal waterways subject to heavy shipping traffic. This fundamental research approach aims at quantifying the (impact of) ship-induced hydrodynamics on a particular design of nature-friendly bank protection (as illustrated in Figure 1.2(b)). Its layout is of interest for installation in confined waterways since it takes up little space in the waterway's wet section and its riverine environment.

To meet this twofold general objective, the following specific research questions will be answered:

1. **What are the characteristics of the ship wave climate in a confined, non-tidal and nature-friendly protected waterway?**

The hydraulic boundary conditions for the ship wave climate are defined by the relation between the dimensions of the waterway and the characteristics of the shipping traffic. The magnitude and behaviour of the ship-generated waves depend on a ship's sailing characteristics and its sailing environment.

On that account, the ship wave climate is characterized based on its input and output variables. The input is defined by the hydraulic boundary conditions for shipping traffic. The ouput is determined by (i) the magnitude of the ship-generated waves, (ii) their wave-structure interaction with the off-bank timber piling, and (iii) the ship waves' behaviour in the shallow water area behind the off-bank timber piling.

2. **To which extent do ship-induced hydrodynamics contribute to sediment dynamics behind the off-bank timber piling?**

The open structure of the nature-friendly bank protection makes water exchange between the fairway and the shallow water area possible. It is however unclear whether this off-bank timber piling configuration provides sufficient protection against ship-induced hydrodynamic forcing in order to maintain a dynamic balance in its bed sediment budget behind the off-bank timber piling, i.e. a 'controlled' (cyclic) bed erosion and accretion, and to prevent bank erosion.

Therefore, ship-induced hydrodynamics and their relative importance to sediment dynamics are investigated for individual ship passages in the shallow water area behind the off-bank timber piling. Suspended sediment transport towards the fairway is considered as a proxy for bed and bank erosion. In this way, shipping traffic's role as a system-driving parameter for (short-term) morphological changes is estimated.

3. **Is this type of nature-friendly bank protection effective to obviate river bed and bank erosion?**

The nature-friendly bank protection under study consists of a double wave attenuating configuration: (i) the off-bank timber piling, and (ii) the reed belt before the river bank. In a confined, non-tidal waterway, flood and ship waves are considered to be the external hydrodynamic forcing parameters on the river bank.

Accordingly, the effectiveness of this type of nature-friendly bank protection is monitored on various locations to assess if this double wave attenuating configuration is technically sound to prevent river bed and bank erosion, i.e. whether or not significant long-term morphological changes do occur along the riverine area.

Because ship-generated waves interact with topographic boundaries, and the cross sectional and longitudinal profile of a nature-friendly protected waterway might further complicate the ship waves' behaviour, the hydrodynamic performance of this nature-friendly bank protection is investigated based on an experimental field study.

1.3 Outline

Now the framework of the research is presented which led to the three formulated research questions, you are guided through this PhD-manuscript in 5 Chapters to find them answered.

Chapter 2 briefly discusses the basics of ship-generated waves and their behaviour in a confined waterway.

Chapter 3 introduces the study area for this experimental field study, i.e. the confined, non-tidal Lys. Subsequently, it provides a detailed description of the designed and constructed monitoring systems.

The subsequent 3 chapters each correspond to one of the three research questions in Section 1.2.

Chapter 4 elaborates on the characteristics of the ship wave climate in this confined, non-tidal and nature-friendly protected waterway. It consists of two main parts. The first part deals with the characteristics of shipping traffic on the Lys. The second part handles the ship wave-structure interaction with various configurations of the off-bank timber piling and discusses the ship waves' shallow water behaviour. For the latter part, the developed analysis methodology for ship-generated wave measurements is additionally described.

Chapter 5 treats the relative importance of ship-induced hydrodynamics to sediment dynamics in the shallow water area behind the off-bank timber piling.

Chapter 6 addresses the effectiveness of the nature-friendly bank protection under study to obviate bed and bank erosion.

Chapter 7 presents the general conclusions of this PhD-research and summarizes the acquired knowledge for each of the three research questions separately. It concludes with suggestions for further research.

2

Ship waves in a confined waterway

2.1 An introduction to ship waves

From a hydrodynamical point of view, a sailing ship resembles to flow around a body (Schiereck, 2001). The ship experiences frictional resistance (due to motion of the ship's hull through a viscous fluid), eddy resistance, air resistance and wave-making resistance (due to the energy that must be supplied continuously by the ship to the wave system created on the water surface) (SNAME, 1988b).

In order to overcome its resistance, the sailing ship transfers energy to the water body in the form of a water displacement from the front to the back of the ship. Its forward motion results in a pressure distribution and corresponding velocity pattern according to Bernoulli's principle (SNAME, 1988b). Along a streamline around the ship's hull, for 2 arbitrary points A and B, the Bernoulli equation states that (in an incompressible, frictionless fluid):

$$\left(z + \frac{p}{\rho g} + \frac{V_s^2}{2g} \right)_A = \left(z + \frac{p}{\rho g} + \frac{V_s^2}{2g} \right)_B = constant \qquad (2.1)$$

where z is the vertical distance from the reference level [m]; p is the pressure [Pa]; g is the acceleration of gravity, $g = 9.81 \, \mathrm{m\,s^{-2}}$; ρ is the fluid density, for fresh water: $\rho = 1000 \, \mathrm{kg\,m^{-3}}$ and V_s is the ship's sailing speed [$\mathrm{m\,s^{-1}}$] (relative to the water's flow velocity).

Figure 2.1 shows that, at the bow and stern, the pressure is increased whereas along the ship's hull a water level depression is observed; the velocity distribution changes accordingly. This wave pattern is frequently named the ship's 'primary'
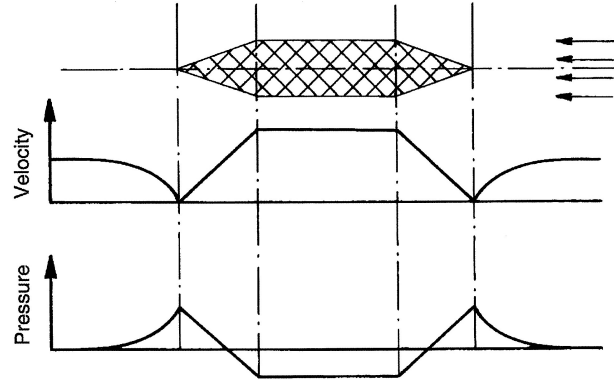
Figure 2.1: Illustration of the water pressure and velocity distribution of an ideal fluid along a simple wedge-shaped hull of a ship (source: Bertram (2000)). This Bernoulli wave pattern is frequently named the ship's 'primary' wave pattern.

wave pattern. The 'primary' wave pattern propagates in the sailing direction, and has a wave length which is about the ship's length L (Schiereck, 2001). Its amplitude is quadratically dependent on the ship's sailing speed V_s (relative to the water's flow velocity), although its general wave shape is not (Bertram, 2000). Note that a ship's sailing speed V_s is restricted to the celerity of its own generated 'primary' wave pattern, which depends on the ship length, unless the ship is able to plane (e.g. pleasure cruising) or it is being towed (Schiereck, 2001).

Transverse and diverging waves are caused by the pressure pattern due to discontinuities in the ship's hull profile, which are found at the bow and stern (Schiereck, 2001) (Figure 2.2). They form interference cusps, of which the (constant) wave envelope, i.e. the cusp locus line, makes an angle of 19°28 with the ship's sailing line in deep water. Accordingly, the direction of wave propagation for this cusp locus line is at an angle of about 35°to the sailing line; hence, the angle of attack towards a river bank parallel to the sailing line is 55°. The diverging waves are dominant in Figure 2.2, which shows a typical subcritical wave pattern (for depth-based Froude number $Fr_d < 0.75$, equation 2.6). These interfering transverse and diverging waves were first investigated by Lord Kelvin in 1887, and are referred to as the 'secondary' Kelvin wave pattern.

In deep and unconfined water, this Kelvin wave envelope can propagate over long distances (several kilometers), in which the maximum wave height of the transverse waves decreases with the square root of the distance to the sailing line and the maximum wave height of the diverging waves (and interference cusps) diminishes with the cubic root (Osborne and Boak, 1999; PIANC, 2008; Schiereck, 2001). Conversely, the 'primary' wave pattern is displayed only locally and has a small amplitude (Garel et al., 2008).
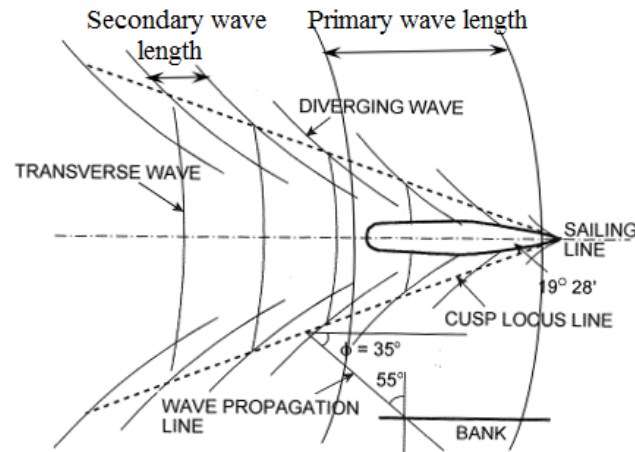
Figure 2.2: Illustration of the 'secondary' wave pattern, consisting of transverse and diverging waves. They interfere and form a cusp locus line (the Kelvin wave envelope), which makes an angle of $19°28$ with the sailing line of the ship in deep water and in shallow water for $Fr_d < 0.75$ (source: Schiereck (2001)).

2.2 Ship waves in confined water

The aforementioned ship resistance is sensitive to the effects of waterway confinedness, which is indicated by a (significant) change in the potential flow around a ship's hull. Because of the limited depth and width of an inland waterway, the pressure and velocity distribution around the ship's hull are more pronounced, leading to an increased sinkage, trim and resistance for the sailing ship (Figure 2.3) (SNAME, 1988b). A return current takes place in the opposite direction to the ship's motion. The enlarged sinkage and trim due to the proximity of the river bed (small under keel clearance), is named the squat effect. It is proportional to the square of the sailing speed V_s and occurs when the depth to draught ratio is less than 4 (USACE, 2006).

The water motions due to a ship passage can be approximated by a 1-D flow situation, where the ship is at rest and the water flows around its hull with a velocity equal to its sailing speed V_s (relative to the water's flow velocity) (Figure 2.4). Schijf (1949) was the first to use this approach, and following assumptions were hereby made: the ship's sailing line is in the axis of the waterway, and the ship sails in a horizontal position; the ship and waterway cross section are prismatic; the return current and drawdown are constant over the waterway cross section; and the ship's sinkage, i.e. the squat, equals the drawdown (Schiereck, 2001).

Because of the increased ship resistance, the Bernoulli equation 2.1 along a streamline between the cross sectional waterway area without (point A) and with

a ship (point B), becomes (illustrated in Figure 2.4B):

$$z_A + \frac{\rho g h}{\rho g} + \frac{V_s^2}{2g} = z_B + \frac{\rho g(h - \Delta h)}{\rho g} + \frac{\alpha(V_s + u_r)^2}{2g} \qquad (2.2)$$

where $z_A = z_B$; $p = \rho g(h(-\Delta h))$ equals the hydrostatic pressure, in which h is the water depth [m] and Δh is the drawdown [m]; u_r is the return current [m s^{-1}] and $\alpha = 1.4 - 0.4V_s/V_l$ is a parameter which takes into account the ratio of a ship's sailing speed V_s to its limit speed V_l (advocated by Przedwojski et al. (1995), found in GBB (2010)).

The continuity equation, which indicates the conservation of mass between the 2 points A and B, equals:

$$A_w V_s = (A_w - A_s - b\Delta h)(V_s + u_r) \qquad (2.3)$$

where A_w is the waterway cross sectional area [m^2]; and A_s is the immersed midship cross sectional area [m^2].

Combination of the equations 2.2 and 2.3 gives the average drawdown Δh and return current u_r occasioned by a ship passage. Note that these equations also hold for a trapezoidal cross section of the waterway when the water depth h is replaced by the average water depth $h_m = \frac{A_w}{W_{SWL}}$, using the ratio of the waterway cross sectional area A_w to its width on the still water level W_{SWL} (GBB, 2010).

A ship's limit speed V_l is now not only dependent on the celerity of its 'primary' wave pattern, but also on the resistance conditions because of waterway confinedness. The 'primary' wave pattern acts in an area of reduced water depth and it runs against the return current u_r, which is scaled with the ship's sailing speed V_s and blockage coefficient m (PIANC, 2008). When the return current u_r becomes critical, the limit speed V_l is reached (GBB, 2010; Schiereck, 2001).

The ship's limit speed V_l can be calculated as:

$$V_l = Fr_{d,cr} \cdot \sqrt{gh} \qquad (2.4)$$

where the critical depth-based Froude number $Fr_{d,cr}$ for a ship is obtained from (Schijf (1949), adapted by Lataire et al. (2009)):

$$Fr_{d,cr} = \left(2\sin\left(\frac{\arcsin(1 - m^{-1})}{3}\right)\right)^{3/2} \qquad (2.5)$$

where m is the blockage coefficient, i.e. the space a ship occupies in the waterway's cross section. It is defined by the ratio of the waterway cross sectional area A_w to the immersed midship cross sectional area $A_s = B \cdot D$, in which B is the ship's beam [m] and D is the ship's actual draught. The midship section coefficient $\beta = 0.995$ is considered negligible and therefore not taken into account (value for inland shipping traffic, advocated by Georgakaki and Sorensen (2004)).
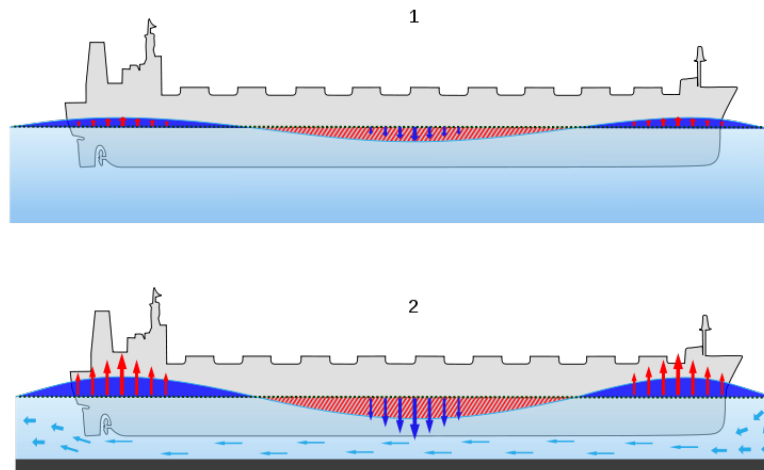
Figure 2.3: 1. In deep water, a sailing ship causes a pressure distribution and velocity profile around its hull according to Bernoulli's principle. 2. In confined water, sailing results in a more pronounced potential flow around the hull, and an increased sinkage and trim because of small under keel clearance (source: Wikipedia (2013))
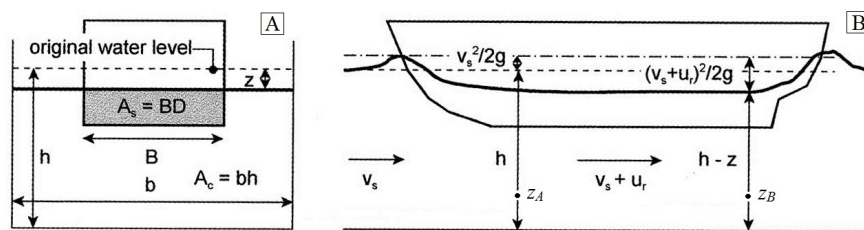
Figure 2.4: Longitudinal and cross section of the 1-D flow approximation of water motions due to a ship passage in a confined waterway. The symbol of the water level depression z corresponds to Δh in equation 2.2, the symbol A_c to A_w in equation 2.3 (source: Schiereck (2001)).

The Kelvin wave envelope might have an altered angle of attack towards the river bank in shallow water (SNAME, 1988b). This angle variation can be estimated using the depth-based Froude number Fr_d:

$$Fr_d = \frac{V_s}{\sqrt{gh}} \qquad (2.6)$$

Until a depth-based Froude number $Fr_d < 0.75$, the deep water conditions are preserved (GBB, 2010; Schiereck, 2001). A further increase of the depth-Froude number towards $Fr_d = 1$ results in a widening of the Kelvin wave envelope until a maximum angle of 78°is obtained for the cusp locus line to the sailing line at $Fr_d = 1$. The wave height, of the predominantly diverging waves, also reaches a maximum when Fr_d approaches 1 (Houser, 2011), and is thus dependent on the sailing speed V_s. A higher increase of $Fr_d > 1$ results in a decrease of the Kelvin wave envelope's angle but the 'secondary' wave pattern now only consists of diverging waves (SNAME, 1988b).

Figure 2.5 illustrates the ship-generated wave and flow pattern of a displacement ship, sailing in a confined waterway with a trapezoidal cross section. Although the duration of its passage is very limited at a certain location, its motion is associated with a complex wave and flow pattern, of which the different hydrodynamic components are superimposed.

At the top of Figure 2.5, the ship's 'primary' wave pattern is shown. At a certain location, it successively consists of a small water level rise, i.e. the bow wave H_{bow}, a drawdown Δh along the ship's hull passage, and another surge, i.e. the transversal stern wave H_{stern} (cf equation 2.2).

At the bottom of Figure 2.5, the behaviour of the 'primary' and 'secondary' wave patterns, and associated currents, in the trapezoidal cross section is depicted. To preserve continuity of flow, the velocity distribution between the ship and river bank changes accordingly; which might result in a high return current u_r (Bhowmik et al., 1995; Mazumder et al., 1993). The transversal stern wave H_{stern} mainly affects the riverine area. This (sloping) shallower water area results in a local depth-Froude number $Fr_d \geq 1$ (because of the limited water depth and/or drawdown), which goes from $Fr_d \geq 1$ to $Fr_d < 1$ at the transition of the drawdown trough to the still water level. This is indicated by the wave breaking, and associated slope supply flow. The Kelvin wave envelope approaches the river bank at an angle of 55°(thus $Fr_d < 0.75$), in which both the transverse and diverging waves are discernible. Superposition of the diverging bow waves and the transversal stern wave occurs but it is not relevant for the design of a bank protection since the distance to the river bank is smaller than the ship length times the tangent of 55°(GBB, 2010) (this generally holds for goods traffic).

Note that for short displacement ships, e.g. push tugs or tug boats, the superposition between the 'primary' wave pattern (the transversal stern wave) and

'secondary' bow wave pattern might become important, dependent on their sailing speed and sailing distance to the river bank (GBB, 2010).
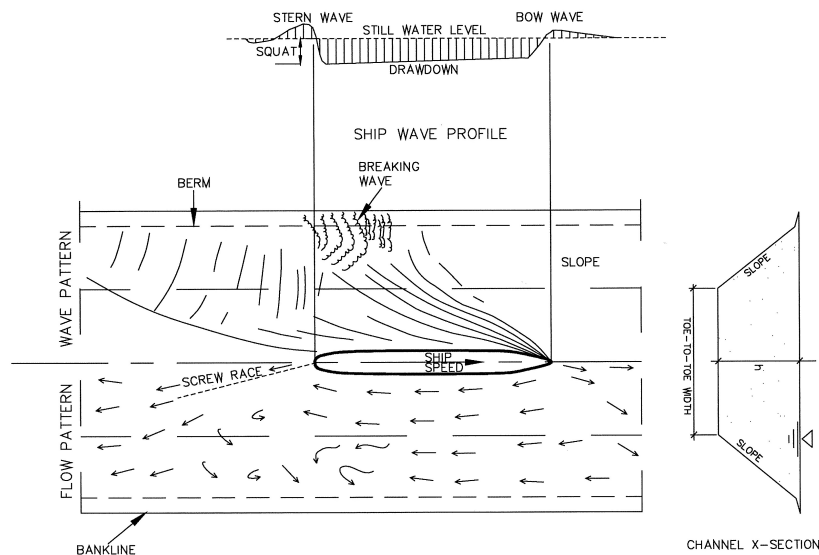
Figure 2.5: Planview of the ship-induced water motions, i.e. wave and flow pattern, on the river bed and banks at a certain location along a confined waterway with trapezoidal cross section (source: USACE (2006)).

The relative importance of the 'primary' and 'secondary' wave patterns depends on the ship type. In a broad sense, inland shipping traffic can be subdivided into two groups, displacement and planing ships. The first group, e.g. goods traffic, always sails at subcritical speed ($Fr_d < 1$) (because of blockage coefficient restrictions, see equation 2.5). These ships have a large underwater volume and corresponding water displacement. Their 'primary' wave pattern is of great importance, whereas their 'secondary' wave pattern wil be less pronounced because of their slow sailing speed V_s.

The latter group, e.g. pleasure cruising, is able to sail at (super)critical speed ($Fr_d \geq 1$). Their underwater volume is small and thus, their 'primary' wave pattern is of little importance but they are able to plane on the water, i.e. the ship rides its own bow wave. The ship's planing speed depends on its ship length (GBB, 2010). To reach the planing speed range, a ship tries to overcome the steep slope of its 'secondary' bow wave. It needs therefore a high engine power, which results in the largest 'secondary' wave heights (occurring in the semi-planing speed range) (PIANC, 2008).

2.3   Conclusion

A sailing ship causes two different types of wave patterns: the Bernoulli wave pattern and the transverse and diverging Kelvin wave pattern, which are referred to as the 'primary' wave pattern and the 'secondary' wave pattern respectively. The first wave pattern is only displayed locally around the ship, the latter wave pattern travels a much longer distance.

Sailing in a confined waterway increases the ship resistance, as a result of which the potential flow around the ship hull becomes more pronounced. The more confined the waterway's dimensions, the more important the hydrodynamics of the ship's 'primary' wave pattern become. This holds specifically for displacement ships, e.g. goods traffic, to which the 'primary' wave pattern is of greatest importance. The 'primary' wave-induced water motions, i.e. the drawdown Δh and transversal stern wave H_{stern}, together with the return current u_r, act as the most important energy contributor towards the river bed and banks (Bauer et al., 2002; Ten Brinke et al., 2004; Verney et al., 2007). The 'secondary' wave pattern, which consists of transverse and diverging waves, generally has a limited wave height, except when ships are able to sail in the semi-planing speed range (e.g. pleasure cruising).

The ship's sailing speed V_s dictates the amplitude of both ship wave patterns, and will therefore be an important parameter for the quantification of the (impact of) ship-induced hydrodynamics.

3

Experimental field setup for the monitoring of ship wave action

3.1 Introduction

Heavy shipping traffic complicates the development of nature-friendly bank protection on confined, non-tidal waterways. For its proper design, accurate input data on the magnitude of ship-induced hydrodynamic forcing is essential.

A significant variability exists in ship data records on different times at the same locations, and between different locations (Parnell and Kofoed-Hansen, 2001; Soomere et al., 2003). On the one hand, ship wave characteristics, such as propagation directions, wave heights and wave periods, vary with ship design and operation (different types, laden or light draught, sailing speed). On the other hand, ship-generated waves interact with topographic boundaries, and the bathymetry of the waterway might further complicate the ship waves' behaviour by means of reflections, amplification and resonance (Stockstill and Berger, 2001). Consequently, a ship passage alters, locally and temporarily, the hydraulic boundary conditions of the waterway significantly.

This variability in ship waves' behaviour, together with varying methodologies and assumptions on which analytical solutions are based (cf Section 2.2), make that ambiguity is likely to persist for the quantification of (the impact of) ship-induced hydrodynamics in the absence of direct measurements (a.o. Dam et al. (2008); Taylor et al. (2007); Torsvik et al. (2009)). By field monitoring, the contribution of various controlling variables can be measured and taken into account

accordingly.

In this PhD-research, a stand-alone monitoring system is designed and constructed, which accurately measures the magnitude of ship-induced hydrodynamic forcing on and the response of a particular type of nature-friendly bank protection (Figure 1.2(b)). After the stand-alone monitoring system was installed in the field, the instrumentation was re-engineered and extended to develop a mobile monitoring system, enhancing the dynamic measurement possibilities.

This chapter introduces the study area chosen for the experimental study on the hydrodynamic performance of this type of nature-friendly bank protection. Subsequently, a detailed description of the fixed and mobile monitoring system is provided, together with good installation practices.

3.2   Study area

Within the context of the Trans-European Transport Network (TEN-T, EU (2006)), which aims at improving the transport mobility within Europe, the connection of the Seine and Scheldt river basins is one of the 30 TEN-T priority projects (EU, 2007-2020). The main objective of the priority project 30 'inland waterway Seine-Scheldt' is to optimise the connection between the French inland waterway network and ports and the Belgian, Dutch and German waterway networks and ports.

A part of this project, the improvement of the navigability between Deûlémont and Ghent, is situated in the Lys river basin. The Lys is a European standard scale ECMT-IV inland waterway (ECMT, 1992). Adaptations include a.o. the deepening of the Lys' waterway profile and the enlargement of locks to upgrade the waterway to a narrow (one-way traffic) ECMT-Vb waterway (tonnage up to 4500 ton, with a draught restriction of 3.5 m, Maes et al. (2006)).

To comply with the European Water Framework Directive (EU, 2000), the Flemish government decided to directly incorporate measures to restore this heavily modified water body to a waterway having a good ecological potential. Aside from the improvement of fauna migration and the enhancement of river dynamics, this involved the installation of nature-friendly bank protections (Maes et al., 2006).

Hence, the Lys is a nice example of reconciliation of various 'stakeholder' needs, i.e. the economic EU Trans-European Transport Network and the environmental EU Water Framework Directive. The most downstream part of the Lys is selected as study area.

3.2.1   History of the Lys

Forming a subbasin of the river Scheldt catchment, the Lys is a typical lowland river, which runs through a part of northern France and western Belgium (Figure

3.1(a)). In the seventies, the meandering course of the river Lys was straightened and a calibrated channel was excavated to allow inland navigation up to ECMT-class IV (tonnage of 1350 ton, ECMT (1992)) (Figure 3.1(b)). This resulted in the construction of several locks with a small head, regulating the water level and resulting in very small flow velocities.

The channelised Lys was designed with a trapezoidal cross sectional area of $144\,m^2$, 50.7 m wide (at still water level) and 3.5 m deep (Figure 3.4). Armoured concrete slabs were placed as revetment under a 10/4 slope, supported by a horizontal concrete beam which was installed in an underwater berm 1.5 m wide at a regulated water depth of 1.3 m. Underneath, the 12/4 underwater slope remained unprotected, like the river bed (Figure 3.2).

In the past decade however, the demand of benefit maximization in goods traffic urged the waterway administration to allow ships up to ECMT-class Va (tonnage up to 3000 ton with no imposed draught restrictions, ECMT (1992)). Heavy shipping traffic resulted however in the failure of the armoured concrete revetment (Figure 3.3(a)). The revetment was undermined and broke, which resulted in progressive bank erosion. Instead of the 10/4 design slope, progressive bank erosion adjusted the river banks to a natural geomorphology (Figure 3.3(b)).
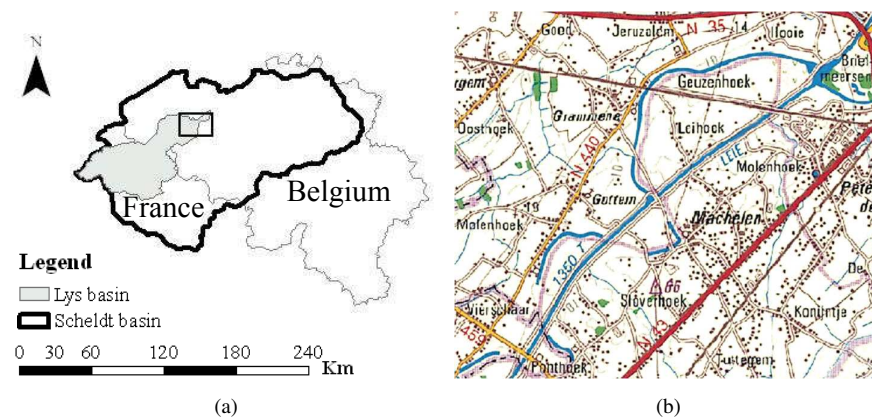
Figure 3.1: (a) Location of the Lys subbasin within the Scheldt river basin. (b) The meandering course of the Lys (blue line) was straightened and calibrated for ECMT-IV shipping traffic (source: DOV (2009)).
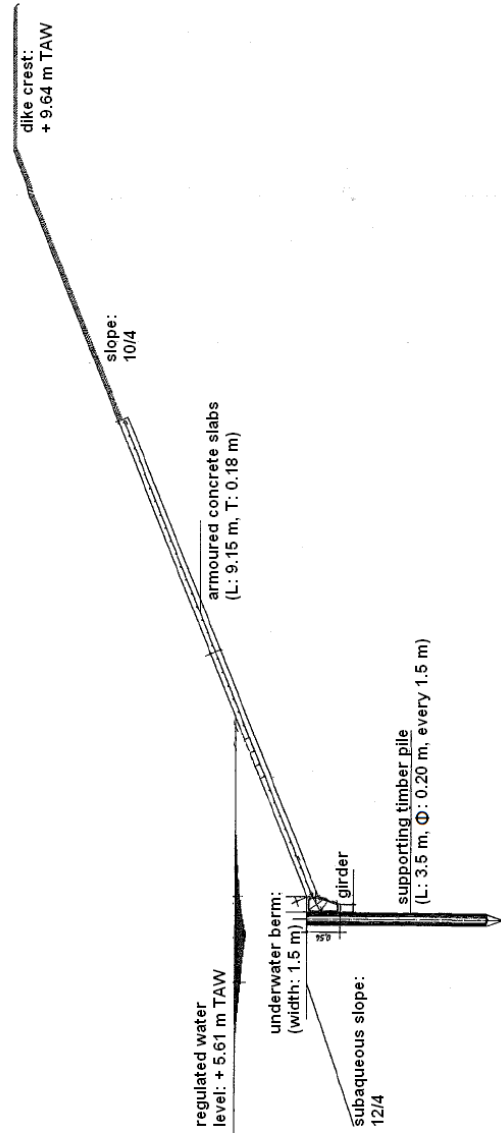
Figure 3.2: Cross sectional view of the original bank protection in the calibrated Lys (for ECMT-IV shipping traffic). Armoured concrete slabs, installed under a 10/4 slope, protect the river bank, the river bed is unprotected. (English adaptation of a technical drawing of W&Z).

(a)

(b)

Figure 3.3: Heavy shipping traffic resulted in the failure of the armoured concrete revetment (*a*) Initially, the concrete slabs were undermined and broke (*b*) Frequent ship-induced hydrodynamic forcing progressively scoured semi-circular embayments into the river banks.

3.2.2   The Lys nowadays (and in the future)

Semi-circular embayments were scoured into the river banks, in which a vertical cut-bank gradually developed with at its base a gently sloping beach of eroded sediments (Figure 3.3(b)). Given these environmental boundary conditions and having limited riverine space available, the waterway authorities decided to install a type of nature-friendly bank protection, which consists of off-bank timber piling, which separates the fairway from the shallow water and riverine area behind, and a reed belt at the base of the vertical cut-bank (cf Figure 1.2(b) and 3.5). From 2008 onwards, heavily eroded locations along the most downstream part of the Lys were tackled using this type of nature-friendly bank protection.

The first, off-bank wave attenuating barrier is made up of a closed row of timber piles, having a length of 5 m and a diameter of 0.2 m. They are piled until a freeboard of 0.50 m to the regulated water level is obtained, and bank-connected. Water exchange between the fairway and the shallow water area is provided with lateral in- and outflow openings, of varying length. This shallow water area has a variable depth, dependent on the eroded slope. The second, natural wave attenuating barrier consists of reed patches, planted at the base of the vertical cut-bank.

The bank protection's working principle relies on a reduction of ship wave energy by the row of timber piling to a lower, manageable level in the shallow water area behind, where ship wave energy is further dissipated by bottom friction and attenuated through the reed belt before reaching the river bank.

In the near future, the (theoretical) trapezoidal cross sectional area will be dredged to 177 m^2 and will have a water depth of 4.5 m in the fairway (deepening of the profile in orange in Figure 3.4). The cross sectional area behind the off-bank timber piling remains unaffected (Maes et al., 2006).

Shipping traffic is heavy in the most downstream part of the Lys; a monthly average of 1600 ships passes through the lock at Sint-Baafs-Vijve (W&Z, 2009-2011). It consists for the greatest part of goods traffic. Pleasure cruising is limited to occasional passages during fair weather days. A speed limit of $V_s = 12\,\mathrm{km\,h}^{-1}$ (3.3 m s^{-1}) is imposed on the Lys.

3.3   Site selection for the monitoring systems

Site selection for the large, fixed monitoring system was guided by the need to find a nature-friendly protected location in a rather straight section of the waterway. This allows ships to sail at their maximum speed V_s and hence, to cause maximum ship-induced hydrodynamic forcing on the nature-friendly bank protection, the river bed and the river bank.

A site in Machelen, situated southwest of the city of Deinze, satisfied these criteria (Figure 3.1(b), and Figure 3.6B and 3.6C). It is located 1.5 km upstream of
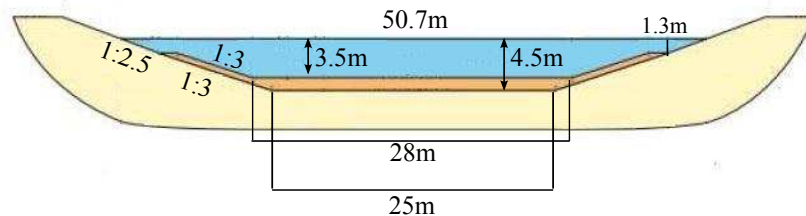
Figure 3.4: The Lys' theoretical trapezoidal cross sectional area, nowadays (blue) and in the future (orange).

the waterway's bifurcation into the Lys derivation canal, leading navigation into the adjacent basin of the Gentse Kanalen, and the Tourist Lys, a smaller tributary which discharges into the Scheldt at Ghent. At this site, which is nature-friendly protected since March 2008, the off-bank timber piling has a length of 160 m. It is bank-connected piled (length of 5.1 m and 4.8 m for the up- and downstream piling respectively), and lateral water in- and outflow openings are present on both sides (as indicated on the location and cross section maps of W & Z (drawn up date: April 27, 2011)). A reed belt additionally protects the natural river bank over 60% of its alongstream length.

The flexible, mobile monitoring system, which was subsequently developed, was applied at various nature-friendly protected locations which differ in off-bank timber piling configuration (Figure 3.6B and 3.6D).

Since 8 of the 10 measurement locations are situated in the most downstream part of the Lys, a short description of the Lys' boundary conditions in this section is given in following subsections. These hydro-environmental boundary conditions are largely determined based on field samples, taken in the nature-friendly bank protection where the fixed monitoring system is installed. Since spatial heterogeneity in natural properties (e.g. grain size distribution, flow patterns) is undoubtedly present, it should be noted that the measured (and calculated) (threshold) values are location-dependent.

3.3.1 Hydrodynamics

The regulated water level of +5.6 m TAW (Tweede Algemene Waterpassing, Belgian reference datum) in the section downstream the lock of Sint-Baafs-Vijve corresponds to an average discharge of 30 $m^3 s^{-1}$ (HIC, 1983-2012). Peak discharges of 200 $m^3 s^{-1}$ occur occasionally, resulting in high water levels.

For the monitoring period from July 2009 to September 2010, the water level raised to more than 6.10 m TAW during 16.5 days (HIC, 2009-2010). During these flood wave conditions, the off-bank timber piling, and often the reed belt,
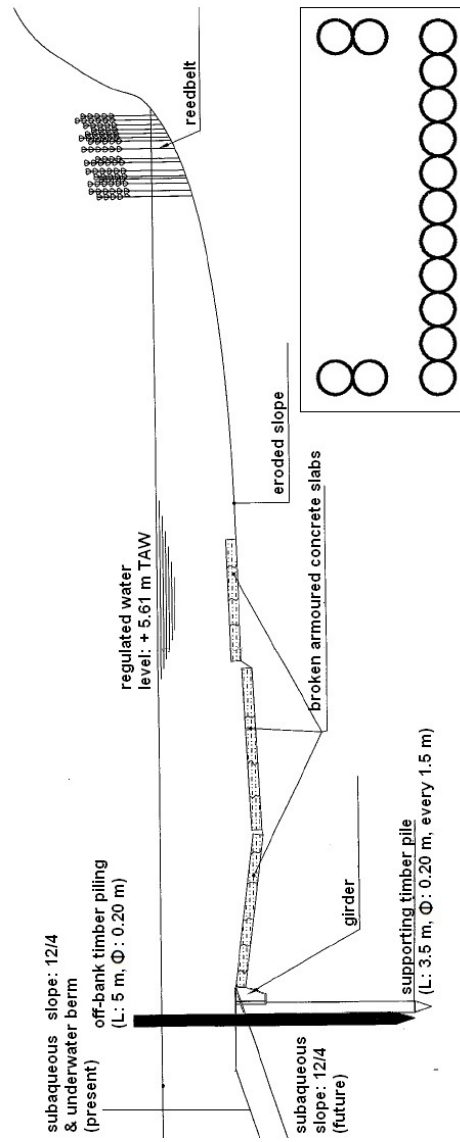
Figure 3.5: Cross sectional view of the new bank protection in the upgraded Lys (for ECMT-Vb shipping traffic). River banks are nature-friendly protected using off-bank timber piling in combination with a reed belt along the (vertical) cut-bank. Inset: plan view of the off-bank and bank-connected timber piling, with lateral water in- and outflow openings (English adaptation of a technical drawing of W&Z).
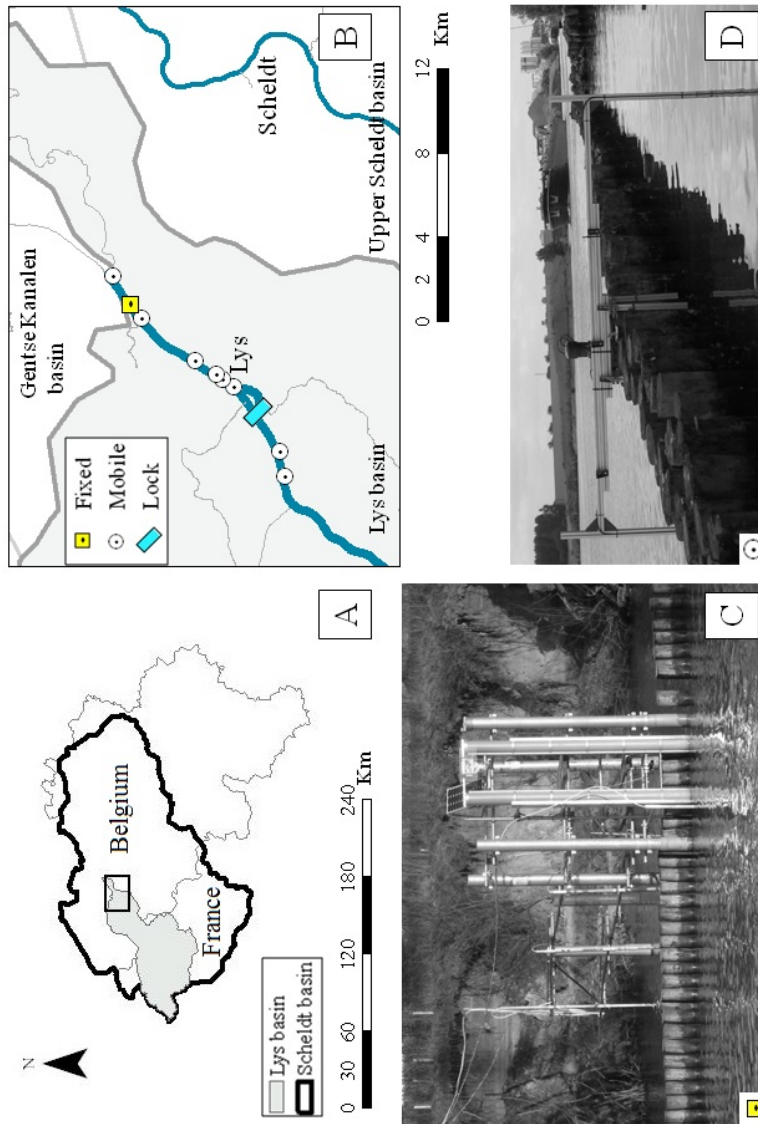
Figure 3.6: Measurement locations along the Lys: A. Situation of (the most downstream part of) the Lys basin; rectangle marks detailed view of B.; B. Indication of measurement locations with fixed and mobile monitoring systems; C. The fixed monitoring system; D. The mobile monitoring system.

were submerged. Discharge data were however not available (during the entire monitoring period), nor was the average cross sectional flow velocity measured.

Lock-induced translation waves are noticeable during the day, leading to small water level fluctuations.

Over a cross sectional measurement transect (of the fixed monitoring system, see Section 3.4.1), flow velocity is measured at various distances from the off-bank timber piling and at various heights z above the river bed during normal weather conditions (Table 3.1). During these steady flow conditions, i.e. without a ship passage, the average flow velocity is low in the measured verticals, $u_X = 2.0{\cdot}10^{-2}\,\mathrm{m\,s^{-1}}$ (in streamwise direction), and its magnitude is similar over the measurement transect (column 2 in Table 3.1). Because of the Lys' canalised layout, this is as to be expected.

Bed shear velocity, u_*, and bed shear stress, τ, are calculated using (Dyer (1986), cited in Kim et al. (2000); checked for fluvial studies by Biron et al. (2004)):

$$\tau = \frac{1}{2}\rho C(\overline{u_X'^2} + \overline{u_Y'^2} + \overline{u_Z'^2}) \tag{3.1}$$

$$u_* = \sqrt{\frac{\tau}{\rho}} \tag{3.2}$$

where u_X', u_Y' and u_Z' are respectively the fluctuating velocity components in horizontal (stream- and crosswise) and vertical direction (the overbar indicates the average over the sampled period of 230 s, and $\sum u' = 0$ in X, Y and Z-direction over the sampled period); C is a proportionality constant, here $C = 0.19$ (as applied in Biron et al. (2004); Kim et al. (2000)).

The Lys' slow flow velocity u_X causes low bed shear stresses τ, which are also rather uniform over the measurement transect (column 4 in Table 3.1).

Table 3.1: Flow characteristics along the cross sectional measurement transect of the fixed monitoring system, under steady flow conditions (measured on May 24, 2011)

Location [*]	Average velocity u_X [m s^{-1}] [**] (at height z [m])	Shear velocity u_* [m s^{-1}]	Bed shear stress τ [N m^{-2}] (at height z [m])
-1	$2.2{\cdot}10^{-2}$ (1.10)	$4.1{\cdot}10^{-3}$	$1.7{\cdot}10^{-2}$ (0.10)
3	$1.8{\cdot}10^{-2}$ (0.47)	not calculated	not measured
7	$2.0{\cdot}10^{-2}$ (0.29)	$2.7{\cdot}10^{-3}$	$0.7{\cdot}10^{-2}$ (0.07)
9.5	not measured	$3.2{\cdot}10^{-3}$	$1.0{\cdot}10^{-2}$ (0.06)

[*] Distance from the off-bank timber piling:
$-$:location in fairway,$+$: location in nature-friendly bank protection

[**] According to the theoretical Prandtl-Von Karman logarithmic velocity profile, at $z = 0.37h$ the average velocity over the vertical is measured

3.3.2   Sediment dynamics

River bed and bank soil samples were taken on various locations in the shallow water area behind the off-bank timber piling to get a better view on the spatial heterogeneity in bed and bank sediments. Water samples were also taken in this area. Particle size distributions of these samples were determined using a Mastersizer 2000 (Malvern Instruments), and listed in Appendix A.

In what follows, sediment characteristics from these 3 different sources, i.e. the river bed, the river bank and the water column, are separately described.

■ **The river bed**

The sandy river bed of the shallow water area has a top layer composed of sediment having a median grain size of $d_{50} = 197 \pm 13\,\mu$m and ranging from 50 to 409 μm (USDA soil texture classification). The top layer is poorly sorted, which indicates that the bed material was deposited over a wide range of flow velocities (sorting coefficient $S = \sqrt{d_{90}/d_{10}} = \pm 1.80$ with d_{90} and d_{10} respectively the grain sizes for which 90% and 10% by weight of the material is finer (Chanson, 2004b)).

An illustrative comment to this calculated value is the observation that a ship passage is able to cause locally and temporarily considerable higher flow velocities compared to the steady river flow. Associated with these higher velocities is the appearance of suspended sediments clouds in the water column during (and after) a ship passage.

The critical shear stress for incipient motion of the river bed is $\tau_{cr} = 0.16\,\mathrm{N\,m^{-2}}$, calculated from (Chanson, 2004b; Van Rijn, 1993):

$$\tau_{cr} = \theta_{cr}\left(\rho_s - \rho\right)gd_{50} \tag{3.3}$$

where θ_{cr} is the critical Shields parameter; ρ_s is the sediment density, here: $\rho_s = 2650\,\mathrm{kg\,m^{-3}}$; d_{50} is the median grain size: the grain size for which 50% by weight of the sediment sample is finer, here $d_{50} = 1.97{\cdot}10^{-4}$ m.

The critical Shields parameter is $\theta_{cr} = 5.2{\cdot}10^{-2}$, calculated from (Van Rijn, 1993):

$$\theta_{cr} = 0.14D_*^{-0.64} \text{ for } 4 < D_* \leq 10 \tag{3.4}$$

$$\text{where } D_* = \left[\frac{\left(\frac{\rho_s}{\rho} - 1\right)g}{\nu^2}\right]^{1/3} d_{50} = 4.65 \tag{3.5}$$

where ν is the kinematic fluid viscosity, for water: $\nu = 1.1{\cdot}10^{-6}\,\mathrm{m^2\,s^{-1}}$ (in a water temperature of 15°C).

Comparison of the critical shear stress τ_{cr} with the shear stresses τ occasioned by the river flow (Table 3.1) indicates a one order of magnitude difference. Incipient motion of the river bed does not take place (during normal flow conditions).

Inception of sediment suspension is related to the balance between the turbulent velocity fluctuation and the particle fall velocity (normal to the river bed) (Chanson, 2004b):

$$\frac{u_{*cr}}{w_s} = 1 \Leftrightarrow u_{*cr} = w_s \qquad (3.6)$$

where u_{*cr} is the critical shear velocity for incipient bed motion, here: $u_{*cr} = 1.3 \cdot 10^{-2} \, \text{m s}^{-1}$ (calculated with equation 3.2, using the τ_{cr} value) and w_s is the particle fall velocity of the sandy bed sediments, expressed as (formula of natural sands, Soulsby (1997)):

$$w_s = \frac{\nu}{d}(10.36^2 + 1.049 D_*^3)^{0.5} - 10.36 \qquad (3.7)$$

which is valid for all D_* (in the range of $d > 62 \, \mu\text{m}$).

The eroded condition of the river banks and the river bed behind the off-bank timber piling makes that the present (and future) cross sectional areas, as indicated in Figure 3.4, do not correspond with the actual 'field' situation. Moreover, measurement of the bed profile along the measurement transect of the fixed monitoring system, indicates that the river bed is mobile behind the off-bank timber piling (Figure 3.7).

Measurement of the bed profile was carried out with a gauge rod (measurement accuracy of $1 \cdot 10^{-3} \, \text{m}$) until 0.75 m from the off-bank timber piling. Closer to the timber piles, broken concrete slabs hindered an accurate sounding of the river bed. For this measured bed profile, a local cross sectional area of roughly $8 \, \text{m}^2$ is determined, instead of its theoretical triangular area of $1.3 \, \text{m}^2$ (surface areas are calculated for the regulated water level of 5.61 m TAW). Throughout the measured months, a 5-6 % enlarged cross sectional area was observed for this particular cross section, compared to the theoretical trapezoidal area of $144 \, \text{m}^2$ (Table 3.2).

However, since these measurements are carried out (i) locally and temporarily, and (ii) only along a part of the cross sectional profile, it is decided to use the theoretical trapezoidal cross sectional area of $144 \, \text{m}^2$ for theoretical calculations in this PhD-research.

■ The river bank

River bank samples, randomly taken in the bank-water contact zone, show a higher variability in sand and silt sediment mixture, having median grain sizes varying from $d_{50} = 29$ to $205 \, \mu\text{m}$. Cohesive clay material, i.e. $d < 3.9 \, \mu\text{m}$, is limited to maximum 7%. Soil textures are classified as 'silt loam', 'loamy sand', 'sandy loam' or 'sand'.
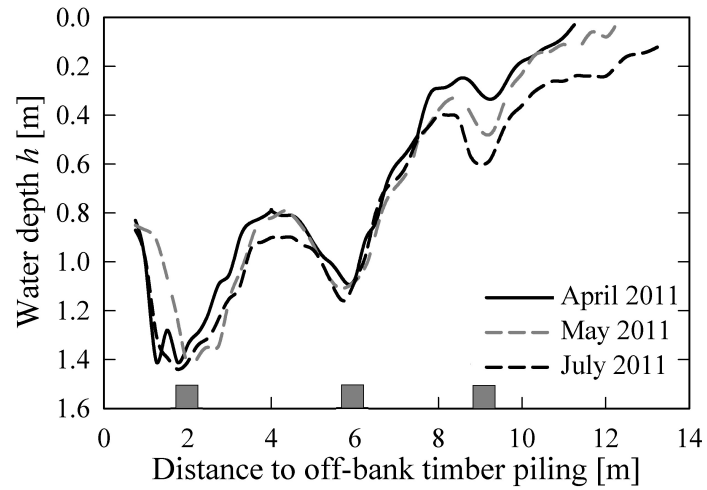
Figure 3.7: Bed profile along the measurement transect of the fixed monitoring system, measured with a gauge rod. The gray rectangles indicate the position of the monitoring system's supporting piles.

Table 3.2: Local and total cross sectional area for the measurement transect of the fixed monitoring system

| | Cross sectional area [m²] | |
	Local	Total
April 2011	7.43	151.83
May 2011	7.90	152.30
July 2011	8.90	153.30

■ **The water column**

Water samples are taken at various heights above the river bed in the shallow water area behind the off-bank timber piling (in a water depth $h = 0.8$ m) during steady flow conditions (on April 14, 2011 25 min after a ship passage). Given that a minimum laser obscuration of 10 % is necessary for particle size analysis with the Mastersizer 2000, water samples are depth-averaged. Particle size analysis of these depth-averaged samples indicates a median grain size $d_{50} = 13 \mu$m for the suspended sediments and classifies 86% of the suspended sediments as 'silt' ($2 \, \mu$m $< d < 62 \, \mu$m).

Table 3.3 gives the suspended sediment concentrations at the sampled heights. Despite the time lag with the hydrodynamic disturbace caused by a ship passage, an equilibrium Rouse-Vanoni concentration profile is not established; instead, the development of local suspension clouds is observed.

According to the Rouse number (equation 3.8), which dictates the mode of sediment transport, the average shear velocity $u_* = 3.3 \cdot 10^{-3}$ m s^{-1} (in steady flow conditions, cf Table 3.1) causes sediment particles with a diameter up to 44 μm to be fully transported as suspended load ($0.8 <$ Rouse $\# < 1.2$) while diameters up to 64 μm might partly be transported in suspension ($1.2 <$ Rouse $\# < 2.5$).

The particle size distributions of the water samples and the bed soil samples support this theoretical Rouse $\#$ classification. The lower boundary limit of the latter's particle size distribution is 50 μm, inferring that dislodged bank material having a smaller particle size than this, i.e the silt and clay fraction, can be advected downstream.

$$\text{Rouse} \, \# = \frac{w_s}{\kappa u_*} \tag{3.8}$$

where κ is Von Karman's constant, $\kappa = 0.4$; w_s is the particle settling velocity [m s^{-1}], calculated using Stokes' equation for the fall velocity of spherical particles with a $d \leq 100 \, \mu$m (Van Rijn (1993)):

$$w_s = \frac{\left(\frac{\rho_s}{\rho} - 1 \right) g d^2}{18 \nu} \tag{3.9}$$

where d is the median particle size diameter d_{50} [m].

It must be noted that natural sediment particles, as in this study, are non-spherical particles to which the abovementioned formula theoretically cannot be applied. However, since the shape effect of non-spherical particles becomes more important for particles having a $d > 300 \, \mu$m (advocated by Van Rijn (1993)), and the particles under study have a $d << 100 \, \mu$m, their terminal fall velocity is determined using the Stokes' equation.

Table 3.3: Suspended sediment concentrations sampled on various heights z above the river bed (water depth $h = 0.8\,\text{m}$). Water samples are taken 25 min after a ship passage on April 24, 2011.

Height z above the river bed [m]	Suspended sediment concentration $SSC(z,t)$ [$\text{g}\,\text{m}^{-3}$]
0.1	67
0.2	49
0.3	121
0.4	125
0.5	107

3.4 A large, fixed and a flexible, mobile monitoring system

3.4.1 Experimental setup

Neglecting the Kelvin's angle at which the cusp locus line of the secondary waves propagates, a perpendicular cross sectional structure was chosen for the measurement setup (Figure 3.8 and Figure 4.6). To hold the measurement infrastructure of the fixed monitoring system, cylindrical galvanised steel piles were opted for as the support frame. Anchored 2 m deep to withstand hydraulic uplift forces, design dimensions were further decided upon survival of an extreme water level rise with a return period of 10 years. This corresponds to a water level rise of 3.3 m above the regulated water level of 5.6 m TAW (return period analysis using the data records of HIC (1983-2012)).

A platform, installed across the off-bank timber piling, supports the securing of a laser distance meter (LD in Figure 3.8) and camera equipment (C in Figure 3.8), and provides extra space for additional devices. Another two steel piles hold the lateral extension of the platform, made of cylindrical galvanised steel tubes, so measurement equipment can be placed in a cross-shore array. The length of the lateral extension spans the shallow water area to the river bank. In this way, access to the platform is also assured. Devices are mounted on these tubes within a housing having adjustable brackets, allowing their easy repositioning (Figure 4.6). The entire monitoring system is powered using a solar panel (SP in Figure 3.8), which continuously feeds batteries to which all measurement equipment is connected. This provides permanent stand-alone data acquisition during summer time, throughout the winter period batteries (Yuasa, 72 Ah for 12 V) need to be additionally charged. Given these robust and flexible design conditions, the monitoring system is also ready-to-use in the post-upgrading waterway configuration (cf Figure 3.4).

A variety of physical processes related to ship-generated waves were taken along in the design of the fixed and mobile monitoring systems. Table 3.4 gives an
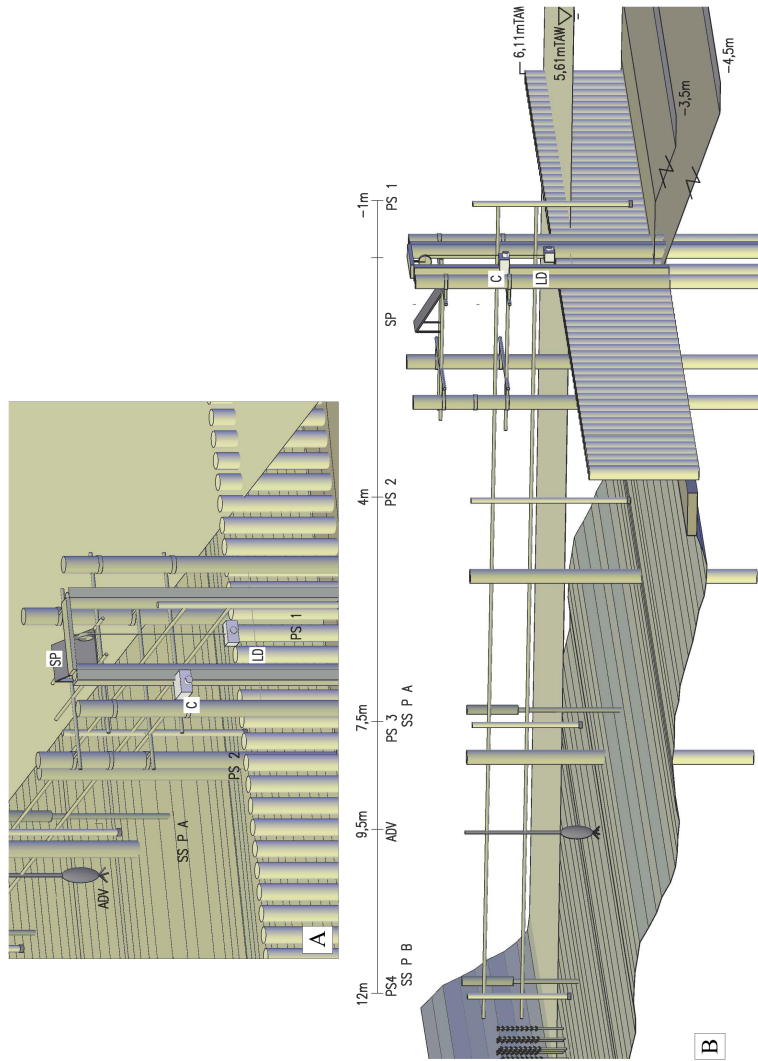
Figure 3.8: Definition sketch of the large, fixed monitoring system, with setup of the measurement equipment: A. Frontal view. B. Cross sectional view

overview of the monitored physical processes, together with the applied measurement equipment at a specific measurement location.

For the mobile monitoring system, designed for swift and easy-to-handle installation, a lighter, more modular method of mounting is chosen (Figure 3.9), which is made out of aluminium parts. The entire monitoring system is easily transportable and the buildup requires limited manpower and only a few hours work. It stays operational for about 6 months using 2 non-rechargeable Lithium D batteries, providing the highest energy capacity (19 Ah for 3.6 V). The mobile monitoring system deals only with the characteristics of wave-structure interaction with the off-bank timber piling. Its modular design is also usable once the waterway is converted to its narrow ECMT-Vb profile.

3.4.2 Measurement equipment

The eligibility criteria for the selection of measurement devices are: good reliability in harsh hydraulic conditions (even during flood events), possibility for stand-alone use and automatic triggering and economical power consumption.

To connect ship data of the lockhouse with measurement data of the fixed monitoring system, a Day and Night Outdoor **Camera** (Abus, Germany) is crosswise directed towards the fairway (C in Figure 3.8). When motion occurs in user-specified cells, the camera starts to record for an appointed period and footage is stored on a SD flash memory card. If the ship's name or the number of certificate of tonnage are registered, both data sources can be linked. Ship data queries are also used to doublecheck the actual number of ship passages along the measurement sites. This is, however, just a rough evaluation of detected ship passages because (small) pleasure cruising can bypass the lock using the meandering loop.

Four Druck PTX 1830 **pressure sensors** (GE Sensing & Inspection Technologies, Leicester, UK) are deployed in a cross-shore array on the fixed monitoring system (PS in Figure 3.8 and Figure 4.6). Pressure sensor 4 (PS 4) is located very close to the river bank, with the other gauges (PS 3 and PS 2) located sequentially further into the waterway, up to a distal point of 15 m from the river bank and 1 m before the off-bank timber piling (PS 1). Two Druck PDCR 1830 pressure sensors are deployed in the mobile monitoring system, one at each side of the timber piling, respectively 1 m in front of the off-bank timber piling (in the fairway) and 2 m behind the off-bank timber piling (Figure 3.9B).

The major difference between these two types of pressure sensors relates to the output signal and, in this specific application, to the method of pressure measurement. PTX 1830 has a venting tube connecting the rear side of the sensor membrane with the atmospheric air pressure, and thus measures relative pressure. The sensor consists of two parts: a transducer, converting the water pressure to an electrical tension and a transmitter, modulating the current of the power supply

Table 3.4: Selected measurement equipment and location for monitored physical processes with fixed and mobile monitoring systems.

Physical processes	Measurement equipment	Measurement location
Incident ship waves	Pressure sensor	In the fairway, before off-bank timber piling
Wave-structure interaction **	Pressure sensor	In the shallow water area, just behind off-bank timber piling
Ship wave refraction and reflection by bottom friction and bank proximity	Pressure sensor	In the shallow water area, at 2 distal points behind off-bank timber piling
Sediment (re)suspension *	Suspended solids profilers	In the shallow water area, at 2 distal points behind off-bank timber piling
Flow velocties and shear stresses *	Acoustic Doppler velocimeter	In the shallow water area
Ship sailing distance from the off-bank timber piling	Laser distance meter	At the off-bank timber piling
Ship sailing speed	Laser distance meter	At the off-bank timber piling

* Physical processes measured during specific measurement campaigns, not continuously
** Physical process also measured with the mobile monitoring system

Figure 3.9: Snapshots of the mobile monitoring system: A. Zoom on position of the monitoring system across the off-bank timber piling. B. Detail of pressure sensor. C. Detail of compact data acquisition unit.

from 4 to 20 mA. PDCR 1830 registers the absolute pressure, which is directly translated into a voltage signal. The PTX 1830 pressure sensors operate at a factory set measurement range from 0 to 1 bar, the PDCR sensors measure from 0 to 1.5 bar. Both types of pressure sensor have a six times permissible overpressure and the signal precision to linearity is specified to be $\pm 0.06\%$ of full-scale of the best straight line. All pressure sensors were laboratory calibrated via progressive stepwise hydraulic pressure generation with a pressure calibrator, determining scaling and offset parameters of each sensor. Output voltages at fixed pressures were recorded for 100 bursts and averaged.

Because ship waves at a specific location disturb local hydrodynamic conditions only within a small time window, it is irrelevant to consider the atmospheric pressure fluctuation in data records. Therefore, the use of PDCR pressure sensors is slightly preferred as they are more energy-efficient (1.8 mA vs. pressure dependent power consumption), require less electronics, and all equipment can be placed underwater. The current loop indeed makes the PTX 1830 pressure sensor less sensitive to disturbances but the distance between sensor and data acquisition of the mobile monitoring system can be kept significantly shorter and therefore, within acceptable limits.

The **laser distance meter** DLS-B 15 (Dimetix, Herisau, Switzerland) is mounted on the front side of the platform, perpendicular to the waterway's cross section (LD in Figure 3.8). The device is attached to a pulley with a spring damper system, which assures that a fixed height above the free water surface is kept during water level rise. In this way, a good contact with the reflection plate on the opposite river bank is established at all times, imperative for a proper distance measurement. The laser beam continuously measures the cross sectional width. When a ship passes, the measured distance is reduced to the spacing between the hull of the ship and the position of the laser distance meter, giving the ship's sailing distance from the off-bank timber piling. Indirectly, ship speed is derived combining the duration of ship passage with ship length data. These ship characteristics (ship dimensions, navigation direction, power, load) are obtained from the lockhouse at Sint-Baafs-Vijve, located 8 km upstream of the measurement site.

Two **suspended solids profilers** ASM-IV (Argus, Ritterhude, Germany) are deployed in the shallow water area (SSP in Figure 3.8 and Figure 4.6). The profiler is 2.4 m long and consists of a battery powered central unit in the head of the instrument and a 1.44 m long stainless steel rod with an active board of backscatter infrared laser sensors (850 nm), equally placed at 0.01 m distance of one another (Figure 4.6D). Both instruments are fixed onto a moveable lateral arm in order to have the possibility of measuring a suspended solids concentration profile in the water column on variable distances from the off-bank timber piling, taking into consideration a distance of five times the pile diameter to the supporting steel piles in order to avoid disturbed suspended solids patterns. The device detects sus-
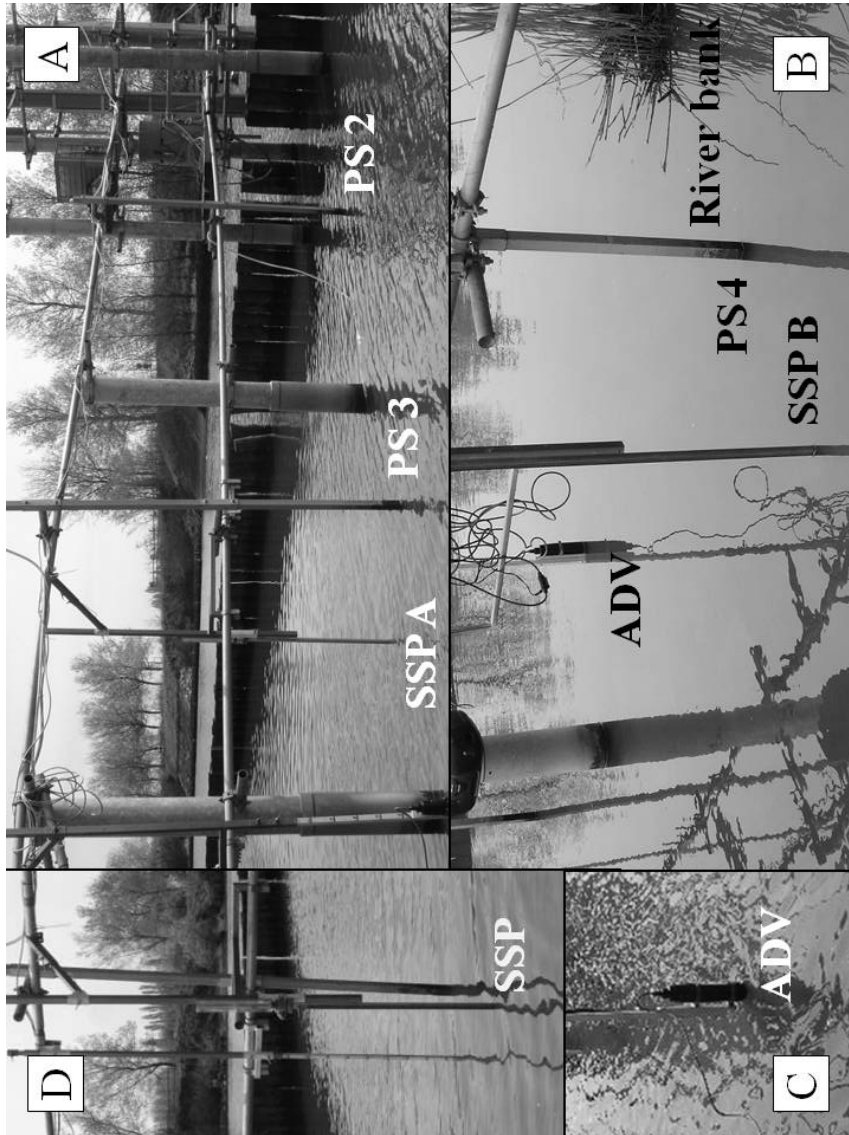
Figure 3.10: Snapshots of the fixed monitoring system: A. Zoom on measurement equipment behind the off-bank timber piling. B. Zoom on measurement equipment close to the river bank. C. Detail of acoustic Doppler velocimeter. D. Detail of suspended solids profiler

pended solids in the water column and records their reflections and the dynamic parameters at the user-defined (maximum) frequency of 1 Hz. At this sampling rate, the profiler's calibration is carried out using *in situ* water samples, taken manually or automatically by an ISCO sampler (Full-size portable sampler, Teledyne ISCO, Lincoln, USA) close to the profiler's location. By analysing these water samples on organic matter and suspended sediment content, the turbidity signal of the profiler can be fitted to a particular suspended sediment concentration, leading to a calibration curve for these specific hydro-environmental conditions. To prevent (bio)fouling, the suspended solids profilers are cleaned before every measurement day.

An **acoustic Doppler velocimeter** (ADV Vectrino, Nortek AS, Rud, Norway) is applied in the shallow water area simultaneously with the suspended solids profilers (ADV in Figure 3.8 and Figure 4.6). When a ship is approaching and passing the fixed monitoring system, flow velocities are recorded in 3-D with a frequency of 25 Hz. By doing so, the relative importance of the flow velocities perpendicular and parallel to the sailing direction is quantified. Positioning of the device near the bottom gives the possibility to calculate bottom shear stresses (Figure 4.6C).

3.4.3   Data acquisition

The continuously monitoring devices, i.e. camera, pressure sensors and laser distance meter, of the large, fixed monitoring system deliver an output signal that is transmitted through cables to locked storage boxes located on the river bank. The storage boxes contain the battery power supply and solar panel charger together with the data logger and camera screen.

The data logger has a signal conditioning unit where the current modulated signal of the relative PTX 1830 pressure sensors is converted to a voltage modulated signal, varying between 0.48 and 2.42 V. Applying sensor specific scaling and offset calibration values, voltage output is a linear function of the measured water pressure. Output from the pressure sensors is separately connected to an analogue low-pass filter to eliminate high-frequency noise. Subsequently, data acquisition hardware converts on-line the voltage signals of all channels into digital data, using a sampling frequency set to 10 Hz. After Analogue-to-Digital (A/D) conversion, the raw data is stored in binary format (which requires the least disk space) on a memory card located in the data logger. The A/D converter has a 12 bit resolution, resulting in 4096 bit levels for a 2 V range and a measurement accuracy of $0.3 \cdot 10^{-3}$ bar/bit (3.6 mm water column). The laser distance meter is connected by means of a digital serial output. Its raw data is simultaneously appended to the binary file containing the pressure time series. Off-line, the raw data is prepared for processing by reorganising it from a per time in a per channel structure. The signal processing and analysis methodology for pressure time series is described

in Section 4.3. Data from temporally applied measurement equipment is not stored in the data logger but handled immediately during these field campaigns.

For the mobile monitoring system, data acquisition and storage are assembled in a compact waterproof PVC housing which can be mounted underwater (Figure 3.9C). Water pressure variations are registered directly as voltage fluctuations such that only high-frequency noise elimination must be done using a low-pass filter subsequently. Conversion of the voltage signals to digital data is done using a sampling frequency set to 8 Hz. After A/D conversion, the raw data are also stored in binary format on a memory card. The mobile data logger has a largely improved resolution of 24 bit. Still, electrical noise inhibits the use of the full A/D conversion range because of the small signal. Practical measurement resolution is therefore limited to 16 bit, which results in $0.1 \cdot 10^{-3}$ bar (1 mm water column) being the smallest measureable pressure variation.

3.5 Conclusion

In order to account for the different controlling variables that influence ship-induced hydrodynamic forcing on the nature-friendly bank protection under study, an experimental field approach is chosen to evaluate its hydrodynamic performance.

To this end, 2 monitoring systems were developed and constructed. Both are applied in the most downstream part of the Lys. The Lys is a European standard scale ECMT-IV waterway, along which nature-friendly bank protections are recently installed to obviate progressive bank erosion (within the framework of the EU TEN-T project 'inland waterway Seine-Scheldt'). A speed limit of $V_s = 12 \, \text{km} \, \text{h}^{-1}$ is imposed on the waterway.

A large monitoring system was constructed at a fixed location. It accurately measures the magnitude of ship-induced hydrodynamic forcing on and the response of the nature-friendly bank protection. Therefore, a variety of physical processes related to ship-generated waves are taken along its design, a.o. incident ship-generated waves, wave-structure interaction with the off-bank timber piling, sediment supsension, ...

The hydro-environmental boundary conditions at this nature-friendly protected site indicate that, during steady (and normal) flow conditions, i.e. without shipping traffic, the Lys' flow velocity u_X is low. Associated bed shear stresses are lower than the critical bed shear stress $\tau_{cr} = 0.16 \, \text{N} \, \text{m}^{-2}$, which means that incipient motion of the river bed does not take place. Soil and water sample analysis revealed that (i) the river bed has a sandy top layer, (ii) the river bank in the bank-water contact zone has a higher variability in sand and silt sediment mixture, (iii) the water column contains a background silty suspended load with $d_{50} = 13 \mu$m, and (iv) silty particles ($d < 64 \, \mu$m) are (partly) transported in suspension and can be advected downstream given the river flow's shear velocity characteristics (based

on the Rouse #).

After the fixed monitoring system was installed in the field, the instrumentation was extended to develop a mobile monitoring system. This flexible monitoring system was applied at various locations to evaluate various configurations of off-bank timber piling on their wave-structure interaction.

4

Ship wave climate in a confined, non-tidal, nature-friendly protected waterway

4.1 Introduction

The ship wave climate in a waterway is dependent on its hydraulic boundary conditions (cf Section 3.2). Confined dimensions of a waterway enlarge the magnitude of the 'primary' ship wave pattern, which, in turn, depends on the ship's specific characteristics like dimensions, power, sailing speed, (laden) draught,…. Inland waterways and their hydraulic structures (e.g. locks) are therefore classified in terms of ship types (ECMT-classes), which are in this PhD-research used to categorize the results of ship-induced hydrodynamic forcing. Table 4.1 gives an overview of the ship properties for the relevant ECMT-classes on the Lys. Ships within each class do not differ distinctly in shape design; they are all of very full form so as to maximise carrying capacity at shallow draughts and to maintain low air draughts (Georgakaki and Sorensen, 2004).

In order to characterize the ship wave climate on the Lys, this chapter combines its input and output variables, and consists therefore of 2 main parts: the first part describes the characteristics of shipping traffic (input) (Section 4.2); the second part discusses the magnitude and behaviour of 'primary' and 'secondary' ship wave patterns in this confined, non-tidal and nature-friendly protected waterway (output) (Section 4.4 and 4.5). For the latter analysis, measurements of

ship-generated waves are used. The developed analysis methodology for these
wave measurements is described in Section 4.3.

To define the characteristics of shipping traffic on the Lys, ship data records are
obtained from the nearby lockhouse at Sint-Baafs-Vijve, except for (small) plea-
sure cruising that can bypass the lock. Additional ship characteristics are deduced
from these data or are measured using the fixed monitoring system. Table 4.2 gives
an overview of all ship characteristics used.

To determine the relative importance of both ship-generated wave patterns,
monitored data are used which were measured by the fixed and mobile monitoring
systems (as described in Section 3.4).

Table 4.1: Classification of inland waterways based on ship types (ECMT, 1992)

	Length L	Beam B	Design draught D_{design}	Tonnage
	[m]	[m]	[m]	[ton]
ECMT-I	38.5	5.05	1.8−2.2	250−400
ECMT-II	50−55	6.6	2.5	400−650
ECMT-III	67−80	8.2	2.5	650−1000
ECMT-IV	80−85	9.5	2.5−2.8	1000−1500
ECMT-Va	95−105	10.4−11.4	2.5−4.5	1500−3000
ECMT-Vb[*]	172−185	11.4	2.5−4.5	3200−6000

[*] in the (future) Lys: up to 4500 ton after the 1 m deepening of the trapezoidal
profile.

Table 4.2: Ship characteristic data

Ship data from lockhouse	Deduced ship characteristics	Measured ship characteristics
Locking time	Sailing speed V_s	Duration of ship passage
Ship dimensions	Limit speed V_l	Sailing distance to
Sailing direction	depth-based Froude-number Fr_d	off-bank timber piling y
Installed power	Displacement Δ	
Tonnage	ECMT-class	
Amount of cargo		

4.2   Characteristics of shipping traffic on the Lys

Ship data records from the lockhouse (from July 2009 to May 2011) give a broad
picture of the characteristics of the shipping traffic sailing on the downstream sec-
tion of the Lys ($N = 36037$: ($N_{tot} = 36251$) − ($N_{incomplete} = 216$)). 93.4% of
the ships, and hence, their ship-induced hydrodynamics, fit within the calibration
standards of this ECMT-IV waterway. After all, the traditional 'older' ships of
ECMT-0, I, II, III and IV are constructed concurrently with the inland waterways.
Nowadays, reduction of specific freight costs (and improved steerability (PIANC,
2008)) lead to an enlargement of the ship's dimensions, maximized to just match
the existing hydraulic infrastructure, i.e. ECMT-Va up to a ship length $L = 110$ m.
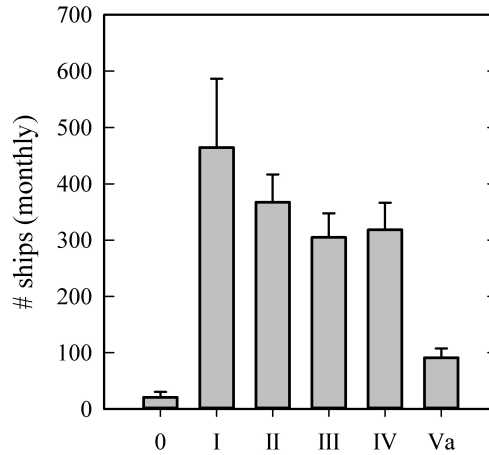
Figure 4.1: Composition of the average monthly shipping traffic which locks at Sint-Baafs-Vijve ($\pm$ 1 standard deviation (SD)), categorized by ECMT-class (based on data from W&Z (2009-2011)). ECMT-I lockings are the most frequent; the number of locked ECMT-II, III and IV ships is rather similar while ECMT-Va shipping traffic is clearly much less. ECMT-0 classifies all other ships having a length $L < 38$ m, e.g. passenger boats, push tugs,....

Navigation statistics show that the majority (89%) of shipping traffic consists of self-propelled ship types. Convoys occupy the second place (9.5%). Convoys include self-propelled ships pushing another one (85%) and push tugs or tow boats with a barge (15%); and have a maximum overall length equal to the maximum length of an ECMT-Va ship. The remainder of the shipping traffic (1.5%) includes service boats, pontoons and passenger boats. Only 1 locking of pleasure cruising was recorded, which underlines that, generally, pleasure cruising bypasses the lock.

On monthly average, 1567 ships lock at Sint-Baafs-Vijve (Figure 4.1). The most frequently recorded lockings are from ECMT-I shipping traffic, which includes 13% barges or pushed motor ships. ECMT-class II, III and IV ships comprise rather similar proportions whereas ECMT-Va ships correspond to just a few lockings a day. ECMT-class 0 classifies all other ships having a length $L < 38$ m, e.g. passenger boats, push tugs,....

The confined dimensions of the Lys make that the pressure and velocity distribution around a ship's hull are more pronounced, as a result of which a ship experiences an increased frictional resistance (cf Section 2.2). However, the effective width of the waterway influenced by a ship's long period 'primary' wave pattern and return current u_r, is restricted laterally. Its distance d_{LP} can be determined by $d_{LP} = \pi/2(L + 3B)$, which is valid for a trapezoidal cross sectional profile with an equal slope on both river bank sides (GBB, 2010). For the Lys,

this formula gives an approximate influence width ranging from 85 m to 247 m for a light draughted ECMT-I ship to a loaded ECMT-Va ship respectively. This indicates that shipping traffic of all ECMT-classes affects the entire cross sectional width of the Lys, except for a push tug or tow boat alone ($d_{LP} = 46$ m, and these have a small draught).

4.2.1   Ship's displacement Δ

Following Archimedes' buoyancy principle, the actual weight of a ship equals the weight of water displaced by its hull (SNAME, 1988a). The ship's volumetric displacement Δ [m^3], i.e. its underwater volume, is calculated as:

$$\Delta = C_B L B D \qquad (4.1)$$

where $C_B = 0.85$ is the block coefficient, L is the ship's length overall [m]; B is the ship's beam [m]; D is the ship's actual draught. Note that the ship's block coefficient depends on its loading condition; however, since inland shipping traffic has a full form, an average value of $C_B = 0.85$ is used (advocated by Georgakaki and Sorensen (2004)).

   Data records on the draught of a ship indicate the buoyant position of the ship at its design load line, i.e. the design draught (cf Table 4.1). The actual draught D of a ship however varies with its loading condition. To estimate a ship's actual draught D, use is made of information regarding inland navigation available in a report of the EU Artemis project (Georgakaki and Sorensen, 2004). It states that a light draughted ship rarely sails with a draught less than 0.4 times its design draught, in order to maintain adequate stability and good balance (Georgakaki and Sorensen, 2004). The varying draught D to variable loading conditions are calculated using a linear correlation (R^2=0.99) set up by the European Development Centre for Inland- and Coastal Navigation (Georgakaki and Sorensen, 2004):

$$\frac{deadweight}{deadweight_{\text{design}}} = 1.3377 \frac{D}{D_{\text{design}}} - 0.3421 \qquad (4.2)$$

where $deadweight$ is assumed to be equal to the ship's carrying cargo [ton], $deadweight_{\text{design}}$ to the ship's tonnage [ton] and D_{design} corresponds to the design draught [m]. Since deadweight tonnage is the 'gross' carrying capacity of a ship and tonnage its 'net' carrying capacity, some inaccuracy is involved in the use of this equation, leading to an underestimation of the draught.

   It is evident that the larger a ship's dimensions are, the larger its immersed volume and hence, water displacement become. Based on their weight, a one order of magnitude difference is already observed between ECMT-I and ECMT-Va shipping traffic, displacing 166 and 1183 m^3 respectively. This increase in underwater volume between the ECMT-classes results in an even more pronounced difference
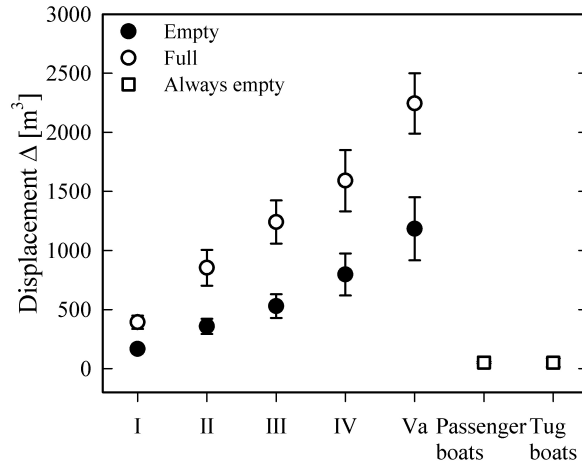
Figure 4.2: Average displacement Δ ($\pm$ 1 SD) of inland shipping traffic, categorized by ECMT-class and utilized carrying capacity (Full: utilized carrying capacity $> 80\%$) (calculated with the number of data records shown in Figure 4.3). The larger a ship's dimensions are, the larger its water displacement becomes.
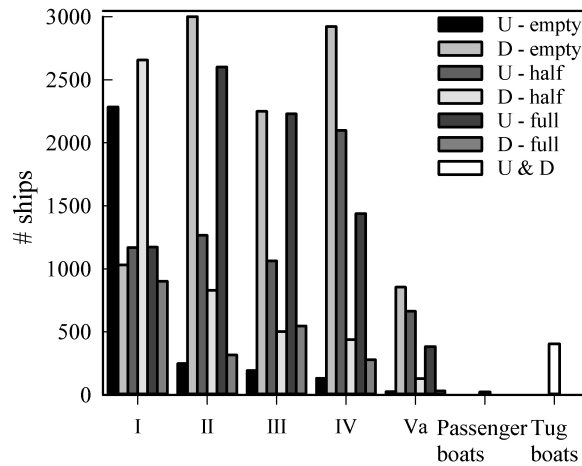
Figure 4.3: Composition of the shipping traffic on the Lys, from July 2009 to May 2011, in absolute numbers, categorized by ECMT-class. Upstream sailing generally indicates laden transport for ships of ECMT-II, III, IV and Va.

for (fully) loaded ships, where ECMT-Va ships occupy 5 times the volume of an ECMT-I ship (Figure 4.2). The displacement Δ of tug and passenger boats is negligible compared to the displaced volumes induced by goods traffic. Convoys mainly consist of two coupled ECMT-I ships, of which the overall displacement Δ equals the sum of both underwater volumes. Mean displacement Δ values are obtained using the number of data records of Figure 4.3.

Figure 4.3 illustrates the composition of the shipping traffic. Up- and downstream sailing reflects the main (un)loading direction on the Lys, i.e. 83% of the ships transports cargo upstream (U) whereas 60% does not transport cargo downstream (D). Upstream sailing corresponds to loaded transport for ECMT-II, III, IV and Va shipping traffic; of which the majority of ECMT-II and III ships utilizes its full carrying capacity (30% half vs 65% full (utilized carrying capacity $> 80\%$)). Draught restrictions result in capacity loss for ECMT-IV and Va ships, 60% sails half loaded and only 37% fully loaded. Remarkably, roughly 70% of the ECMT-II and III ships, and 80% of the ECMT-IV and Va ships sail empty downstream. ECMT-I ships sail equally with light or laden draught upstream while 80% carries cargo downstream. Only 20% is fully loaded (up- and downstream sailing). In 70% of the lockings, tug boats (N_{tug} = 405) were pushing or towing a barge. Passenger boats (N_{pas} = 23) are seldom locked.

Since the Lys' flow velocity is small (cf Section 3.3.1), no difference in magnitude of ship-induced hydrodynamic forcing is expected for up- or downstream sailing.

4.2.2 Ship's limit speed V_l

A speed restriction of $V_s = 12\,\mathrm{km\,h^{-1}}$ ($3.3\,\mathrm{m\,s^{-1}}$) applies to the Lys. Apart from this speed limit, a ship's sailing speed V_s is (theoretically) bounded by its limit speed V_l. It is calculated using equation 2.4, in which the average water depth of the Lys is used $h_m = \frac{A_w}{W_{SWL}} = 2.85\,\mathrm{m}$, and the critical depth-based Froude equation 2.5 is entered. Equation 2.5 includes also the Lys' dependent blockage coefficient m.

Important to note with these theoretical calculations is that they are determined using the calibrated values for the waterway's cross sectional area A_w and depth h. In reality, the actual water level is frequently higher at the location of the fixed monitoring system, and its cross sectional profile differs from the calibrated trapezoidal profile (see Section 3.3.2). Given the eroded condition of large stretches of the Lys' river banks, a deviant cross sectional area is expected to be found along its course. The more a particular cross section deviates from the calibrated profile, the higher (or lower) a ship's limit speed V_l will be. Consequently, the calculated values for ship-related variables, like the ship's limit speed V_l, are minimum values.
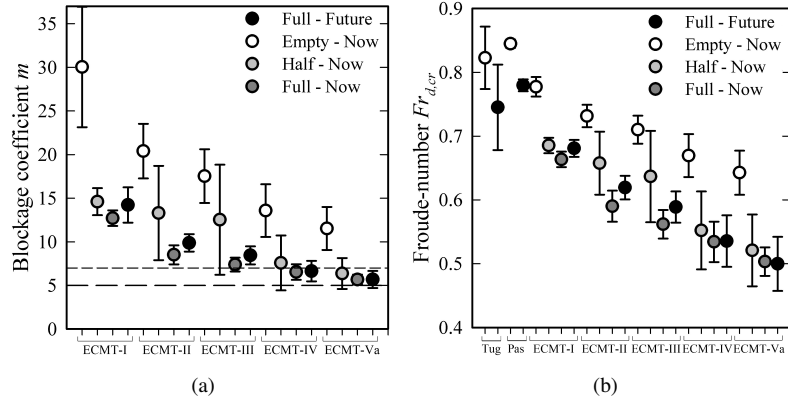
Figure 4.4: Parameters determining the ship's limit speed V_l, categorized by ECMT-class and utilized carrying capacity (Full: utilized carrying capacity $> 80\%$). (a) Average blockage coefficient m ($\pm$ 1 SD): the larger a ship's midship section, the lower its blockage coefficient. (Long and short dashed line indicate $m = 5$ and $m = 7$ respectively) (b) average critical Froude number $Fr_{d,cr}$ ($\pm$ 1 SD) reflects the blockage coefficient differences, within and between the ECMT-classes.
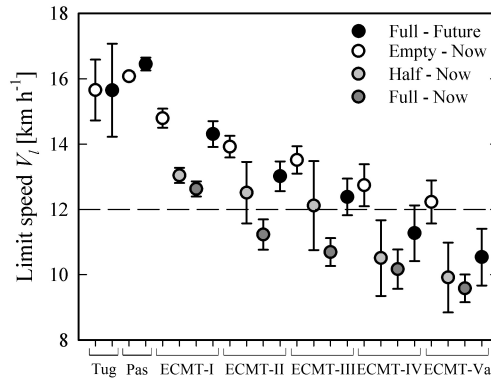
Figure 4.5: Average limit speed V_l ($\pm$ 1 SD) of shipping traffic in the Lys, categorized by ECMT-class and utilized carrying capacity (Full: utilized carrying capacity $> 80\%$). The speed limit $V_s = 12\,\mathrm{km\,h^{-1}}$ is indicated with a long dashed line. All light draughted ships are able to exceed the imposed speed limit while the limit speed is below for fully loaded ships as from ECMT-II.

The blockage coefficient m must ideally be higher than 7 (with lowest limit on 5) to minimize the sailing ship's resistance (De Rouck, 2008-2009). Figure 4.4(a) indicates the average blockage coefficient m, categorized by ECMT-class and utilized carrying capacity (only self-propelled ship types are taken into account). Squat is not taken into account in the blockage coefficient's determination. Passenger and tug boats are not displayed, their blockage coefficients equal 57 and 61 respectively. ECMT-IV and Va ships experience an increased resistance when carrying cargo; fully loaded ECMT-III ships sometimes. Comparison of the actual and future blockage coefficients for (full) laden draught indicates an increased blockage coefficient because of the enlarged waterway cross section. No significant difference for fully loaded ECMT-IV and Va ships is however observed.

In the current data set, only 18 ship records had an actual draught D of more than 3 m (using equation 4.2) while 4574 ships had a design draught D_{design} exceeding 3 m. For the future situation, calculations are based on this design draught D_{design}, taking into account the draught restriction of 3.5 m. This restriction had to be applied for 1104 ship records, indicating 18 unique ECMT-IV ships and 66 ECMT-Va ships which will not be able to sail fully loaded on the Lys.

From July 2009 to May 2011, 1.6% of the locked ships sailed with a blockage coefficient $m < 5$, indicating that, generally, a captain tried to avoid these very confined conditions in order to be able to sail with considerable speed. In the future waterway layout, 4.6% of the fully loaded shipping traffic will have a blockage coefficient $m < 5$. Frictional resistance might be further increased when a sailing ship has no over depth of 30-40% to its draught (De Rouck, 2008-2009). For the Lys, this holds when 1.2 m water depth is maintained under the keel, which is not the case for fully loaded shipping traffic of all ECMT-classes and for half loaded ships as from ECMT-class IV.

Critical depth-based Froude numbers $Fr_{d,cr}$ reflect the blockage coefficient differences, ranging from $Fr_{d,cr} = 0.64$ to 0.77 for empty ECMT-Va to I ships and from $Fr_{d,cr} = 0.50$ to 0.66 for fully loaded ECMT-Va to I ships respectively.

The limit speed V_l is well below the imposed speed limit for fully loaded shipping traffic as from ECMT-class II whereas light draughted ships of all ECMT-classes are able to exceed this limit (Figure 4.5). The limit speed V_l ranges from $V_l = 12.2\,\text{km}\,\text{h}^{-1}$ (ECMT-Va) to $14.8\,\text{km}\,\text{h}^{-1}$ (ECMT-I) for light draughted shipping traffic, and from $V_l = 9.6\,\text{km}\,\text{h}^{-1}$ (ECMT-Va) to $12.6\,\text{km}\,\text{h}^{-1}$ (ECMT-I) for fully loaded shipping traffic. Tug boats and passenger boats are able to sail at somewhat higher limit speeds than light draughted shipping traffic.

In the future situation, only fully loaded ECMT-IV and Va will not be able to sail beyond this speed limit. This limit speed V_l will be somewhat reduced when the frictional resistance of the long period 'primary' wave pattern on river bed and bank leads to a stern or bow heavy trim.

4.3 Analysis methodology of the ship characteristic pressure time series

By analogy with the generally adopted method for (wind) wave analysis, signal analysis of ship waves is handled by combining processing steps in the time and frequency domain. Various ways of implementing this methodology on ship waves are however found in literature. A classification can be made between methods interpreting the ship wave pattern in itself (e.g. Chwang and Chen (2003); Hofmann et al. (2008)) and methods separating the ship wave pattern into the 'primary' and 'secondary' wave pattern (e.g. Teschke et al. (2008); Verney et al. (2007)). Since one of the objectives is to estimate the magnitude and behaviour of every ship wave pattern individually, a method in accordance with the latter approach is opted for (see research question 1 in Section 1.2).

Pressure data (pre-)processing and analysis are carried out using a self-designed routine, implemented in Labview (National Instruments), which is partly based on the established in-house knowledge about wind waves. The data processing consists of the sequential execution of following steps: 1. a ship wave event is detected and selected in the pressure time series; 2. correction and filtering of the signal takes place in the frequency domain; 3. the ship wave parameters are determined after transformation of the pressure time series to a water elevation time series.

4.3.1 Identification and selection of a ship event

In the raw pressure time series, a minimum water level fluctuation of 0.06 m and an interval time of 100 s between two pressure peaks are set as conditions to be met upon selection as a ship wave event (Figure 4.6A). Furthermore, this peak detection algorithm is carried out on the reverse pressure time series in order to minimize multiple selection of the same ship event (avoidance of both drawdown and stern wave detection). The amplitude of the peak, i.e. the maximum drawdown Δh_{max}, and the location of the peak, i.e. the occurrence time of the maximum drawdown $t_{\Delta h_{max}}$, are both identified and collected in the ship event data base.

The cutoff length for an isolated ship wave event includes the pressure time series from 120 s (2 min) before the occurrence time of the maximum drawdown $t_{\Delta h_{max}}$ until 600 s (10 min) after (Figure 4.6B). Shipping traffic is however dense on the Lys, and regularly ships follow or cross each other closely with little clearance. This hampers the correct selection and cutoff of an identified ship wave event in two ways. On the one hand, the determined criteria of the peak detection algorithm occasionally result in the non-separation of two ships following or crossing each other more closely than the interval criterion of 100 s. They are treated as one ship event. On the other hand, dense shipping traffic results in the interference of several ships' wave patterns. An identified ship wave event may consist of the su-

perposition of various wave signals, which leads to a misrepresentation of a single ship's hydrodynamics. The latter problem is tackled by dynamically adapting the cutoff length of a particular ship event i, based on the time interval between this event and both the preceding $i-1$ and next $i+1$ ship events. Table 4.3 shows the decision matrix for the cutoff length.

4.3.2   Filtering of the 'primary' and 'secondary' ship wave patterns out of the selected ship event

The pressure time series of a selected ship event is detrended by subtracting the average hourly water pressure. It then consists of pressure fluctuations due to wind- and ship-generated waves. Their contribution can be separated out because wind- and ship-generated waves are characterised by different wave periods, i.e. a wave period below and above 2 s respectively (in confined waterways). In addition, ship wave energy occurs in bimodal peaks (for displacement ships). The ship's 'primary' wave pattern, which has generally a long period, and its 'secondary' wave pattern, which has a shorter period, are distinguished from one another by their difference in wave period. The 'primary' long period wave pattern is filtered out on the condition of a period $T_{LP} \geq 10$ s. The 'secondary' shorter period wave pattern is situated in the interval ($2\,\text{s} < T_{SP} < 10\,\text{s}$) between the 'primary' wave pattern and the wind-generated waves.

As separation is carried out based on distinct wave periods, and hence, wave frequencies ($f = 1/T$), a fast Fourier transform with a 10 % cosine tapered window is applied to convert the pressure time series into the frequency domain. After correction of the pressure signal for depth attenuation using linear wave theory (based on Ellis et al. (2006)), band pass filters are used to separate out the 2 ship wave patterns. A low pass filter (frequency $f < 0.1$ Hz) preserves the long period 'primary' wave pattern; a band pass filter between $0.1 < f < 0.5$ Hz determines the short period 'secondary' waves. Subsequently, an inverse Fourier transform converts both the frequency series back to the time domain. A water elevation time series is now obtained for both wave patterns (Figure 4.6C and D).

4.3.3   Determination of the characteristic wave parameters of the 'primary' and 'secondary' ship wave pattern

Figure 4.7 indicates the characteristic wave parameters for both ship wave patterns, which are obtained using the zero downcrossing method. For every ship wave pattern, the wave height and wave period are computed for all two consecutive zero downcrossings within the ship event. A sorting routine selects the largest wave height and its wave period out of all the zero-downcrossing intervals. This results in the transversal stern wave H_{stern} and the 'primary' wave period T_{LP}, and the maximum 'secondary' wave height $H_{SP,max}$ and its wave period $T_{SP,max}$.
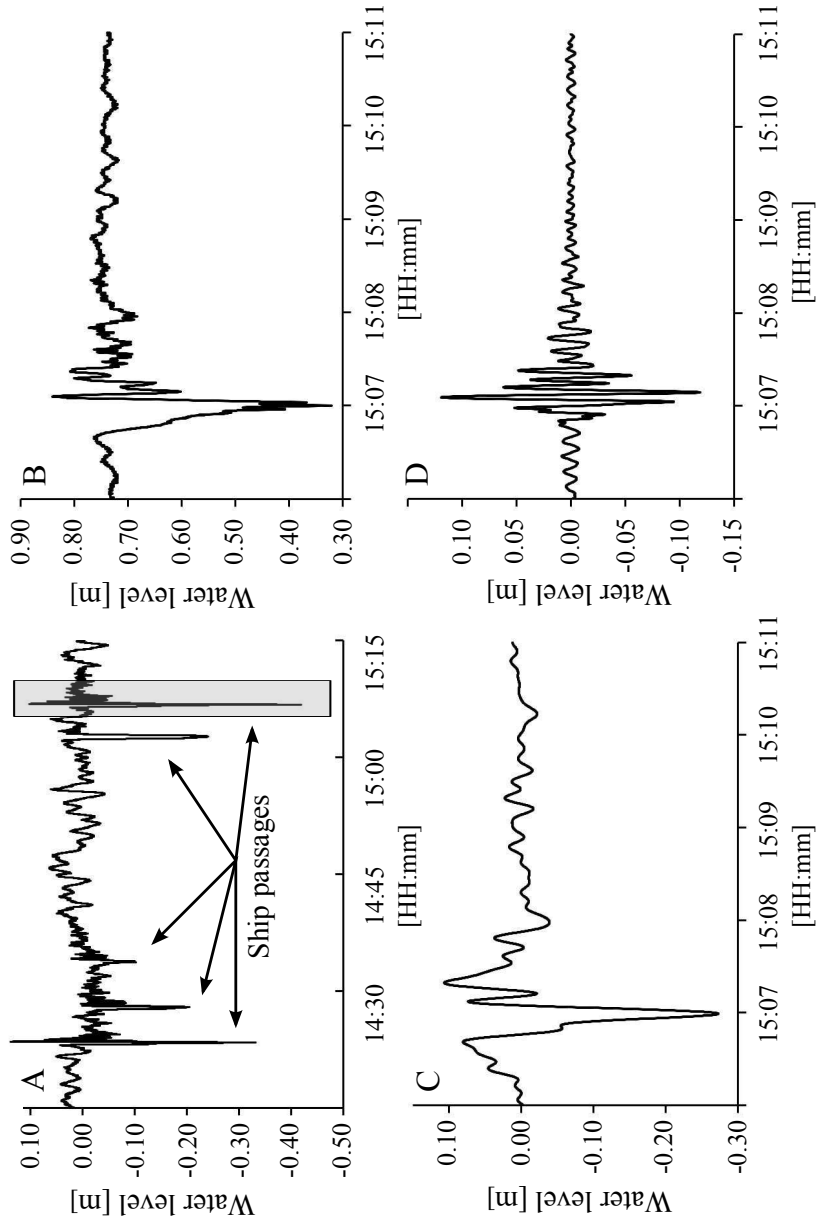
Figure 4.6: Example of the analysis methodology for ship wave events A. Hourly time series of water level fluctuations, with indication of 5 ship passages; B. Zoom on one selected (isolated) ship event; C. Filtered out long period 'primary' wave pattern; D. Filtered out short period 'secondary' wave pattern

Table 4.3: Decision matrix on the cutoff length of a ship event i, based on the time interval between this event and the preceding $i-1$ and next $i+1$ ship events

event t_{i-1} / event t_{i+1}	$t_{i-1} < 180$ s		180 s $< t_{i-1} < 600$ s		$t_{i-1} > 600$ s	
	begin	end	begin	end	begin	end
$t_{i+1} < 180$ s	$t_{\Delta h_{max,i}} - 45$ s	$t_{\Delta h_{max,i+1}} - 45$ s	$t_{\Delta h_{max,i}} - 60$ s	$t_{\Delta h_{max,i+1}} - 45$ s	$t_{\Delta h_{max,i}} - 120$ s	$t_{\Delta h_{max,i+1}} - 45$ s
180 s $< t_{i+1} < 600$ s	$t_{\Delta h_{max,i}} - 45$ s	$t_{\Delta h_{max,i+1}} - 60$ s	$t_{\Delta h_{max,i}} - 60$ s	$t_{\Delta h_{max,i+1}} - 60$ s	$t_{\Delta h_{max,i}} - 120$ s	$t_{\Delta h_{max,i+1}} - 60$ s
$t_{i+1} > 600$ s	$t_{\Delta h_{max,i}} - 45$ s	$t_{\Delta h_{max,i}} + 600$ s	$t_{\Delta h_{max,i}} - 60$ s	$t_{\Delta h_{max,i}} + 600$ s	$t_{\Delta h_{max,i}} - 120$ s	$t_{\Delta h_{max,i}} + 600$ s
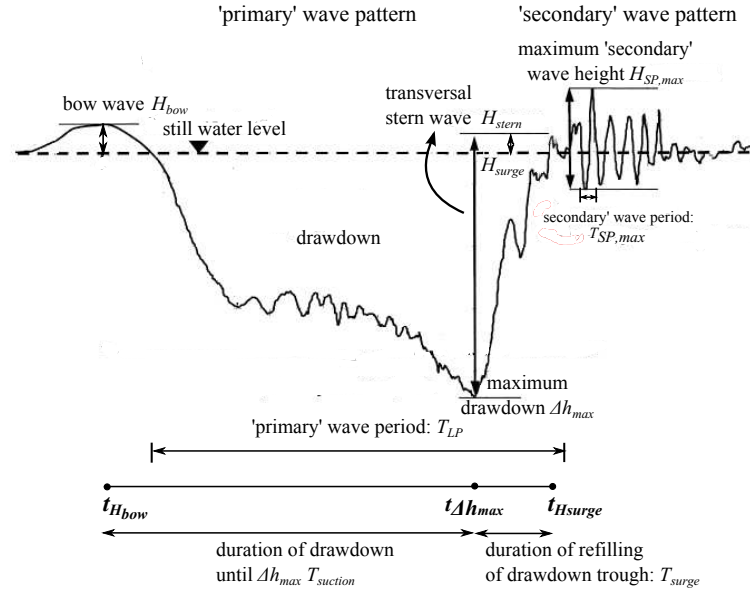
Figure 4.7: Characteristic wave parameters of the 'primary' and 'secondary' wave pattern, determined from the water elevation time series. Illustration of these ship wave patterns for a heavy trimmed displacement ship.

For the 'primary' wave pattern, following additional parameters are determined: the bow wave H_{bow} (and its occurrence time $t_{H_{bow}}$); the maximum water level rise after the maximum drawdown occurred H_{surge}; the drawdown duration until the maximum drawdown Δh_{max} is reached: $T_{suction} = [t_{H_{bow}}; t_{\Delta h_{max}}]$; the duration of refilling of the maximum drawdown: $T_{surge} = [t_{\Delta h_{max}}; t_{H_{surge}}]$.

4.4 Ship wave-structure interaction and (confined) shallow water behaviour

Ship wave-structure interaction and shallow water behaviour are discussed for a week-long subsample of the monitored data, from May 24-31, 2011. During this measurement period, settled weather conditions prevailed, resulting in a freeboard of 0.50 m between the top of the off-bank timber piling and the still water level at the location of the fixed monitoring system.

330 ship passages were monitored with adequate completeness and quality to be analysed. 9 ship events corresponded to pleasure cruising while 216 different displacement ships were recorded. Thereof, 72 ships crossed the measurement transect multiple times. Up- and downstream sailing were in balance, of which the majority of upstream shipping traffic carried cargo (and vice versa). Table

4.4 gives an overview of the monitored shipping traffic. As is to be expected, since the Lys has a very small flow velocity (cf Section 3.3.1), no differences in magnitude of the ship-generated wave patterns were found between up- and downstream sailing. Both sailing directions are therefore merged in the result interpretation, where ECMT-class and utilized carrying capacity are applied as principal categorical variables. Note that the small number of ship events in some categories (e.g. fully loaded ECMT-Va) might slightly bias the results.

A fourth of the ship passages are isolated ship events, which have a measured ship wave signature of 720 s (12 min). Another fourth of the ship passages is characterized by a wave event duration of less than 350 s (5.8 min). This indicates that, especially during daylight hours, shipping traffic is dense.

ECMT-I, II and III ships each occupied 20% of the monitored ship events, of which 8 ECMT-I ship passages consisted of 2 coupled ships. 26 % and 11 % of the monitored records corresponded to ECMT-IV and Va respectively. Pleasure cruising accounted for the remaining 3 %. The number of ECMT-II, III and IV ship passages match comparatively well with the overall monthly navigation statistics (Figure 4.1), whereas relatively less ECMT-I and more ECMT-Va ships sailed along.

Table 4.4: Monitored up- and downstream shipping traffic over the measurement period May 24-31, 2011, categorized by ECMT-class and utilized carrying capacity (Full: utilized carrying capacity > 80%)

	Carrying cargo?	# ships	ECMT-I	ECMT-II	ECMT-III	ECMT-IV	ECMT-Va
	Empty	15	13	0	2	0	0
UP	Half	68	8	11	12	25	12
	Full	88	12	27	24	22	3
	Empty	100	5	26	24	30	15
DOWN	Half	26	13	4	3	5	1
	Full	24	8	3	8	4	1
	Total	U: 171 - D: 150	59	71	73	86	32

Although the limit speed V_l decreases with increasing ECMT-class (Figure 4.5), a difference in sailing speed V_s between the ECMT-classes is less clearly observed. Average sailing speeds, which depend on the utilized carrying capacity, are comparable; and sailing speeds range from $V_s = 6.5\text{-}7 \, \text{km} \, \text{h}^{-1}$ to $15.5 \, \text{km} \, \text{h}^{-1}$ ($14 \, \text{km} \, \text{h}^{-1}$ for ECMT-class Va) (Figure 4.9).

One-third of the passing ships exceeded the speed limit of $V_s = 12 \, \text{km} \, \text{h}^{-1}$, irrespective of ECMT-class. Generally, light draughted ships always sail above the speed limit while cargo carrying ships only occasionally exceed this threshold (fully loaded ships never do, except for a single ECMT-I ship passage). Captains tend to sail very close to their ship's limit speed, which is always above the imposed speed limit for unladen ships.

The limit speed V_l can only be overtopped unsteadily if a ship separates from its own bow wave system. The higher a ship's ECMT-class, the more frequent the ship exceeds its limit speed (Figure 4.9 and 4.8). 30% of the ECMT-Va ships
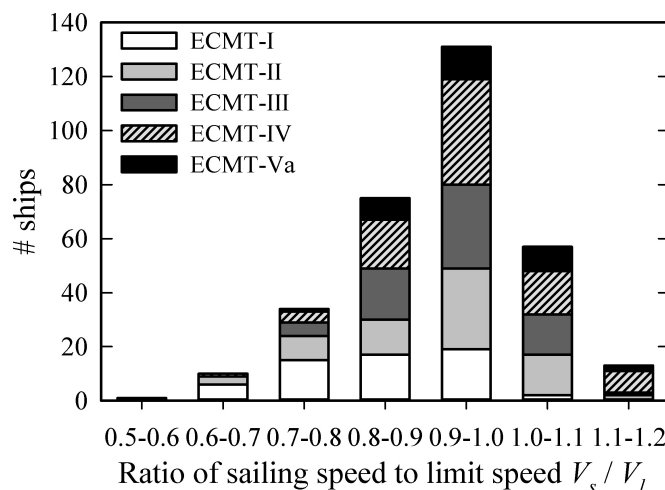
Figure 4.8: Number of ships, categorized by ECMT-class, that sails at a specific ratio of sailing speed to limit speed V_s/V_l, i.e. the relative ship speed. The higher a ship's ECMT-class, the more frequent it exceeds its limit speed. 67 ships, which are all light draughted, sailed at a ratio $V_s/V_l \geq 1$

sails above their limit speed while only 4% of the ECMT-I ships surpasses it. To cross its limit speed, a ship needs a large engine power, which is standard in larger, modern motor ships but restricted in smaller, traditional ships. This is reflected in the ratio of sailing speed to limit speed V_s/V_l, i.e. the relative ship speed, which increases from an average $V_s/V_l = 0.83$ for ECMT-I to $V_s/V_l = 0.96$ for ECMT-Va. In total, 67 ships, which are all light draughted, sailed at a ratio $V_s/V_l \geq 1$.

Ships mainly sail in the middle of the waterway, which implies that, on average, ships sail at a distance of 15 m (ECMT-Va) to 17.8 m (ECMT-I) from the off-bank timber piling (distance to ship's hull). Within the ECMT-classes, a ratio of 65 to 35% for centric to eccentric sailing was found for this monitoring period, except for ECMT-class III which has a ratio of 80 to 20%. Deviation of centric sailing generally occurred when ships had to cross each other. A minimum distance of 9 m to the off-bank timber piling was always kept, while the maximum distance was 20-25 m. Small differences in sailing speed with increasing distance to the off-bank timber piling reflect the principal (un)loading direction on the Lys (cf Table 4.4), and hence, sailing speed might be higher further away from the off-bank timber piling. However, the ratio of sailing speed to limit speed V_s/V_l shows no correlation with ship eccentricity.

Ship hydrodynamics are registered with 4 pressure sensors (PS), crosswise installed at various distances from the off-bank timber piling (Figure 3.8). Table 4.5 shows their layout for this monitoring period. The very shallow water conditions
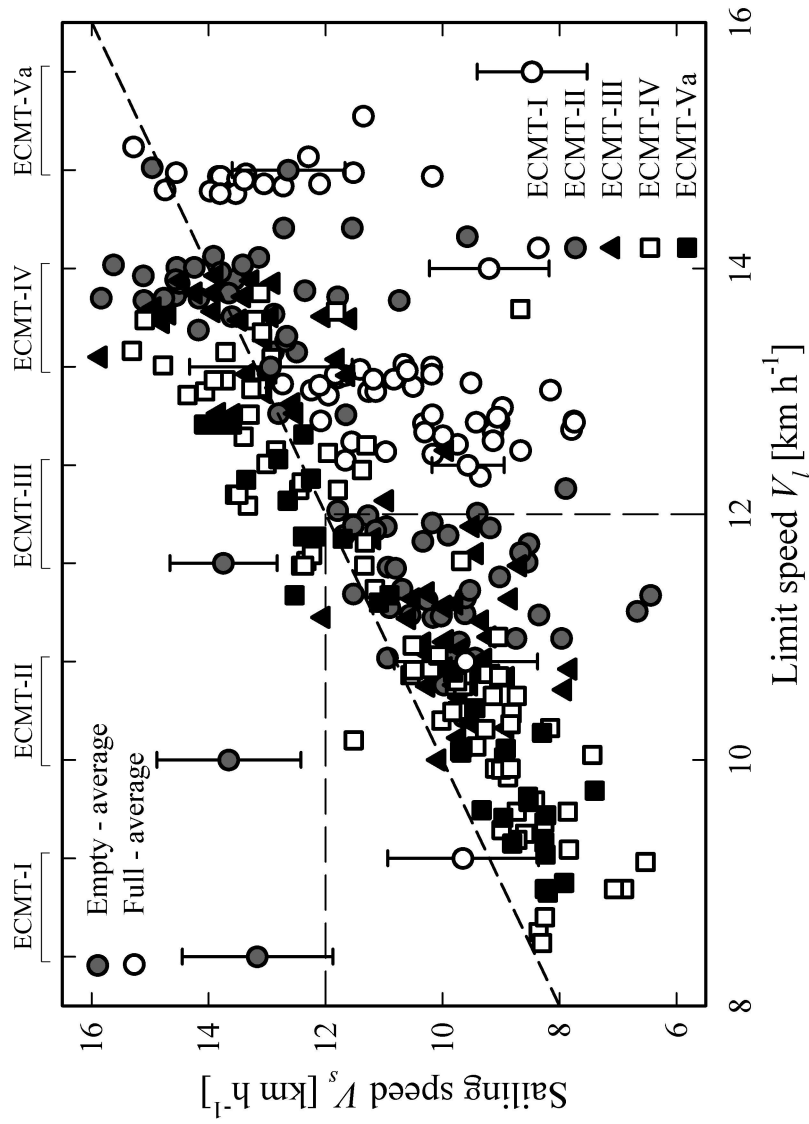
Figure 4.9: Ship's sailing speed V_s in relation to its limit speed V_l, categorized by ECMT-class. The average sailing speeds ($\pm$ 1 SD), which depend on utilized carrying capacity, are quite comparable between the ECMT-classes. The speed limit $V_s = 12\,\text{km}\,\text{h}^{-1}$ is indicated with a long dashed black line; one-third of the passing ships exceeded this threshold.

at pressure sensor 4 (PS 4), located at a distance of 2 m from the river bank, resulted in a frequent surfacing of the sensor, i.e. whenever the drawdown of a ship exceeded 0.09 m. This takes place during 270 ship passages (85 %), and as such pressure sensor 4 was left out for the result interpretation.

Table 4.5: Location and position of the pressure sensors for the measurement period of May 24-31, 2011.

	Distance to timber piling [m]	Water depth [m]	Height above river bed [m]
PS 1	-1.0	2.85	2.08
PS 2	4.0	1.00	0.20
PS 3	7.5	0.67	0.28
PS 4	12.0	0.24	0.15

### 4.4.1 Long period 'primary' wave pattern

The long period 'primary' wave pattern, and associated currents below and beside the ship, alter with increasing sailing speed V_s, and hence, with a changing ratio of sailing speed to limit speed V_s/V_l. This key parameter, indicating the transition from a sub- to supercritical return current u_r ($V_s/V_l < 1 \rightarrow V_s/V_l \geq 1$) (cf Section 2.2), is therefore used as explanatory variable.

In what follows, the characteristic wave parameters of the 'primary' wave pattern are discussed, which are normative for the 'primary' wave-induced forcing on the nature-friendly bank protection, the river bed and the river bank. The height of the bow wave H_{bow} is less pronounced than the transversal stern wave H_{stern}. On that account, the bow wave H_{bow} is not considered.

■ **The maximum drawdown** Δh_{max}

The drawdown effect is directly related to the ship's underwater volume and corresponding water volume that needs to be displaced. The drawdown Δh is thus expected to increase with increasing ECMT-class (Figure 4.10). This holds for light draughted shipping traffic, where the average maximum drawdown equals $\Delta h_{max} = 0.07$ to 0.26 m for ECMT-I to IV and Va ships. (Fully) loaded shipping traffic however shows that the buildup of the drawdown trough is also dependent on the ship's sailing speed V_s. Except for ECMT-I ships, which have a (smaller) average maximum drawdown of $\Delta h_{max} = 0.09$ m, the differences in maximum drawdown are very small between the ECMT-classes. An average maximum drawdown of $\Delta h_{max} = 0.17$ m was measured for cargo carrying ships as from ECMT-class II. Large maximum drawdowns $\Delta h_{max} \geq 0.3$ m regularly occurred for ECMT-IV shipping traffic (and occasionally for ECMT-II, III and Va).

When a ship approaches its limit speed V_l, a strong increase in maximum drawdown Δh_{max} takes place (Figure 4.11). The lower a ship's blockage coefficient
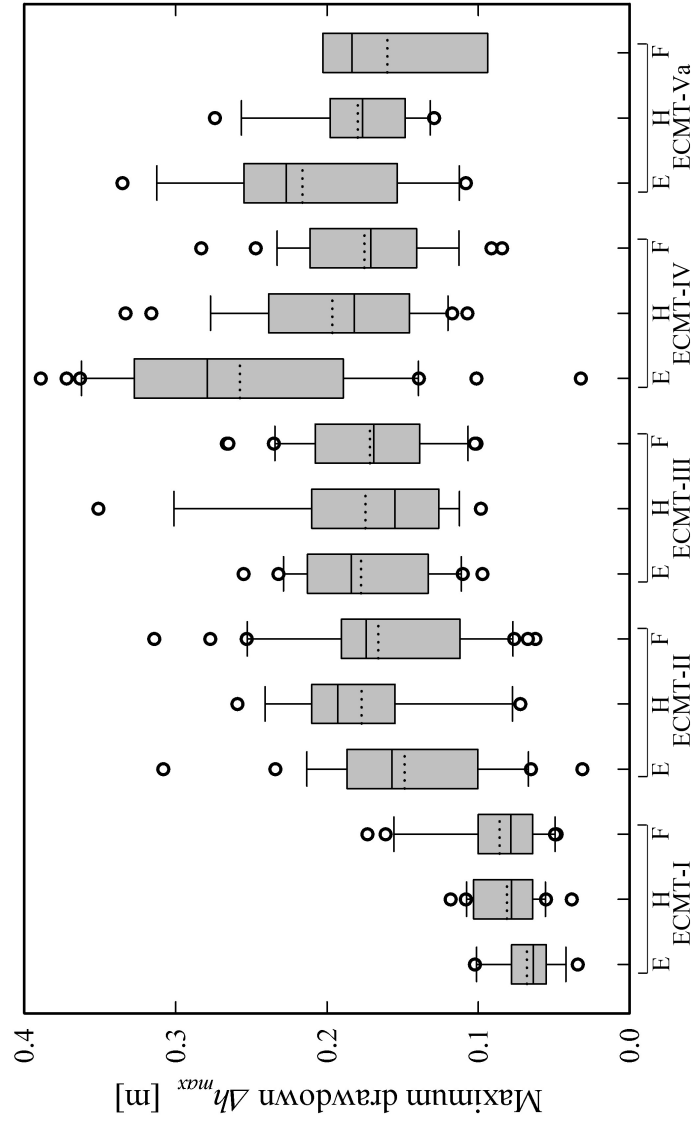
Figure 4.10: Boxplot of the maximum drawdown Δh_{max}, categorized by ECMT-class and utilized carrying capacity (E: Empty, H: Half, F: Full: > 80%) (at PS 1). For light draughted shipping traffic, the maximum drawdown increases with increasing ECMT-class. Cargo carrying ships as from ECMT-II cause a similar maximum drawdown, what indicates that its magnitude is not only dependent on the ship's underwater volume, but also on its sailing speed. Large maximum drawdowns $\Delta h_{max} \geq 0.3$ m regularly occurred for ECMT-IV shipping traffic. Besides the median (full line), a dotted line indicates the mean for every category. The category Full of ECMT-class Va has only 4 ship events, no 10th and 90th percentiles can be calculated.

m, roughly reflected by its higher ECMT-class, the higher the increase in maximum drawdown. For example, an ECMT-IV ship sailing at ratio $V_s/V_l = 0.8$ has a maximum drawdown $\Delta h_{max} = 0.13$ m, while sailing at $V_s/V_l = 1$ increases the maximum drawdown to about $\Delta h_{max} = 0.33$ m, or to 250 %! Displacement flows are maximal when sailing occurs close to the limit speed ($V_s/V_l = 1$), and increase with increasing ship beam B and draught D.

The drawdown Δh generally decreases with increasing distance from the ship. Given the Lys' confined dimensions, the entire cross sectional area is however affected by the 'primary' wave pattern (cf Section 4.2). This implies that (i) within every ECMT-class, no difference in maximum drawdown Δh_{max} is observed (at PS 1) for increased sailing distance to the off-bank timber piling y, and (ii) no difference in maximum drawdown Δh_{max} (or occurrence time $t_{\Delta h_{max}}$) is found over the measurement transect (from PS 1 to PS 3). Note that, statistically, there is a significant difference between the maximum drawdowns Δh_{max} at PS 1 and PS 3 for ECMT-I to III (paired t-test, 95% confidence level). This difference amounts however to a very small decrease from PS 1 to PS 3 of about 0.015 m. The magnitude of the drawdown trough is thus preserved on the condition that the water level is sufficiently high.

Taking into account the local topography of the bed profile (cf Figure 3.7), this results very often in the surfacing of a part of the river bed behind the off-bank timber piling (close to the river bank). During 85 % of the ship events, at least, 2 m of the river bed surfaces, and 4 ship events even caused surfacing of the river bed up to 4 m from the river bank (one-third of the width of the shallow water area).

To reach the maximum drawdown Δh_{max}, it takes for the majority of the ships almost the duration of their passage along the measurement transect, which indicates that ships are generally stern heavy trimmed (Figure 4.12(a)). For ECMT-I, the maximum drawdown Δh_{max} always occurred when the ship's stern passed the measurement transect. For the other ECMT-classes, the maximum drawdown Δh_{max} took place after two-third of the ship crossed it (98 % for ECMT-II and III - 80 % for ECMT-IV and Va).

Drawdown velocity is calculated by dividing the maximum drawdown Δh_{max} (Figure 4.10) by the time it takes to reach the maximum drawdown $T_{suction}$ (Figure 4.12(a)). Average drawdown velocities are similar for all ECMT-classes, and range from $0.2 \cdot 10^{-2}$ to $1.5 \cdot 10^{-2}$ m s^{-1} (except for ECMT-I: up to $0.9 \cdot 10^{-2}$ m s^{-1}). Figure 4.12(b) shows however that drawdown velocity rapidly increases with increasing ratio of sailing speed to limit speed V_s/V_l. Since the largest maximum drawdowns for $V_s/V_l \geq 1$ occur within ECMT-classes IV and Va (cf Figure 4.11), a similar drawdown velocity for e.g. an ECMT-II or ECMT-IV ship passage induces the highest impact on river bed and bank for the latter ship event (e.g. high shear stresses).
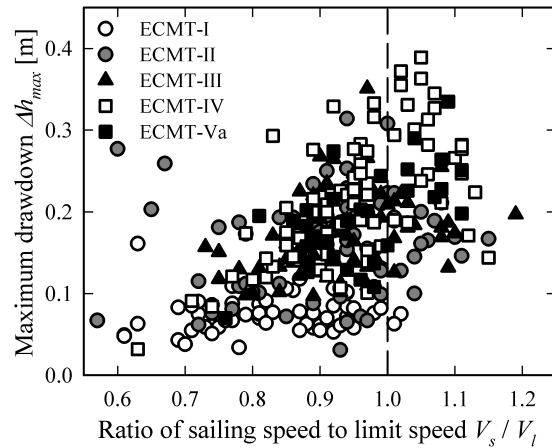
Figure 4.11: The maximum drawdown Δh_{max} in relation to the ratio of sailing speed to limit speed V_s/V_l, categorized by ECMT-class. When a ship approaches (and exceeds) its limit speed V_l ($V_s/V_l \geq 1$), a strong increase in maximum drawdown takes place. The lower a ship's blockage coefficient m, roughly reflected by its ECMT-classification, the higher the increase in drawdown trough. (A dashed line indicates the ratio $V_s/V_l = 1$).
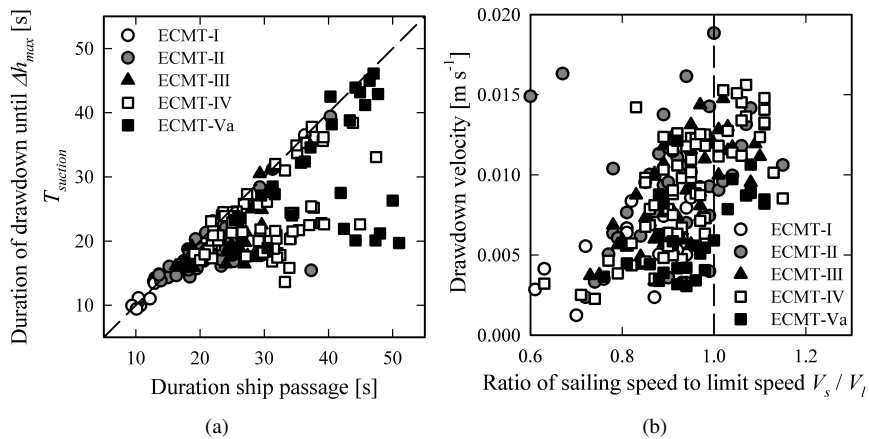
Figure 4.12: (a) The time it takes for a ship to reach its maximum drawdown Δh_{max}, categorized by ECMT-class. For the majority of the shipping traffic, it takes almost the duration of their passage at the measurement transect, which indicates that ships are generally stern heavy trimmed (b) Drawdown velocity in relation to the ratio of sailing speed to limit speed V_s/V_l, categorized by ECMT-class. It rapidly increases with increasing ratio of sailing speed to limit speed V_s/V_l. (A dashed line indicates the ratio $V_s/V_l = 1$).

- **The return current** u_r

The lateral distribution of the return current u_r spans the entire cross sectional width, and it might, together with the displacement flow, lead to an increased suspended sediment concentration. The ship's return current u_r, together with its sailing speed V_s, are the hydrodynamic relevant velocities in the Lys since it has a very small flow velocity (cf Section 3.3.1). The return current u_r is considered to be the effective velocity to the ground.

During the monitoring period of May 24-31, 2011, the return current u_r is not measured. Instead, its maximum value is calculated using the Bernoulli equation 2.2. Solving this equation with the maximum drawdown Δh_{max}, the ship's sailing speed V_s and the parameter α, which depends on the ratio V_s/V_l, gives an estimation of the maximum return current $u_{r,max}$ caused by the ship's passage. Note that for this theoretical calculation the same important remarks hold as for the determination of the limit speed V_l (cf Section 4.2.2).

For light draughted shipping traffic, the average maximum return current $u_{r,max}$ increases with increasing ECMT-class, from $u_{r,max} = 0.20\,\mathrm{m\,s^{-1}}$ to 0.68 $\mathrm{m\,s^{-1}}$ for ECMT-I to ECMT-IV respectively (Figure 4.13). ECMT-Va ships have a somewhat lower average of $u_{r,max} = 0.60\,\mathrm{m\,s^{-1}}$ but high return currents up to about $u_{r,max} = 1\,\mathrm{m\,s^{-1}}$ occur within ECMT-IV and Va. For cargo carrying ships, the differences between the ECMT-classes are less marked, i.e. the average maximum return current equals roughly $u_{r,max} = 0.50\,\mathrm{m\,s^{-1}}$, except for the lower ECMT-I value $u_{r,max} = 0.20\,\mathrm{s^{-1}}$. Within ECMT-I and II, carrying cargo results in a slight increase in maximum return current $u_{r,max}$; within ECMT-III, IV and Va, an increasing underwater volume does not give rise to a higher maximum return current $u_{r,max}$.

An increase of the blockage coefficient m is thus less important to the magnitude of a sailing ship's maximum return current $u_{r,max}$ than the approach to its limit speed V_l (Figure 4.14). A higher ratio of sailing speed to limit speed V_s/V_l significantly increases the maximum return current $u_{r,max}$ caused by a ship's passage. This is rather independent of its ECMT-classification although exceedance of the ratio $V_s/V_l = 1$ indicates that the highest values of maximum return currents $u_{r,max}$ correspond to light draughted ECMT-IV and ECMT-Va ships. The higher ECMT-I outlier ($u_{r,max} = 0.40\,\mathrm{m\,s^{-1}}$ for $V_s/V_l = 0.61$) corresponds to 2 fully loaded and coupled ships; the ECMT-II outlier ($u_{r,max} = 0.26\,\mathrm{m\,s^{-1}}$ for $V_s/V_l = 0.57$) indicates a fully loaded ship sailing close to the off-bank timber piling.

On average, the magnitude of the maximum return current $u_{r,max}$ amounts to 6%, 15% and 20% of the ship's sailing speed V_s for ECMT-I, ECMT-II and ECMT-III, and ECMT-IV and ECMT-Va shipping traffic respectively.
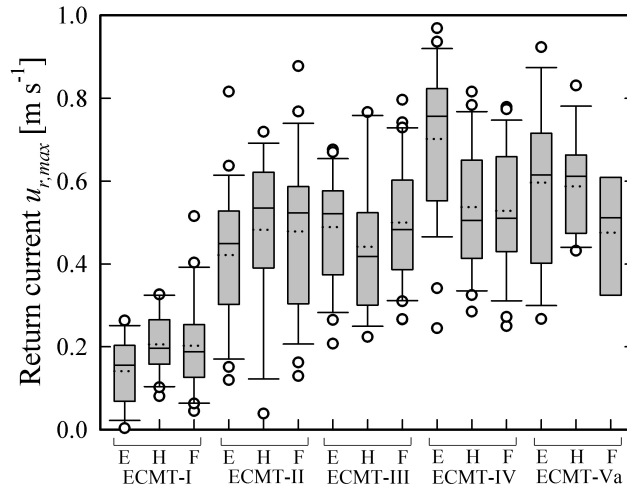
Figure 4.13: Boxplot of the maximum return current $u_{r,max}$ generated by a ship's sailing, categorized by ECMT-class and utilized carrying capacity (E: Empty, H: Half, F: Full: > 80%). (Besides the median (full line), a dotted line indicates the mean for every category. The category Full of ECMT-class Va has only 4 ship events, no 10th and 90th percentiles can be calculated.)
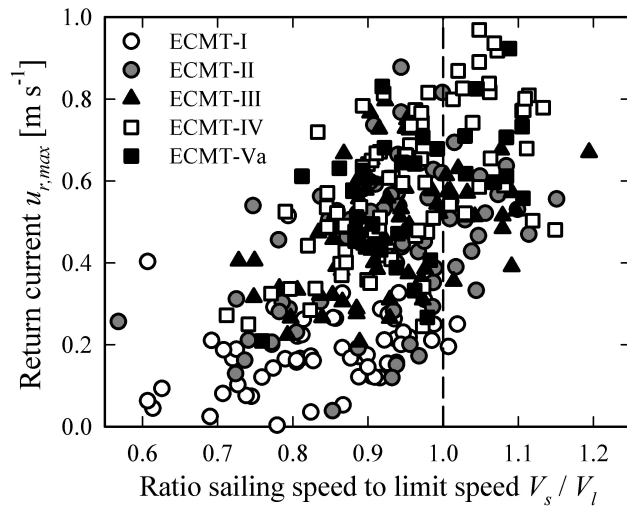

Figure 4.14: The maximum return current $u_{r,max}$ in relation to the ratio of sailing speed to limit speed V_s/V_l, categorized per ECMT-class. The magnitude of the maximum return current significantly increases when the ship's sailing speed V_s approaches its limit speed V_l, independent of its ECMT-class. (A dashed line indicates the ratio $V_s/V_l = 1$).

■ **The transversal stern wave** H_{stern}

The transition of the drawdown trough to the undisturbed water level is characterised by a transversal stern wave H_{stern}. Besides the maximum drawdown Δh_{max}, its height is determined by a following small water level rise H_{surge} (as indicated in Figure 4.7).

This small water level rise H_{surge} generally accounts for 20 to 35% of the transversal stern wave H_{stern} when the ship sails below its limit speed V_l (at PS 1). When the sailing speed V_s approaches the limit speed V_l, its part reduces to roughly 15-20%. The reduced water depth from PS 1 to PS 3 leads to a very small, yet significant, extra surge of 0.02-0.03 m at PS 3 (paired t-tests, 95% confidence interval). Combination of the slightly higher surge H_{surge} and less deep maximum drawdown Δh_{max} results in an identical transversal stern wave H_{stern} at PS 1 and PS 3 (paired t-tests, 95% confidence interval).

As the transversal stern wave H_{stern} is strongly related to the maximum drawdown Δh_{max}, its height is largely determined by the drawdown characteristics (Figure 4.15 and 4.16). For light draughted shipping traffic, it increases with increasing ECMT-class from an average $H_{stern} = 0.13$ m to 0.36 m for ECMT-I to ECMT-IV. ECMT-Va ships have a somewhat lower average: $H_{stern} = 0.31$ m. Except for ECMT-I ships ($H_{stern} = 0.14$ m), (fully) loaded shipping traffic results in a similar average stern wave height $H_{stern} = 0.25$ m. Maximum values can rise to $H_{stern} = 0.45$-0.50 m for all ECMT-classes but ECMT-I. Higher transversal stern waves occur more frequently for light draughted ships, as indicated in Figure 4.16 too. A higher ratio of sailing speed to limit speed V_s/V_l results in a higher transversal stern wave H_{stern}.

A ship's transversal stern wave H_{stern} might break when the ship sails close to its limit speed V_l because it comes from the area behind the stern and tries, following its dynamics, to overtake the ship (GBB, 2010). Given that the Lys is a confined waterway, and the off-bank timber piling yields a clear porosity effect, the probability that a transversal stern wave breaks, or at least causes a significant slope supply flow, is high because of the (very) shallow water conditions near the river bank. Figure 2.5 illustrates this phenomenon.

The behaviour of the transversal stern wave can be assessed by two breaker criteria (according to GBB (2010)), in which the conditions at PS 3 are considered to be representative for the shallow water and riverine area. Figure 4.17 indicates the combination of the two breaker criteria: 1. in the vertical axis: the 'primary' wave steepness $s = H_{stern}/d_{ship-PS3} > 0.15$: the ratio of the transversal stern wave H_{stern} to its length, which is about the ship's length (cf Section 2.1). However, the wave length is limited because of the shorter distance between the ship's trajectory and the river bank $d_{ship-PS3}$, and 2. in the horizontal axis: the (local) squared depth-Froude number $Fr_d^2 = (V_s + u_{r,max})^2/g(h - \Delta h_{max}) > 1.5$, taking into account the ship's sailing speed V_s, its maximum return current $u_{r,max}$
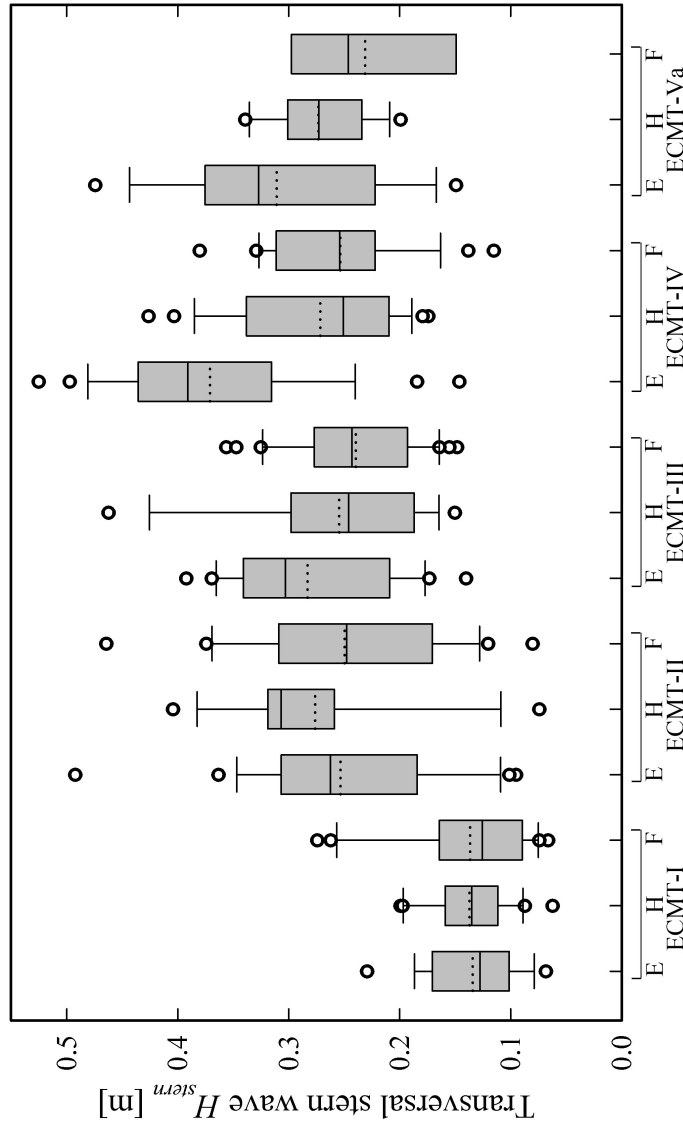
Figure 4.15: Boxplot of the transversal stern wave H_{stern}, categorized by ECMT-class and utilized carrying capacity (E: Empty, H: Half, F: Full: > 80%) (at PS 3, since the transversal stern wave mainly affects the shallow water and riverine area). Its height is strongly correlated to the maximum drawdown Δh_{max}, but depends also, for a small yet varying part, on the following water level rise. For light draughted shipping traffic, the transversal stern wave increases with increasing ECMT-class. Cargo carrying ships as from ECMT-II cause a similar average transversal stern wave. Besides the median (full line), a dotted line indicates the mean for every category. The category Full of ECMT-class Va has only 4 ship events, no 10th and 90th percentiles can be calculated.
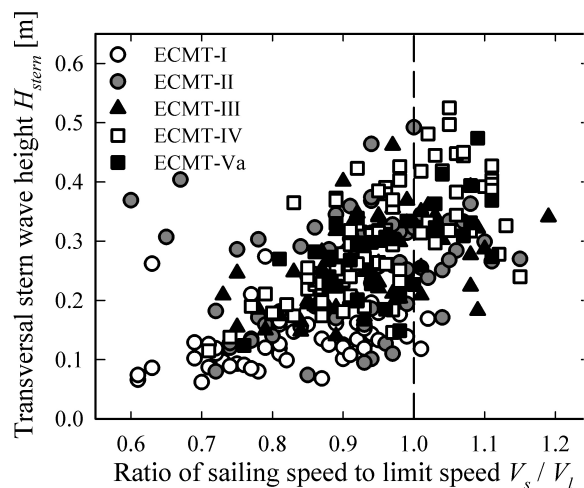
Figure 4.16: The transversal stern wave H_{stern} in relation to the ratio of sailing speed to limit speed V_s/V_l, categorized by ECMT-class. A higher ratio of sailing speed to limit speed V_s/V_l results in a higher transversal stern wave H_{stern}. (A dashed line indicates the ratio $V_s/V_l = 1$)

and its maximum drawdown Δh_{max} at PS 3. The dashed line indicates the transition between unbroken transversal stern waves without and with significant slope supply flow; the full line indicates the transition between unbroken and broken transversal stern waves with significant slope supply flow.

The latter breaker criterion, which indicates the flow characteristics at the transition of the maximum drawdown trough towards an undisturbed water level, is clearly the governing parameter. For 284 ship passages, the (local) depth-Froude number equals $Fr_d^2 \geq 1.5$. On that account, a significant slope supply flow accompanied the transversal stern wave, which had characteristics similar to a hydraulic jump. According to the classification in Chanson (2004a), this hydraulic jump generally had an undular wave front ($1.5 < Fr_d^2 < 2.9$, 169 ship passages) or showed a (weak) jump ($Fr_d^2 \geq 2.9$, 115 ship passages). Note that this classification is only indicative since no observations took place, and undular wave fronts might be observed until $Fr_d^2 = 16$ (Chanson, 2004a). For 26 ship passages, the transversal stern wave did not break but a significant slope supply flow occurred ($1 < Fr_d^2 < 1.5$).

The (turbulent) characteristics of the transversal stern wave H_{stern}, and its accompanying slope supply flow, depend on the refilling velocity of the drawdown trough. For 133 stern heavy trimmed ships, where the maximum drawdown Δh_{max} occurred just before the transversal stern wave H_{stern}, the refilling velocity of the drawdown trough is calculated by dividing the transversal stern wave

(a)

(b) zoom on (a)
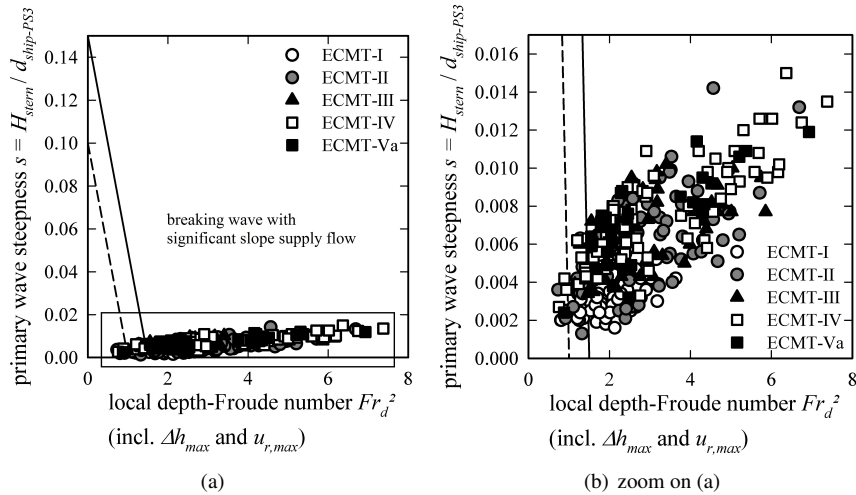
Figure 4.17: Combination of the 2 breaker criteria of the transversal stern wave height H_{stern}, which characterize its breaking behaviour, categorized by ECMT-class (according to GBB (2010)). The (local) depth-Froude number Fr^2, indicating the flow characteristics at the transition of the maximum drawdown trough towards an undisturbed water level, is clearly the governing parameter. For 284 ship passages, the transversal stern wave H_{stern} had characteristics similar to a hydraulic jump.


(a)

(b)
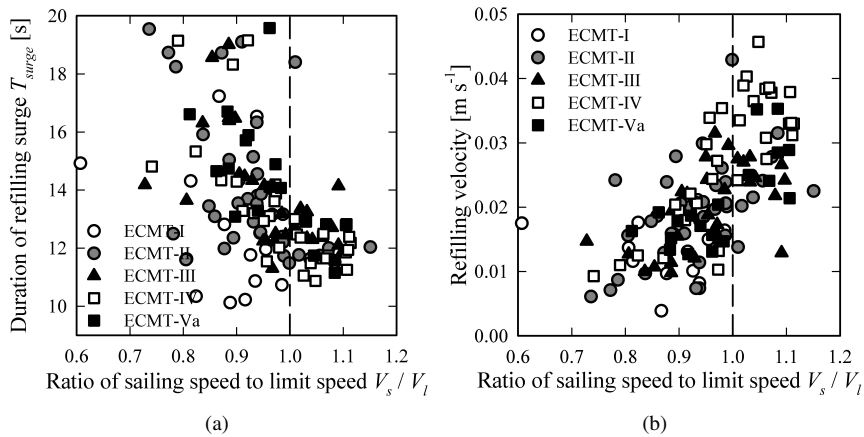
Figure 4.18: (a) Duration for refilling of the drawdown trough in relation to the ratio of sailing speed to limit speed V_s/V_l, categorized per ECMT-class. Its duration tends to decrease quadratically for a higher ratio of sailing speed to limit speed V_s/V_l, levelling off at 11 s. (b) Refilling velocity of the drawdown trough in relation to the ratio of sailing speed to limit speed V_s/V_l, categorized per ECMT-class. (A dashed line indicates the ratio $V_s/V_l = 1$).

H_{stern} (Figure 4.15) by the time it takes to refill the maximum drawdown trough T_{surge} (Figure 4.18(b)). This duration tends to decrease quadratically for a higher ratio of sailing speed to limit speed V_s /V_l, levelling off at $T_{surge} = 11$ s.

Refilling velocity ranges from $0.5 \cdot 10^{-2}$ to $4.5 \cdot 10^{-2}$ m s^{-1}, and increases rapidly with increasing ratio of sailing speed to limit speed V_s/V_l (Figure 4.18(a)). Refilling velocities can thus be up to 2.5 times higher than drawdown velocities (cf Figure 4.12(b)). The highest refilling velocities are occasioned by ECMT-IV shipping traffic.

4.4.2   Short period 'secondary' wave pattern

The short period 'secondary' wave pattern originates at the ship's bow and stern and consists of transverse and diverging waves which form interference cusps (as described in Section 2.1). The maximum wave height in this wave train $H_{SP,max}$ is considered to be normative for the 'secondary' wave-induced forcing on the nature-friendly bank protection, the river bed and the river bank.

For this analysis, a subset of 187 ship passages is used because only for these events the maximum 'secondary' wave height $H_{SP,max}$ corresponded for all pressure sensors, i.e. it took place at (nearly) the same time at all pressure sensors. An identical selected maximum 'secondary' wave height at all locations is essential to determine its reduction (see below).

The 'secondary' wave height is mainly dependent on the ship's sailing speed V_s. Because of the (relative) slow sailing speed of displacement ships, a small maximum 'secondary' wave height $H_{SP,max}$ is measured (compared to the 'primary' transversal stern wave H_{stern}) (Figure 4.19). For the majority of the ship passages, the maximum 'secondary' wave height amounts to less than $H_{SP,max} \leq$ 0.08 m. The largest values, up to $H_{SP,max} = 0.13$ m, are occasioned by light draughted ECMT-I ships, which are able to sail at the highest speed (Figure 4.9). Note that the ratio of sailing speed to limit speed V_s/V_l is of no importance because the 'secondary' wave pattern is not bound to the limit speed criterion; instead, 'secondary' waves are able to act and propagate like free water waves (within the boundary conditions of a ship's wave-making resistance, reflected in its depth- and length-based Froude numbers).

Exceedance of the depth-based Froude number $Fr_d = 0.8$ (at PS 1, equation 2.6) never takes place (only 16 ship passages caused a $Fr_d > 0.7$). The angle of attack towards the river bank equals thus approximately 55° for the (dominant) diverging waves, like in deep, unconfined water (cf Figure 2.2). In one-third of the ship events, the maximum 'secondary' wave height $H_{SP,max}$ is measured before or at stern passage along the measurement transect. Superposition of the maximum 'secondary' wave height $H_{SP,max}$ and the transversal stern wave H_{stern} occurs in half of the ship passages, and for all ships with a ratio of sailing speed to limit

speed $V_s/V_l \geq 1$.

No reduction in 'secondary' wave height is measured based on the difference between the incident maximum height $H_{SP,max,i}$ at PS 1 and transmitted maximum wave heights $H_{SP,max,t}$ at PS 2 and PS 3 (significant difference amounts to $2 \cdot 10^{-3}$ m, paired t-tests, 95% confidence interval).
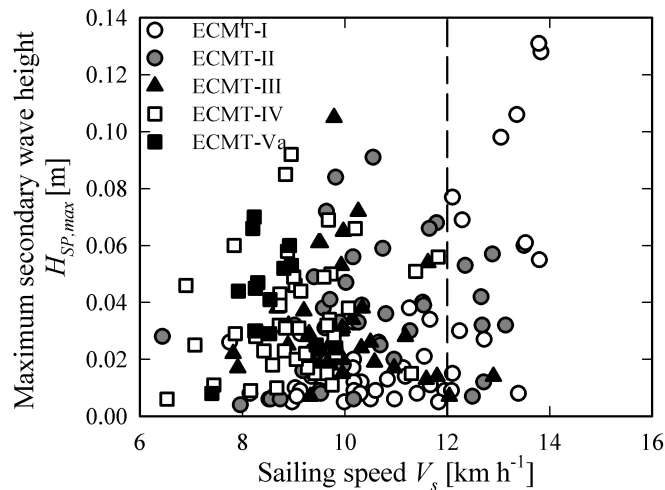

Figure 4.19: Maximum 'secondary' wave height $H_{SP,max}$ in relation to the ship's sailing speed V_s (at PS 1), categorized per ECMT-class. The (relative) slow sailing speed of displacement ships results in a small maximum 'secondary' wave height $H_{SP,max}$. Light draughted ECMT-I ships generate the highest maximum 'secondary' wave heights. The imposed speed limit $V_s = 12\,\mathrm{km\,h^{-1}}$ is indicated with a long dashed line.

4.4.2.1   Pleasure cruising

The short period 'secondary' wave pattern is normative for the potential impact of pleasure cruising, of which the largest waves occur when sailing takes place in the semi-planing speed range. Compared to displacement shipping traffic, its frequency of occurrence is very low within this monitoring period.

4 ship events corresponded to speed boats, the other 5 passages were motor boats. Pleasure cruising's sailing speed ranged from $V_s = 6.7$ to $14\,\mathrm{km\,h^{-1}}$ (Figure 4.20). Note that these values are not calculated but estimated based on the camera footage (no data records on ship length L). Maximum short period wave heights, about $H_{SP,max} = 0.04$-0.06 m for motor boats and more variable (and higher) for speed boats, fall within the range of goods traffic. Speed boats however, with their specific hull design and quasi no displacement, will generate higher waves when their sailing speed approaches the semi-planing range.
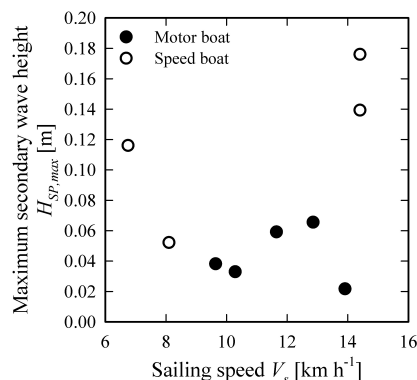
Figure 4.20: Maximum 'secondary' wave height $H_{SP,max}$ of pleasure cruising in relation to its sailing speed V_s (at PS 1). Maximum 'secondary' wave heights, about $H_{SP,max} = 0.04$-0.06 m for motor boats and more variable (and higher) for speed boats, fall within the range of goods traffic for this monitoring period.

4.5 Ship wave transmission and reduction by various configurations of off-bank timber piling

During the months June - December 2011, several off-bank timber piling configurations are successively investigated on their wave-structure interaction, i.e. ship wave transmission and reduction, making use of the mobile monitoring system.

Table 4.6 gives an overview of the 9 monitored locations, Appendix B provides additional figures of the various configurations of off-bank timber piling.

At 2 locations (1 and 3), a double row of off-bank timber piling is installed parallel to the fairway. The other 7 locations are piled with a single row parallel to the fairway. The lateral water in- and outflow to the shallow water riverine area is bounded by the length of the bank-connected timber piling, which determines the variable width of the water in- and outflow openings. Except for location 3 and 4, all locations have a single or double row of bank-connected timber piling. Thereof, 2 locations are entirely closed laterally (location 1 and 2). To check the influence of the various bank-connected piling configurations on the ship wave behaviour, the monitoring system was always installed in the middle of the off-bank timber piling.

The length of the off-bank timber piling varies significantly between the locations, but the width of the shallow water area is rather similar. Locations 1, 2, 6 and 7 are close, i.e. a distance of less than 200 m, to a widening of the cross sectional area (e.g. secondary channel, turning basin).

At the time of result interpretation, no ship data were available from the lockhouse at Sint-Baafs-Vijve. Analysis of the hydrodynamic behaviour of the timber

Table 4.6: Characteristics of the 9 locations where ship wave reduction and transmission by various configurations of off-bank timber piling is monitored.

Location	Bank side	Row of timber piling	Length [m] timber piling *	Bank-connected? - length *[m]	Width shallow water area at monitoring system[m]
1	Left	Double	79	Yes - 100% closed	8
2	Left	Single	76	Yes - 100% closed	15
3	Left	Double	51	No	10
4	Right	Single	180	No	13
5	Right	Single	340	Yes - 5 m	12
6	Left	Single	176	Yes - 5 m	10
7	Right	Single	200	Yes - 5 m	15
8	Left	Single	165	Yes - Up: 6.2 m & Down: 5.4 m	12
9	Right	Single	253	Yes - 6 m	15

* source: location and cross section maps of W & Z (drawn up date: April 27, 2011)

piling is focussed on the differences between the incident and transmitted wave heights, H_i and H_t respectively, for both ship wave patterns separately. In total, 2800 ship events were measured. All locations were monitored for about one week, except for location 1 which was monitored for 3 weeks. Table 4.7 lists the general information for every monitored period. Relative differences in water depth before and after the off-bank timber piling are around 50-55%, but are distinctly higher for locations 1, 4 and 9.

Table 4.7: The number of ship events analysed for the measurement periods at the 9 locations, with indication of the average water depth at the pressure sensors of the mobile monitoring system.

Location	Measurement period	# ship events	Water depth [m]		
	2011		PS 1	PS 2	% (PS 2 / PS 1)
1	08/06 − 30/06	653	1.75	1.50	86
2	06/09 − 14/09	219	1.40	0.82	59
3	14/09 − 20/09	173	1.88	0.86	46
4	20/09 − 27/09	215	2.10	1.63	78
5	27/09 − 07/11	405	2.30	1.30	57
6	07/11 − 17/11	364	2.40	1.15	48
7	17/11 − 24/11	253	2.17	1.01	47
8	24/11 − 30/11	251	2.10	1.12	53
9	30/11 − 07/12	267	1.70	1.10	65

4.5.1 Long period 'primary' wave pattern

The incident transversal stern wave has an average height $H_{stern,i} = 0.17 - 0.22$ m (lowest mean value: location 1 - highest mean value: location 3) (Figure 4.21). Except for the somewhat lower values at location 1 and 2, 25% of the transversal stern waves is generally higher than 0.25 m. Their magnitude amounts to a maximum $H_{stern,i} = 0.40$ m to 0.55 m (lowest maximum value: location 9 - highest maximum value: location 3). Minimum values are very small, which indicates that pleasure cruising took place throughout the entire monitoring period.

The boxplots of the transversal stern wave show a rather similar wave height distribution for the various locations. This indicates that (i) although environmental characteristics slightly differ between the locations, this does not significantly affect the incident transversal stern wave height $H_{stern,i}$, and (ii) the varying measurement period (and duration) does not significantly affect the composition of the monitored shipping traffic.

No difference between incident and transmitted stern wave heights, $H_{stern,i}$ and $H_{stern,t}$ respectively, is measured at all locations (paired t-test, 95% confidence interval) (Figure 4.23(a)). Location 4 shows a slightly deviant yet not significant result. No reduction in ship-induced hydrodynamic forcing is thus obtained irrespective of the varying timber piling configurations.
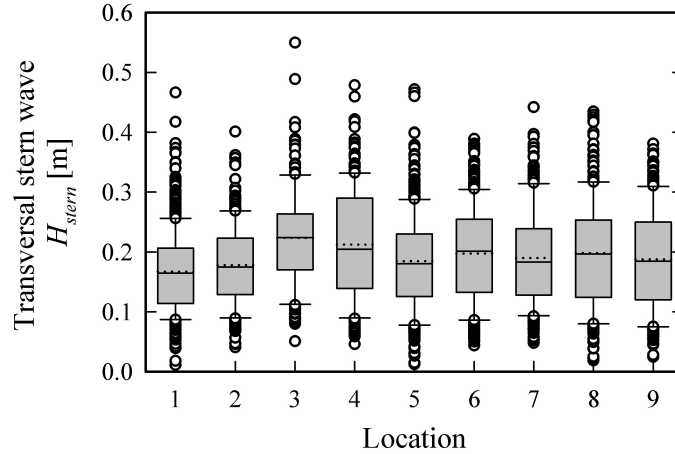
Figure 4.21: Boxplot of the incident transversal stern wave height $H_{stern,i}$ at 9 locations with various configurations of off-bank timber piling. Although environmental characteristics (slightly) differ between the locations, the incident stern waves have a rather similar wave height distribution. Besides the median (full line), a dotted line indicates the mean for every category.

4.5.2   Short period 'secondary' wave pattern

The incident maximum 'secondary' wave has an average height $H_{SP,max,i} = 0.04 - 0.05$ m for all locations (Figure 4.22). 90% of these maximum 'secondary' wave heights is smaller than 0.10 m, except for location 4 where the 90th percentile is at 0.15 m. Large values, frequently up to $H_{SP,max,i} = 0.20$ m and occasionally up to $H_{SP,max,i} = 0.30 - 0.35$ m (at location 1 and 4), are however also measured.

A significant difference between incident and transmitted maximum 'secondary' wave heights, $H_{SP,max,i}$ and $H_{SP,max,t}$ respectively, is found for all locations (paired t-test, 95% confidence interval), which amounts to an average wave height reduction of 0.01-0.03 m (lowest mean value: location 6 - highest mean value: location 4) (Figure 4.23(b)). A very small difference in absolute terms, yet it corresponds to a relative location-dependent wave height reduction of 30% to 60%, i.e. the higher the maximum 'secondary' wave height, the larger its wave height reduction. This wave height reduction is determined based on the wave transmission coefficient $K_T = \frac{H_{SP,max,t}}{H_{SP,max,i}} \cdot 100$. Both the relative wave height transmission and reduction are listed in Table 4.8 for all locations.

Between location 1 and 2, having a row of off-bank timber piling of the same length and being entirely closed laterally, a double row of timber piling resulted in 30% extra wave height reduction (55%) compared to the single row (25%). A similar difference in reduction is obtained between both double piled locations 1 and 3, where closure of the lateral in- and outflow openings resulted in a 55%

Table 4.8: Relative transmission and reduction in maximum 'secondary' wave height between $H_{SP,max,i}$ and $H_{SP,max,t}$ at the 9 locations with various configurations of off-bank timber piling

	Wave height transmission K_T [%]	Wave height reduction $100 - K_T$ [%]	Determination coefficient R^2 of linear regression for K_T
location 1	45	55	0.78
location 2	75	25	0.80
location 3	72	28	0.73
location 4	46	54	0.84
location 5	61	39	0.77
location 6	77	23	0.82
location 7	69	31	0.89
location 8	59	41	0.80
location 9	55	45	0.81

reduction (compared to 28%). However, between location 3 and 4, which do not have a bank-connected row of timber piling, the single row of off-bank timber piling at location 4, being much longer than the double row at location 3, gives also 55% reduction (compared to 28%). Between locations 5 to 9, piled with a single off-bank row of variable length, an increase in length does not result in a significantly higher wave height reduction, e.g the shortest length (165 m, location 8) result in a similar reduction as the longest length (365 m, location 5), being 41% and 39% respectively.

As such, installation of a single or double row of off-bank timber piling does not consistently result in significant differences in wave height reduction, nor does the length of the off-bank timber piling. Between the various locations, large relative differences in wave height reduction are measured but they are rather location-dependent than factor-dependent. The 'good' performance of the off-bank timber piling at location 4 is rather surprising, and no clear explanation is found.
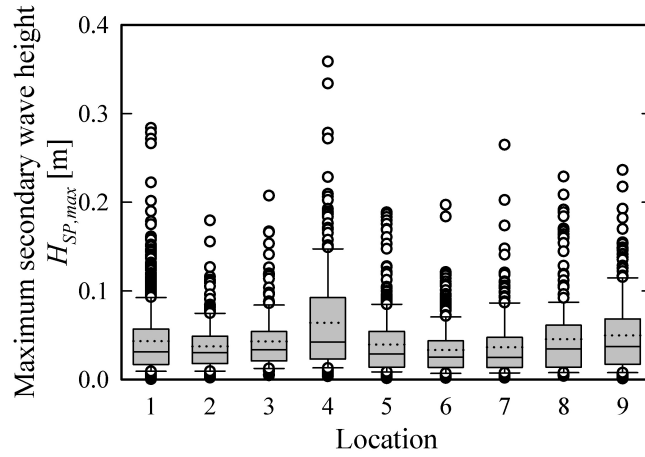
Figure 4.22: Boxplot of the incident maximum 'secondary' wave height $H_{SP,max,i}$ at 9 locations with various configurations of off-bank timber piling. 90% of these maximum wave heights is smaller than 0.10 m, except for location 4 where the 90th percentile is at 0.15 m. Besides the median (full line), a dotted line indicates the arithmetic mean for every category.

(a) $H_{stern,i} - H_{stern,t}$

(b) $H_{SP,max,i} - H_{SP,max,t}$
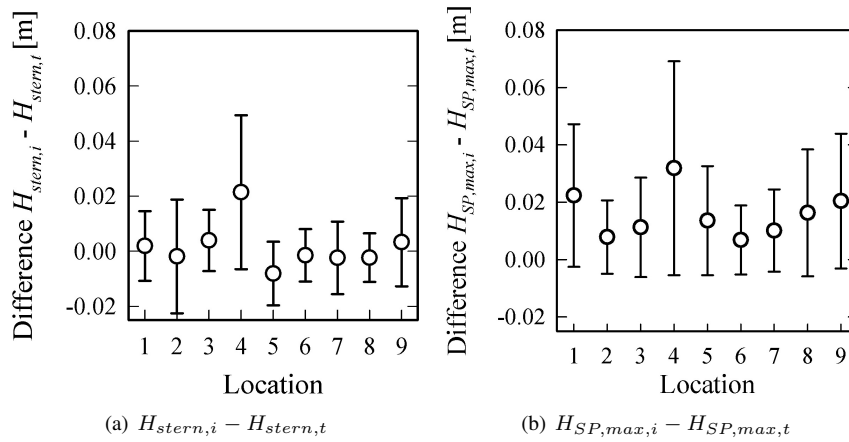
Figure 4.23: Average differences between the incident and transmitted wave heights, H_i and H_t respectively, for both wave patterns at 9 locations with various configurations of off-bank timber piling. Between the locations, no difference in transversal stern wave height H_{stern} is found, and a very small yet significant difference in maximum 'secondary' wave height $H_{SP,max}$.

4.6   Conclusion

Characterization of the ship wave climate on the Lys was accomplished by analysing both its input and output variables, i.e. the characteristics of shipping traffic (input) and the magnitude and behaviour of the 'primary' and 'secondary' wave patterns in this confined, nature-friendly protected waterway (output).

The characteristics of shipping traffic were defined by analysing 36037 data records of ships, locked at Sint-Baafs-Vijve throughout the period July 2009 - May 2011. A sailing ship is bounded to its limit speed V_l, which ranges from $V_l = 12.2 \, \mathrm{km \, h^{-1}}$ (ECMT-Va) to $14.8 \, \mathrm{km \, h^{-1}}$ (ECMT-I) for light draughted shipping traffic, and from $V_l = 9.6 \, \mathrm{km \, h^{-1}}$ (ECMT-Va) to $12.6 \, \mathrm{km \, h^{-1}}$ (ECMT-I) for fully loaded shipping traffic. The imposed speed limit of $V_s = 12 \, \mathrm{km \, h^{-1}}$ can thus easily be exceeded by all light draughted ships.

Sailing at limit speed V_l corresponds to a maximum critical depth-based Froude number $Fr_{d,cr} = 0.77$ (occasioned by light draughted ECMT-I ships), indicating a subcritical sailing regime for displacement ships. A small blockage coefficient $m < 5$ does generally not occur. A captain tries to avoid such a high ship resistance in order to be able to sail at considerable speed. This implies however that he has to limit the ship's cargo.

For 330 ship passages (from May 24-31, 2011), the magnitude of both ship wave patterns was linked to specific ship characteristics. Given the Lys' confinedness, the 'primary' wave pattern clearly dominates the ship wave signature. Maximum values for its characteristic parameters are: a maximum drawdown $\Delta h_{max} = 0.35 \, \mathrm{m}$; a transversal stern wave $H_{stern} = 0.50 \, \mathrm{m}$, and a maximum return current $u_{r,max} = 1 \, \mathrm{m \, s^{-1}}$. These highest values of ship-induced hydrodynamics are caused by light draughted shipping traffic of ECMT-class IV, sailing at a ratio of sailing speed to limit speed $V_s/V_l \geq 1$. The latter aspect is of greatest importance; the higher the ratio V_s/V_l, the higher the ship-induced hydrodynamics. $V_s/V_l \geq 1$ corresponds to light draughted shipping traffic, which generates a more pronounced ship wave signature with increasing ECMT-class. (Fully) loaded shipping traffic of all ECMT-classes (except ECMT-I) causes a similar 'primary' wave pattern (for a similar V_s/V_l). Captains tend to sail close to their ship's limit speed V_l, thereby, if possible, disregarding the imposed speed limit.

Ship wave-structure interaction and shallow water behaviour were examined for the latter monitored data, and (successively) for various configurations of off-bank timber piling throughout June-December 2011. The magnitude of the 'primary' wave pattern, i.e. the maximum drawdown Δh_{max} and transversal stern wave H_{stern}, is preserved on the condition that the water level is sufficiently high in the shallow water area. The intended ship wave reduction by off-bank timber piling is thus not obtained. Instead, the clear porosity effect yields a significant water exchange between the fairway and the shallow water area, which frequently

dries a part of the shallow water riverine area. Combination of the large 'primary' wave transmission and the limited water depth along the river bank might lead to a severe impact of the transversal stern wave H_{stern} on this riverine area.

A small absolute, yet significant, average difference in incident and transmitted maximum 'secondary' wave height $H_{SP,max}$ is observed for the various locations with varying configurations of off-bank timber piling. Relative reduction of maximum 'secondary' wave heights $H_{SP,max}$ ranges from 20% to 55%, but is rather location-dependent than factor-dependent. None of the various configurations of off-bank timber piling does clearly lead to a better result. Maximum 'secondary' wave heights $H_{SP,max}$ occasioned by pleasure cruising might be higher than those generated by goods traffic, especially those generated by speed boats. Pleasure cruising however just occasionally sails along the Lys. Because of their limited occurrence compared to goods traffic, pleasure cruising does not seem to contribute an important hydrodynamic forcing.

The future waterway layout includes an enlarged trapezoidal cross section because of the 1 m deepening of the bed profile. As a result, an increased blockage coefficient m is calculated for all ECMT-classes except for ECMT-IV and Va (because of the (now vs future) difference in blockage coefficient restrictions). The ships' limit speed V_l will increase, which results in a higher amplitude for both ship wave patterns and hence, a larger impact of the ship-induced hydrodynamic forcing. A restriction to the imposed speed limit will therefore be of a even bigger importance. Based on their limit speed V_l, only fully loaded ECMT-IV and Va ships will not be able to exceed this limit.

5

Importance of ship-induced
hydrodynamics
to sediment dynamics

5.1 Introduction

The grouped wave structure and non-linear form make ship-generated waves capable of entraining and suspending (significant) quantities of bed and bank sediments (Bauer et al., 2002; Garel et al., 2008; Houser, 2011; Osborne and Boak, 1999; Parchure et al., 2001; Rapaglia et al., 2011; Schoellhamer, 1996; Verney et al., 2007). They cause pressure changes and shear threshold exceedance (de-Wit and Kranenburg, 1997; Verney et al., 2007). The magnitude of the suspended sediment concentration is commonly related to the relative ship wave height and near-bottom orbital wave velocities (Bauer et al., 2002; Rapaglia et al., 2011). Because of the characteristic ship wave asymmetry in confined water, this suspension phenomenon displays a distinctive temporal structure (Osborne and Boak, 1999).

Direction and magnitude of sediment transport is however not clear-cut determined; it seems largely dependent on the transformation of the ship-generated waves, which travel away from the sailing line and interact with the local bathymetry (Houser, 2011; Osborne and Boak, 1999; Parchure et al., 2001). Research focusing on the far-wave field, i.e. only the 'secondary' wave pattern, indicates a tendency towards landward sediment transport (Osborne and Boak, 1999; Parnell et al., 2007; Ravens and Thomas, 2008) whereas studies involving the near-wave

field, i.e. also the 'primary' wave pattern, point out river bed erosion and bank retreat (Bauer et al., 2002; Garel et al., 2008; Houser, 2011; Nanson et al., 1994; Verney et al., 2007). In any case, the way in which sediment transport is facilitated, is determined by its grain size and erodibility (e.g. continuous advection of cohesive sediments: Bauer et al. (2002); temporal suspension load transport for sandy sediments: Nanson et al. (1994)).

The open structure of the nature-friendly bank protection makes water exchange between the fairway and the shallow water riverine area possible. It is however unclear whether this off-bank timber piling configuration provides sufficient protection against ship wave action in order to maintain a dynamic balance in its bed sediment budget behind the off-bank timber piling, i.e. a 'controlled' cyclic bed erosion and accretion.

This chapter addresses the results of a quantitative field study, which focused on the magnitude of ship-induced hydrodynamics and their relative importance to sediment dynamics in the shallow water area behind the off-bank timber piling. For these short-term morphological changes, sediment transport towards the fairway is considered as a proxy for bed and bank erosion.

5.2   Field setup

The measurement campaign is carried out in early spring, April 13-15, 2011, under normal weather conditions (cf Section 3.3.1). Making use of the fixed monitoring system (cf Section 3.4), instantaneous water level fluctuations, turbidity levels and current velocities are measured for individual ship passages. This measurement transect is situated in a non-vegetated riverine area; a possibly different sediment dynamics in the vicinity of the reed belt is thus not taken into account.

Figure 5.1 provides a schematized overview of the equipment deployment and the cross section's bed profile. In following paragraphs, this field setup is explained tersely; a detailed technical description of the measurement equipment can be found in Section 3.4.2.

Two pressure sensors of the fixed monitoring system are used; the pressure sensor (PS 1 in Figure 5.1) which is located in the fairway, 1 m before the off-bank timber piling (water depth $h_{PS1} = 3.2$ m), and the pressure sensor (PS 2 in Figure 5.1) located 4 m behind the off-bank timber piling, in the shallow water area ($h_{PS2} = 1.1$ m).

The two suspended solids profilers (SSP) are placed 7.5 m and 12 m behind the off-bank timber piling (SSP A and SSP B in Figure 5.1 respectively). The sensor array is oriented downstream, which is defined as the positive X-direction. Given that the maximum water depth is $h_{SSP\,A} = 0.8$ m (at location SSP A), a suspended solids concentration profile of the entire water column can be obtained. *In situ* testing of the profilers revealed however that a significant higher turbidity response to

Figure 5.1: Schematized overview of the equipment deployment on the measurement transect of the fixed monitoring system, and the cross sectional bed profile, with indication of the horizontal ship wave-induced velocity components (cf equation 5.1 and 5.2).

ship wave action mainly occurs in the lowest 0.3 m of the water column. *In situ* calibration of suspended solids profiler A is therefore only carried out for heights $z = 0.1$ m, 0.2 m and 0.3 m above the river bed. Intense mixing of suspended sediments takes place over the entire water column at suspended solids profiler B. In order to balance the immersion time of the sensors during a ship passage, *in situ* calibration is carried out at height $z = 0.10$ m above the river bed. Linear least squares fit calibration curves between turbidity levels and suspended sediment concentrations are obtained for the 5 optical backscatter sensors around these heights, making use of water samples taken at the respective heights. Determination coefficients of the calibration fits are $R^2 = 0.84, 0.72, 0.60$ and 0.70, for the heights $z = 0.1$ m, 0.2 m and 0.3 m at SSP A and $z = 0.1$ m at SSP B respectively. The somewhat lower calibration fit for 0.30 m is due to the higher variability in suspended sandy sediments since not all ship passages cause a suspension process until this height.

An acoustic Doppler velocimeter is installed almost equidistant between both suspended solids profilers, at the edge of maximum water withdrawal because of the ship-induced drawdown (ADV in Figure 5.1). 3-D velocity components are measured for a manually selected time frame around the ship's passage along the measurement transect, i.e. until the ship wave-induced velocities are quasi entirely dampened. Positioned near the river bed (ADV at height $z = 0.05\text{-}0.07$ m above the river bed), these velocity components can be used to estimate the ship-induced hydrodynamic forcing on the river bank and the ship-induced shear stresses on the river bed. Orientation of the orthogonal coordinate system is aligned with the profilers; positive X-direction is downstream and positive Y-direction is crosswise towards the river bank.

5.3   Methodology

5.3.1   Analysis of ship-induced hydrodynamics

The 'primary' and 'secondary' wave patterns, measured with PS 1 and PS 2, are extracted out of the pressure time series using the analysis methodology described in Section 4.3. In the same way, spectral analysis of the directional velocity components provides information on the ship's frequency-dependent wave and turbulence characteristics.

Each velocity component is decomposed in varying wave-induced and turbulence-induced contributions:

$$u_X = u_{X,LP} + u_{X,SP} + u'_X \tag{5.1}$$

where u_X is the horizontal velocity component in the X-direction; $u_{X,LP}$ and $u_{X,SP}$ are the long period 'primary' and short period 'secondary' wave-induced contributions, and u'_X is the fluctuating turbulent component ($\overline{u'_X} = 0$) For u_Y and

u_Z, the horizontal velocity component in the Y-direction and the vertical velocity component in the Z-direction respectively, a similar subdivision is obtained. The magnitude of the vertical velocity component u_Z is very small compared to the horizontal components; its behaviour is therefore disregarded. The prefix 'horizontal' is further omitted in the discussion of velocity results. The horizontal ship wave-induced velocity components are indicated in Figure 5.1.

Summation of the directional wave-induced velocity components leads to the combined wave-induced velocities $u_{X,W}$ and $u_{Y,W}$ in the X- and Y-direction. The resultant of the long period 'primary' U_{LP} and short period 'secondary' U_{SP} wave-induced velocity components determines the instantaneous wave velocity just outside the boundary layer for both wave patterns separately, and is calculated as (similar for U_{SP}):

$$U_{LP} = \sqrt{u_{X,LP}^2 + u_{Y,LP}^2} \tag{5.2}$$

The resultant of the combined wave-induced velocity components U_W is obtained using the same calculation method as equation 5.2. The resultant bank-oriented velocity $U_{W,bank}$ indicates the combined wave-induced velocity directed towards the river bank, and accounts for the ship-induced hydrodynamic forcing on the river bank.

5.3.2   Calculation of ship-induced bed shear stresses

Frictional forces exerted on the river bed are a combination of the ship-generated 'primary' and 'secondary' wave patterns and the river flow. In the Lys, the river flow is very slow (cf. Section 3.3.1). Its added contribution to ship-induced hydrodynamics is therefore considered negligible and is not independently included as a forcing parameter for bed shear stress calculation.

Bed shear stresses are calculated because exceedance of the critical shear stress $\tau_{cr} = 0.16\,\mathrm{N\,m^{-2}}$ (cf Section 3.3.2) indicates incipient motion of the river bed. Subsequently, sediment suspension might take place when the balance between the turbulent velocity fluctuation, which is related to the bed shear velocity u_*, and the particle fall velocity w_s (normal to the river bed) equals 1 (cf equation 3.6).

The combined ship wave shear stress τ_W is obtained by the cross product of the 'primary' and 'secondary' wave contributions, $\tau_{W,LP}$ and $\tau_{W,SP}$, which are separately calculated using the general expression (e.g. found in Soulsby (1997); Van Rijn (1993)) (similar for $\tau_{W,SP}$):

$$\tau_{W,LP} = \frac{1}{2}\rho f_{W,LP} U_{LP}^2 \tag{5.3}$$

The wave friction factor f_W depends on the turbulent characteristics of the flow. In this study, flow is assumed to be hydraulically rough during a ship passage

and the friction factor is obtained from (Soulsby, 1997) (similar for $f_{W,SP}$):

$$f_{W,LP} = 1.39 \left(\frac{U_{LP} T_{LP}}{2\pi z_0} \right)^{-0.52} \tag{5.4}$$

where z_0 is the bed roughness length, taken as $z_0 = 4 \cdot 10^{-4}$ m (mean value for unrippled sand, advocated by Soulsby (1997)); T_{LP} is the 'primary' wave period [s]. The wave period is calculated using data from pressure sensor 2. Both the 'primary' and 'secondary' wave period, T_{LP} and $T_{SP,max}$ respectively, are indicated in Figure 4.7.

As a measure of instantaneous turbulence intensity, turbulent kinetic energy (TKE) is used and calculated from the instantaneous fluctuating velocity components (Dyer, 1986):

$$TKE = 1/2 \left(u_X'^2 + u_Y'^2 + u_Z'^2 \right) \tag{5.5}$$

The turbulence kinetic energy approach is not selected as shear stress calculation method because of impracticability of shear separation between both ship-generated wave components.

5.3.3 Determination of suspended and transported bed and bank sediments

Quantification of sediment dynamics because of ship-induced hydrodynamic forcing on river bed and bank separately, is hampered by the large variability and overlap in bed and bank grain sizes. Suspended sediment concentrations measured by SSP A, positioned at considerable distance from the river bank, indicate the entrained and suspended bed sediments. At SSP B, a mixture of suspended bed and bank particles is reflected in the measured suspended sediment concentration. Relying on the differences in sediment dislodge and transport characteristics for varying grain size (here: (fine) sand - silt), a partial distinction between both sediment sources is made.

Entrained silty bank particles stay, once dislodged, prolonged in suspension and are advected downstream (based on the Rouse #, cf Section 3.3.2). An estimate of the added suspended silt concentration SSC_{silt} [g m^{-3}] to the suspended sediment concentration is obtained by subtraction of *post* and *pre* ship passage suspended sediment concentrations. The *pre* concentration corresponds to the suspended load averaged over a 15 min time frame before a ship passage, the *post* concentration is determined after turbulence due to ship-induced hydrodynamics settled down (based on ADV signal analysis).

Suspension of bank sediments having a mean diameter that falls in the range of the river bed is indirectly regarded in this study. It is argued that dislodgement of sandy sediments results first in near-bank deposition on the river bed, where

they become part of the top bed layer. Their sediment resuspension and transport is taken into account in the calculation of bed sediment dynamics.

Depth-averaged integration of the increased suspended sediment concentration at SSP A, i.e. total suspended sediment concentration minus *pre* ship passage suspended sediment concentration, represents the average concentration of sandy bed sediments (re)suspended over the water column at a time t because of an individual ship's wave action $\overline{C}_{m,bed}(t)$ [g m^{-3}]:

$$\overline{C}_{m,bed}(t) = \frac{1}{h_{SSP\,A}} \int_0^{h_{SSP\,A}} SSC(z,t)dz \qquad (5.6)$$

where $h_{SSP\,A}$ is the water depth at the location of SSP A [m], z is the height above the river bed [m], t is time [s], $SSC(z,t)$ is the suspended sediment concentration at height z and time t [g m^{-3}]. This suspended sediment concentration $SSC(z,t)$, measured at height $z = 0.10$, 0.20 or 0.30 m above the river bed, is assumed to hold for the entire 0.10 m water column below its measurement height at time t, i.e. SSC($z = 0.10$ m,t) holds for a height $z = 0 \mapsto 0.10$ m at time t. Based on this assumption, a weighted depth-averaged suspended sediment concentration is used for the sediment transport calculations.

Integration of this depth-averaged concentration of (re)suspended sandy bed sediments $\overline{C}_{m,bed}(t)$ over the duration of a ship's hydrodynamic disturbance T_0 represents the cumulative concentration of sandy bed sediments (re)suspended because of an individual ship's wave action $\overline{C}_{\sum,m,bed}(T_0)$. It gives a better view on sediment dynamics than the maximum suspended sediment concentration on a certain height above the river bed $SSC(z,t)_{max}$.

The cumulative quantity of (re)suspended bed sediments $\overline{C}_{\sum,m,bed}(T_0)$ [g m^{-3}] follows from:

$$\overline{C}_{\sum,m,bed}(T_0) = \int_0^{T_0} \overline{C}_{m,bed}(t)dt \qquad (5.7)$$

where T_0 is the duration of an individual ship's hydrodynamic disturbance [s].

The time- and depth-averaged quantity of (re)suspended bed sediments $\overline{C}_{m,bed}$ [g m^{-3} s^{-1}] is obtained by dividing equation 5.7 by the duration of a ship's hydrodynamic disturbance T_0.

While transport of the silty bank sediments directly (and continuously) follows from the assumption of downstream advection, suspension transport of the sandy bed (and bank) particles incorporates a temporal aspect in its sediment discharge. Assuming no-slip conditions between the fluid and sediment particles, the crosswise suspended sediment mass flux $q_{m,bed}(t)$ at time t [g m^{-2} s^{-1}], through a vertical plane A parallel to the river bank, is calculated as:

$$q_{m,bed}(t) = \overline{C}_{m,bed}(t) \cdot u_{Y,W}(t) \qquad (5.8)$$

where $u_{Y,W}$ is the crosswise combined wave-induced velocity [m s^{-1}]. Vertical plane A [m^2] has a height equal to the water depth at SSP A $h_{SSP\,A}$ [m] and a unit alongstream width [m].

The cumulative suspended sediment mass transport $Q_{\sum,m,bed}$ [g m^{-1}] per unit alongstream width [m] is then obtained from:

$$Q_{\sum,m,bed}(T_0) = \int_0^{T_0} q_{m,bed}(t) \cdot h_{SSP\,A} dt \qquad (5.9)$$

Because vertical velocity profiles could not be measured with the available measurement equipment, suspended sediment transport had to be estimated from velocity measurements at one height above the river bed. Bearing in mind the wave velocity profile in shallow water (according to linear wave theory, and reported for ships by Mazumder et al. (1993)) and the small bed slope between the non-collocated measurement devices, sediment transport is presumably underestimated. Bed load transport is not considered in this study.

Calibration of the suspended solids profilers was carried out for specific heights above the river bed and sampling took place at discrete time intervals, such that calculation of the integrals in equation 5.7 and 5.9 is discretized accordingly.

5.4 Results

5.4.1 General

Over the 3-day measurement campaign, 70 ships sailed along the nature-friendly bank protection, of which 5 were pleasure cruising while the others carried goods traffic. Thereof, 46 ship passages were monitored with adequate completeness and quality to be analysed. Up- and downstream sailing were in balance. 14 ships were light draughted, 15 ships were fully loaded (utilized carrying capacity > 80%), and 12 ships had a variable carrying capacity < 80%. 2 'compound' ship events took place. One was the result of two crossing ECMT-Va ships; the other was created by two closely following ECMT-III and ECMT-I ships. This implies that for these 4 ship passages ship-induced hydrodynamics and sediment dynamics could not be separated from one another, and hence, they are considered as 2 ship events. In the figures, these 'compound' events are encircled and assigned to the ECMT-class of the largest ship.

Passage of pleasure cruising did not result in substantial wave patterns, and current velocities were only marginally affected. Shear stresses stayed below the critical shear stress $\tau_{cr} = 0.16\,\mathrm{N\,m^{-2}}$. No increased suspended sediment levels were noticed. Pleasure cruising is therefore disregarded in the results' interpretation and discussion.

Table 5.1 lists the characteristics of the shipping traffic, categorized by ECMT-class. Sailing speed V_s is mainly just below the imposed speed limit of $V_s =$

$12\,\mathrm{km\,h^{-1}}$ ($= 3.3\,\mathrm{m\,s^{-1}}$), except for ECMT-class Va (because of blockage coefficient restrictions). The largest relative 'primary' wave height, i.e. transversal stern wave, and the limited relative 'secondary' wave height, $H_{stern}\,h^{-1}$ and $H_{SP,max}\,h^{-1}$ respectively, indicate both that the threshold of breaking is not reached (H h^{-1} = 0.78, advocated by Van Rijn (1990)).

On April 13, 2011, no pressure data were available from the fixed monitoring system. For the 13 ship passages on this day, ship characteristics were deduced from ships having a similar displacement Δ; the sailing distance from the off-bank timber piling y was visually estimated.

5.4.2   Hydro- and sediment dynamic signature of a ship passage

Although the magnitude of ship-induced hydrodynamics varies, the temporal structure of all ship passages is similar. Figure 5.2 illustrates the ship wave action in the confined, non-tidal Lys, displaying the hydro- and sediment dynamic signature of two successive ECMT-IV ship passages along the measurement transect. Table 5.2 gives an overview of their characteristic parameters.

Ship A and B are ECMT-IV ships that are fully loaded and sailing upstream. Ship A, being somewhat heavier than ship B, sails $1.8\,\mathrm{km\,h^{-1}}$ ($0.5\,\mathrm{m\,s^{-1}}$) slower and 5 m closer to the off-bank timber piling (Table 5.2). Approaching the measurement transect, a small water level rise indicates the ship's bow wave H_{bow}. Subsequently, a drawdown Δh, having the largest vertical amplitude, is created during the ship's hull passage. It is followed by the transversal stern wave H_{stern} and the short period 'secondary' wave pattern (which is also noticeable during the drawdown Δh) (Figure 5.2A). Although the pressure sensors are installed before and behind the off-bank timber piling (and in different water depths), no significant difference between the ship wave patterns is observed, which indicates a clear porosity effect through the off-bank timber piling.

Building up the drawdown trough is associated with a sharp increase in 'primary' wave-induced velocity, directed downstream because the ships are sailing upstream, i.e. the ship's return current u_r, and towards the fairway because of the ship's displacement Δ ($u_{X,LP}$ and $u_{Y,LP}$ in Figure 5.2B). When the maximum drawdown Δh_{max} is reached, 'primary' wave-induced velocities also reach their maximum as this corresponds to the lowest water level. Subsequently, these 'primary' wave-induced velocities drop back to almost zero, what roughly coincides with the stern passage along the measurement transect. Thereupon, a second velocity peak is observed, which indicates the transversal stern wave H_{stern}. This refilling of the drawdown trough induces a flow reversal, by which the returning water mass is able to hit the river bank with a potential large impact energy, i.e.

Table 5.1: Characteristics of the 41 monitored ship passages (of goods traffic) during the 3-day measurement campaign, categorized by ECMT-class

	#	Sailing speed V_s [km h^{-1}]	V_s [m s^{-1}]	depth-based Froude Fr_d (Shallow water - PS 2)	Relative wave height H_{stern} h^{-1} (Shallow water - PS 2)	Relative wave height H_{SP} h^{-1} (Shallow water - PS 2)
ECMT-I	15	10.43 ± 2.99	2.90 ± 0.83	0.92 ± 0.26	0.12 ± 0.06	0.02 ± 0.02
ECMT-II	6	11.52 ± 3.71	3.20 ± 1.03	0.97 ± 0.23	0.20 ± 0.09	0.03 ± 0.02
ECMT-III	6	10.86 ± 1.50	3.02 ± 0.42	0.93 ± 0.14	0.17 ± 0.10	0.03 ± 0.01
ECMT-IV	10	10.08 ± 2.25	2.80 ± 0.63	0.88 ± 0.18	0.23 ± 0.09	0.04 ± 0.03
ECMT-Va	4	8.43 ± 1.18	2.34 ± 0.33	0.74 ± 0.10	0.19 ± 0.04	0.01 ± 0.01

the slope supply flow dynamics. The 'secondary' wave pattern is marked by rapid oscillations in 'secondary' wave-induced velocity and direction ($u_{X,SP}$ and $u_{Y,SP}$ in Figure 5.2B). Clearly, the 'primary' wave pattern is the key contributor to ship wave-induced velocities, and its magnitude tends to be highest during the drawdown. The maximum combined wave-induced velocities $U_{W,max}$ are comparable for both ships, but the maximum's direction is oriented for ship A towards the fairway whereas for ship B this is towards the river bank (Table 5.2).

Both ship passages cause a significant increase in bed shear stress, up to one order of magnitude higher than the critical shear stress $\tau_{cr} = 0.16\,\mathrm{N\,m}^{-1}$ (Figure 5.2C). 'Primary' and 'secondary' wave shear stresses, $\tau_{W,LP}$ and $\tau_{W,SP}$ respectively, are quite similar during the formation of the drawdown Δh, but after the transversal stern wave H_{stern}, the latter prevails because of the stern-associated 'secondary' wave pattern. For ship A, which is stern heavy trimmed, the duration of shear threshold exceedance is more prolonged because of its intenser stern-associated 'secondary' wave pattern. The maximum of the combined ship wave shear stress τ_W is also somewhat higher for ship A. Turbulent kinetic energy TKE reaches the highest values during the ship's hull passage and is thus mainly associated with the drawdown hydrodynamics.

Exceedance of the critical shear stress τ_{cr} at bow passage causes an instantaneous increase of the suspended sediment concentrations $SSC(z,t)$ at SSP A (Figure 5.2D) for both ships. Ship wave-induced velocities and associated turbulence lead to two suspension peaks: the first coincides with the drawdown trough, the second results from the transversal stern wave's behaviour. The magnitude of these suspension responses correlates to the strength of the hydrodynamic triggers, and depends on the vertical distance of the measurement height z to the river bed. A small time lag is visible between the maximum suspension levels on the different heights z. Because both ships' 'primary' wave-induced velocities are crosswise skewed towards the fairway, net suspended sand transport takes place towards the fairway, which is considered to be a proxy for bed erosion (Table 5.2).

Closer to the river bank, at SSP B, reduced suspended sediment concentrations are measured during a ship's passage. The ship-induced drawdown Δh results in water withdrawal away from the river bank, and hence, the SSP B. Ship A even causes surfacing of the river bed beyond the profiler's location (Figure 5.2E). The transversal stern wave H_{stern}, and its accompanying slope supply flow, activate sediment (re)suspension near the river bank, of which duration and agitation are closely linked to their hydrodynamic behaviour. Sediments might become available from two sources, the river bed and bank, depending on the magnitude of the combined bank-oriented wave-induced velocities $U_{W,bank}$. Comparison of the *pre*

and *post* suspended sediment levels for the combined ship passages of A and B indicates that the combined bank-oriented wave-induced velocities $U_{W,bank}$ were high enough to dislodge silty bank particles.

In a confined, non-tidal waterway, the slightly different boundary conditions for ship A and B lead to distinctly different ship-induced hydrodynamics, and hence, large contrasts in sediment dynamics, being in this example more marked for ship A.

Table 5.2: Overview of hydro- and sediment dynamic characteristics of two ECMT-IV ships A and B, closely following one another along the measurement transect on April 15, 2011

|	Ship A	Ship B
Length L, Beam B, Draught D [m]	85 - 9.6 - 2.9	80 - 8.2 - 2.7
Displacement Δ [m^3]	2379	1758
Sailing distance to the off-bank timber piling y [m]	12	17
Sailing speed V_s [km h^{-1} (m s^{-1})]	7.6 (2.1)	9.4 (2.6)
Transversal stern wave H_{stern} [m]	0.19	0.16
Maximum 'secondary' wave height $H_{SP,max}$ [m]	0.07	0.16
Duration of ship passage [s]	40	31
Duration of suction $T_{suction}$ [s]	36	27
Duration of surge T_{surge} [s]	16	10
Duration of critical shear exceedance $t > \tau_{cr}$ [s]	118	57
'Primary' wave-induced velocity $U_{LP,max}$ [m s^{-1}]	0.55	0.31
'Secondary' wave-induced velocity $U_{SP,max}$ [m s^{-1}]	0.24	0.24
combined wave-induced velocity $U_{W,max}$ (direction) [m s^{-1}]	0.56 (-22°)	0.49 (132°)
combined bank-oriented wave-induced velocity $U_{W,bank,max}$ [m s^{-1}]	0.43	0.49
Maximum ship wave shear stress $\tau_{W,max}$ [N m^{-2}]	2.55	1.88
Cumulative suspended sand sediments $\overline{C}_{\sum,m,bed}(T_0)$ (river bed) [g m^{-3}]	4900	3100
Suspended sand mass transport $Q_{\sum,m,bed}(T_0)$ (river bed) [g m^{-1}]	-170	-50
Suspended silty sediments SSC_{silt} (river bank) [g m^{-3}]	Ship B too close	120
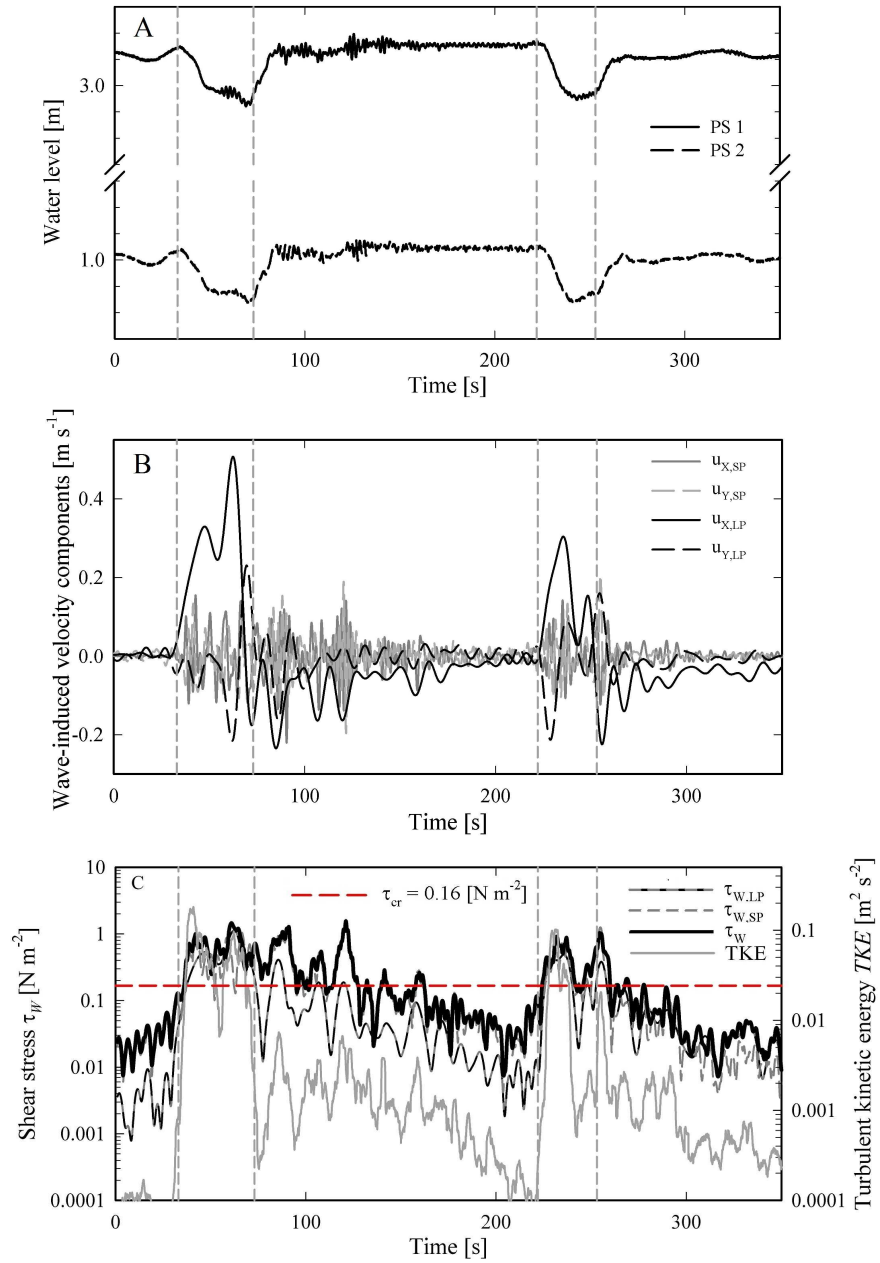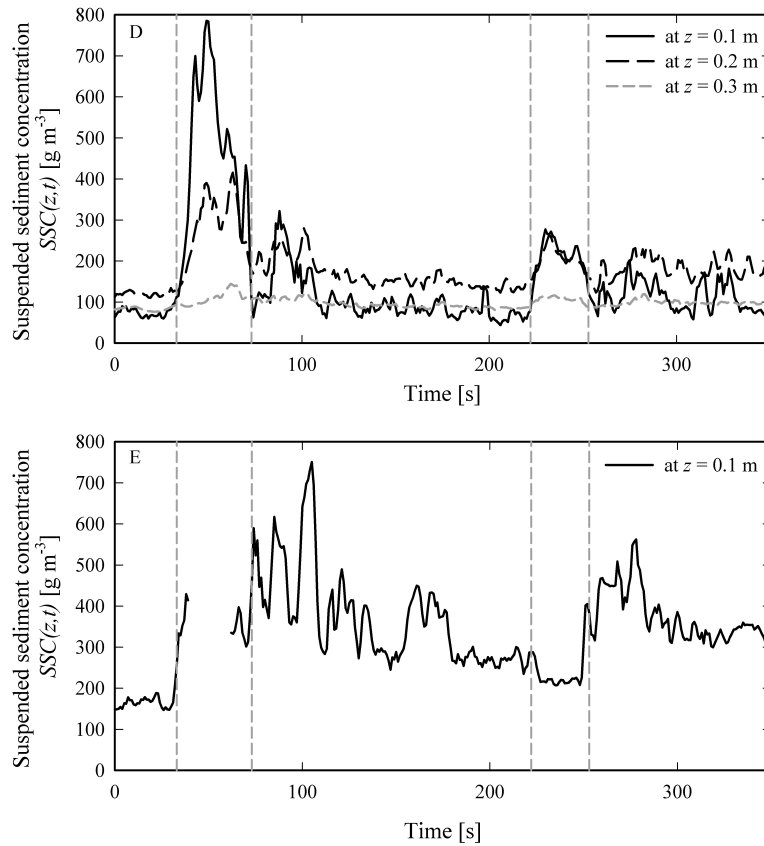
Figure 5.2: Time series of the hydro- and sediment dynamic signature of 2 ECMT-IV ships A (first event) and B (second event). The grey dashed lines mark the ship passage (bow and stern respectively) at the measurement transect. A. Water level fluctuations of the ship's combined 'primary' and 'secondary' wave pattern in the fairway (PS 1) and in the shallow area (PS 2) B. 'Primary' and 'secondary' wave-induced velocity components in streamwise u_X (X-direction, positive downstream) and crosswise u_Y (Y-direction, positive towards the river bank) direction. C. The combined ship wave shear stress τ_W, with indication of the 'primary' and 'secondary' wave-induced contributions, $\tau_{W,LP}$ and $\tau_{W,SP}$ respectively. D. Suspended sediment concentration at different heights z above the river bed, measured with SSP A. E. Suspended sediment concentration at height $z = 0.1$ m above the river bed, measured with SSP B.
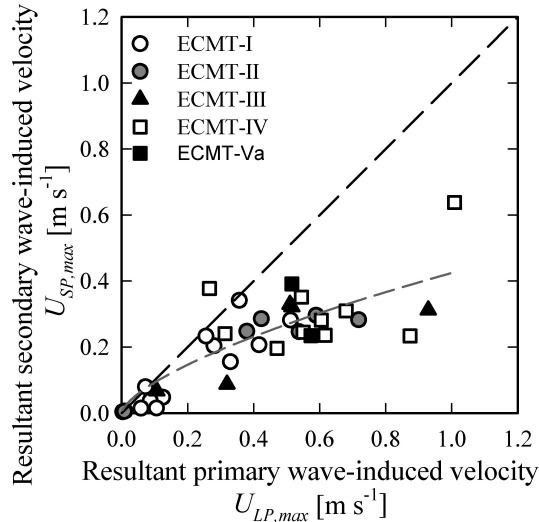
Figure 5.3: Maximum resultant velocity of 'primary' and 'secondary' wave-induced components, $U_{LP,max}$ and $U_{SP,max}$ respectively, of a ship passage, categorized by ECMT-class. The 'primary' wave pattern clearly leads to higher velocities than the 'secondary' wave pattern.

5.4.3   Characteristics of ship-induced hydrodynamics

The Lys' confined dimensions amplify the ship's 'primary' wave pattern and its wave-induced velocity components. Maximum resultant velocities related to the 'primary' wave pattern $U_{LP,max}$ are consistently the highest, up to $U_{LP,max} = 1.0\,\mathrm{m\,s}^{-1}$ (Figure 5.3). No clear distinction is observed between the velocity's magnitude and the ship's ECMT-class, which roughly reflects the differences in blockage coefficient m (cf Section 4.2, Figure 4.4(a)). Maximum resultant velocities associated with the 'secondary' wave pattern $U_{SP,max}$ are roughly 50% of the 'primary's maximum but tend to level off around $U_{SP,max} = 0.4\,\mathrm{m\,s}^{-1}$.

The velocity's maximum is predominantly oriented towards the fairway for the resultant 'primary' wave-induced velocity $U_{LP,max}$ and the angle of attack depends on the sailing direction, being 330° for upstream sailing and 210° for downstream sailing (Figure 5.4). Accordingly, an angle of 30° with the fairway axis is the principal direction of the maximum resultant 'primary' wave-induced velocity. Orientation and angle of attack for the maximum resultant 'secondary' wave-induced velocity $U_{SP,max}$ are rather randomly (Figure 5.4). The maximum of the resultant combined wave-induced velocity $U_{W,max}$ is clearly dominated by the 'primary' wave pattern, which often dictates the angle of attack. The maximum bank-oriented combined wave-induced velocity $U_{W,bank,max}$ hits the river bank obliquely at an angle independent of up- or downstream sailing. Its magnitude is
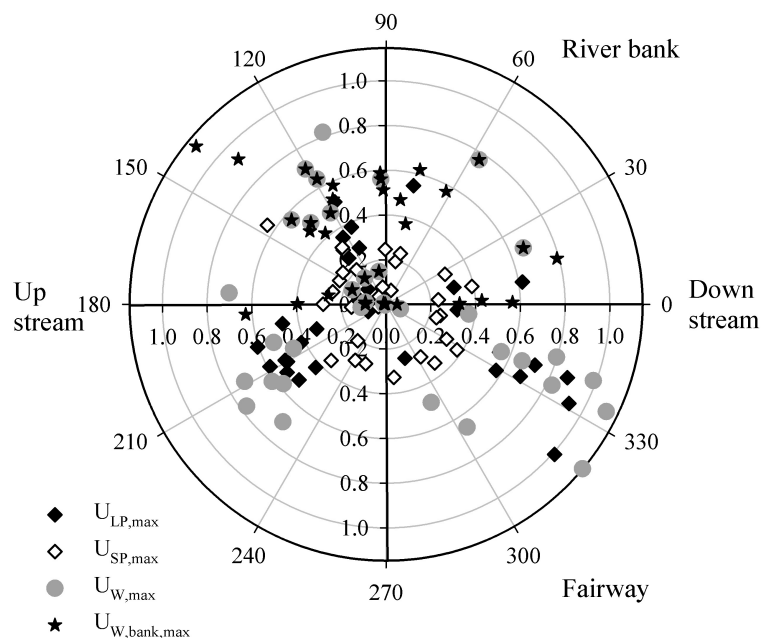
Figure 5.4: Direction and magnitude of the maximum of the resultant wave-induced velocity because of the 'primary' wave pattern $U_{LP,max}$, the 'secondary' wave pattern $U_{SP,max}$, and the combined ship wave patterns $U_{W,max}$. For the latter velocity, the bank-oriented maximum $U_{W,bank,max}$ is also indicated.

considerably high for one-third of the ship passages, amounting to $U_{W,bank,max} = 0.6\,\mathrm{m\,s}^{-1}$ and occasionally even up to $U_{W,bank,max} = 1.0\,\mathrm{m\,s}^{-1}$ (Figure 5.4).

From the data set of ship characteristics, a set of steering parameters determining (part of) the magnitude of the maximum resultant combined wave-induced velocity $U_{W,max}$ [$\mathrm{m\,s}^{-1}$] is found using linear regression modelling. Up- and downstream sailing, sailing speed V_s [$\mathrm{m\,s}^{-1}$], ship displacement Δ [m^3], sailing distance to the off-bank timber piling y [m], the relative transversal stern wave height $H_{stern}\,h^{-1}$ [-] and the relative maximum 'secondary' wave height $H_{SP,max}\,h^{-1}$ [-] are taken into consideration. To set up the model, singular events such as crossing ships and push-towing are omitted. Analysis pointed out that the ship's displacement Δ, its sailing speed V_s and its sailing distance from the off-bank timber piling y explain roughly half of the variance in the maximum resultant combined wave-induced velocity $U_{W,max}$ (at 95% confidence level). An increase in ship displacement Δ adds the most to the velocity's maximum. Up- or downstream sailing direction is found to be insignificant, as expected given the Lys' very small flow velocity (cf Section 3.3.1).

For this specific data set (N=36), following regression model is obtained for $U_{W,max}$:

$$U_{W,max} = 2.3 \cdot 10^{-4}\Delta + 0.1V_s - 0.3 \cdot 10^{-1}y + 0.5 + \epsilon_i \qquad (5.10)$$

where ϵ_i is the random error term ($N(0,\sigma^2)$), which is distributed normally with a mean equal to 0 and a variance σ^2.

Knowledge of the relative transversal stern wave height $H_{stern}\,h^{-1}$ (only available for a subset of data (N=20)) attributes another 12% to statistical determination. The relative maximum 'secondary' wave height $H_{SP,max}\,h^{-1}$ is found to be insignificant.

$$U_{W,max} = 1.8 \cdot 10^{-4}\Delta + 0.3V_s - 0.2 \cdot 10^{-1}y + 2.5H_{stern}\,h^{-1} - 0.6 + \epsilon_i$$
$$(5.11)$$

Note that the fitted coefficients are explanatory for this data set; validation is necessary to enlarge their robustness and reliability to predict other ship wave patterns in the same study site or at other locations.

The critical shear stress $\tau_{cr} = 0.16\,\mathrm{N\,m^{-2}}$ is exceeded in 85% of the ship passages. Duration of shear threshold exceedance is largely correlated with the duration of a ship passage along the measurement transect, which again demonstrates the importance of 'primary' wave-induced hydrodynamics. It lasts 10 s longer than the ship's passage, except for 2 fully loaded ECMT-IV ships, and 1 ECMT-I ship which sails fast at $V_s = 15.8\,\mathrm{km\,h^{-1}}$ ($4.4\,\mathrm{m\,s^{-1}}$) (beyond the limit speed) (Figure 5.5).

Both the maximum 'primary' and 'secondary' wave shear stresses, $\tau_{LP,max}$ and $\tau_{SP,max}$ respectively, are generally higher than the critical shear stress τ_{cr}. The 'secondary' wave pattern induces however higher shear stresses than the 'primary' wave pattern (Figure 5.6). Although wave-induced velocities of the latter are higher, the influence of the wave friction factor f_W and, indirectly, the wave period T is important. The wave friction factor f_W is more pronounced for the 'secondary' wave pattern, which results in higher shear stresses. The 'primary' wave period ranges from $T_{LP} = 30$ to $100\,\mathrm{s}$, while maximum 'secondary' wave periods fluctuate around $T_{SP,max} = 2\text{-}5\,\mathrm{s}$. Consequently, the 'secondary' wave pattern has the largest share in the combined ship wave shear stress τ_W (as also illustrated in Figure 5.2C). Maximum values for the maximum 'primary' and 'secondary' wave-induced shear stresses are up to $\tau_{LP,max} = 2.5\,\mathrm{N\,m^{-2}}$ and $\tau_{SP,max} = 4.1\,\mathrm{N\,m^{-2}}$ respectively, and the resulting combined ship wave shear stress amounts maximally to $\tau_W = 5.1\,\mathrm{N\,m^{-2}}$.
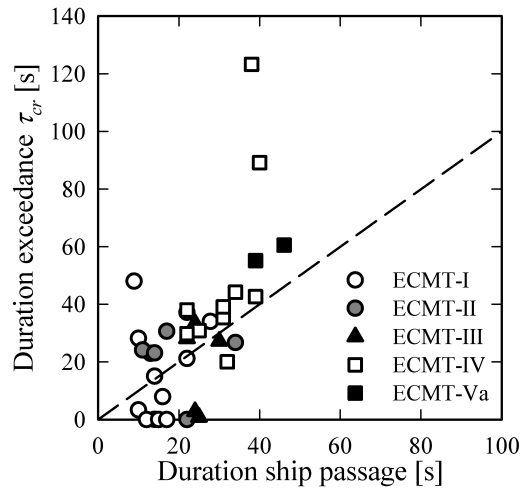
Figure 5.5: Duration of exceedance of the critical shear stress $t > \tau_{cr}$ in relation to the duration of a ship passage along the measurement transect, categorized by ECMT-class. Both are largely correlated, which demonstrates the importance of 'primary' wave-induced hydrodynamics.
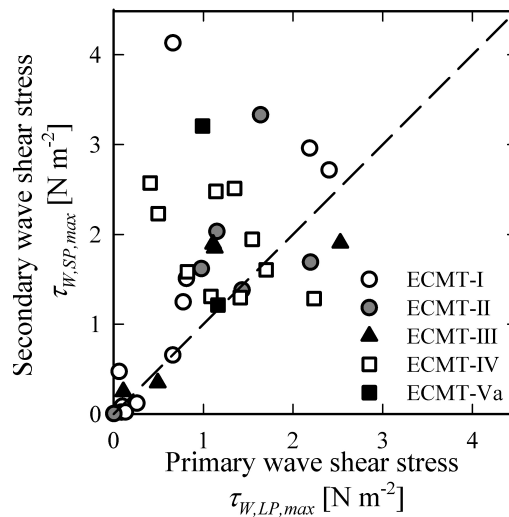
Figure 5.6: Maximum values of the 'primary' and 'secondary' wave shear stresses, $\tau_{LP,max}$ and $\tau_{SP,max}$ respectively, due to a ship passage, categorized by ECMT-class.

5.4.4 Amount of ship-induced suspended bed and bank sediments

The transient nature of ship-generated waves makes that the duration of an individual ship's hydrodynamic disturbance T_0 is limited to 2 to 3 min at the measurement transect.

Statistical regression analysis indicates that half of the variability in the cumulative quantity of (re)suspended bed sediments $\overline{C}_{\sum,m,bed}(T_0)$ [g m^{-3}] can be determined by the maximum resultant combined wave-induced velocity $U_{W,max}$ [m s^{-1}] (R^2 = 0.57, at 95% confidence level). Process and response variables are quadratically linked to one another. Although (re)suspension of the bed sediments depends on critical shear exceedance and associated turbulence, the amount of suspended bed sediments mainly scales with the magnitude of the resultant low-frequency wave-induced velocities U_{LP} (cf Figure 5.4). However, statistical determination of the time- and depth-averaged quantity of suspended bed sediments ($\overline{C}_{m,bed}$) reflects the 'instantaneous' importance of the aforementioned ship-induced hydrodynamics. $\overline{C}_{m,bed}$ is significantly scaled with the maximum combined ship wave shear stress $\tau_{W,max}$ [N m^{-2}], the duration of critical shear exceedance $t > \tau_{cr}$ [s] and, also, the maximum resultant combined wave-induced velocity $U_{W,max}$ (R^2 = 0.70).

For this specific data set (N=36), following regression model is obtained for $\overline{C}_{\sum,m,bed}(T_0)$:

$$\sqrt{\overline{C}_{\sum,m,bed}(T_0)} = 6.5 \cdot 10^1 U_{W,max} + 11 + \epsilon_i \tag{5.12}$$

For this specific data set (N=36), following regression model is obtained for $\overline{C}_{m,bed}$:

$$\sqrt{\overline{C}_{m,bed}} = 3 U_{W,max} + 3.8 \cdot 10^{-2} t > \tau_{cr} - 0.5 \tau_{W,max} + 3 + \epsilon_i \tag{5.13}$$

A clear difference in quantity of suspended bed sediments is noticeable between and within the ECMT-classes, ranging from a moderate suspension of $\overline{C}_{\sum,m,bed}(T_0) = 1000$ g m^{-3} to substantial amounts of $\overline{C}_{\sum,m,bed}(T_0) = 8000$ g m^{-3} (Figure 5.7). An indicator for substantial suspension is the occurrence of a maximum resultant combined wave-induced velocity $U_{W,max}$ higher than 0.4 m s^{-1}.

What remains in the water column after settling of the short-lived suspension peak of sandy sediments, is the suspended load. Figure 5.8 shows the suspended silt concentration added to the suspended load after a ship passage. 16 ship events resulted in the dislodgement of fine-grained, silty bank particles. Thereof, 2 ship events consisted of 2 closely following or crossing ships, of which the crossing of 2 ECMT-Va ships is the most remarkable.
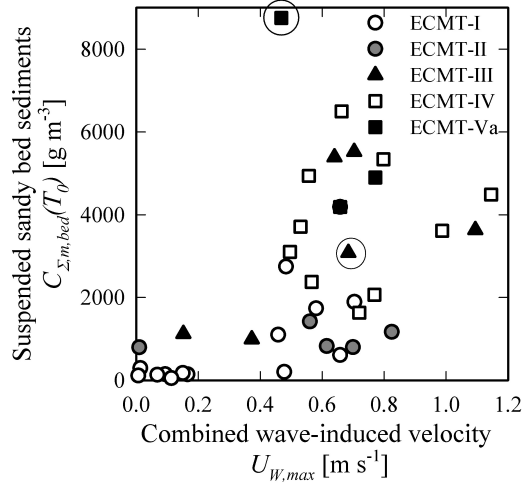
Figure 5.7: Cumulative depth-averaged concentration of suspended bed sediments $\overline{C}_{\Sigma,m,bed}(T_0)$ due to a ship passage in relation to its maximum combined wave-induced velocity $U_{W,max}$, categorized by ECMT-class. An indicator for substantial suspension is the occurrence of a maximum resultant combined wave-induced velocity $U_{W,max} \geq 0.4\,\mathrm{m\,s}^{-1}$. (Encircled values are the 'compound' events, assigned to the ECMT-class of the largest ship).
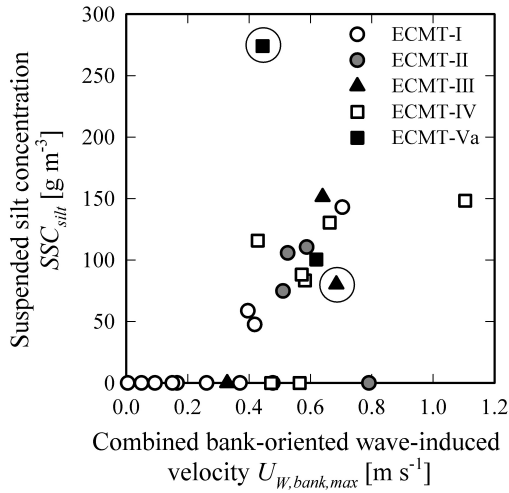

Figure 5.8: Amount of suspended silty bank sediments SSC_{silt} due to a ship passage in relation to its maximum combined bank-oriented wave-induced velocity $U_{W,bank,max}$, categorized by ECMT-class. When the bank-oriented wave-induced velocity exceeds $0.4\,\mathrm{m\,s}^{-1}$, this might lead to a dislodgement of silty bank sediments, which tends to be linearly correlated with this velocity's maximum. (Encircled values are the 'compound' events, assigned to the ECMT-class of the largest ship).

Although ships of all ECMT-classes are able to cause a dislodgement of silty bank sediments (ECMT-class I, II and III because of high sailing speeds V_s), suspension of silty bank sediments is in half of these 16 ship events the result of ECMT-IV or Va ship passages. The amount of these suspended sediments is considerably lower than the suspended quantities of bed sediments. When the maximum bank-oriented combined wave-induced velocity $U_{W,bank,max}$ exceeds $0.4\,\mathrm{m\,s^{-1}}$, this might lead to a dislodgement of silty bank sediments, which tends to be linearly correlated to the velocity's maximum. The angle at which the resultant combined wave-induced velocity attacks the river bank is unimportant for this dislodgement process.

5.4.5 Direction and magnitude of ship-induced sediment transport

Substantial amounts of sandy bed sediments are (re)suspended due to a ship passage but these suspension events do not necessarily lead to a significant net sediment transport. Cumulative crosswise sediment transport over the duration of a ship's hydrodynamic disturbance T_0 might result in both bed accretion and erosion behind the off-bank timber piling (Figure 5.9). Although ships of all ECMT-classes (except ECMT-I) are able to cause, to some extent, suspended sediment transport, significant (yet in absolute values relatively small) net crosswise sediment transport is only effected by ships of ECMT-IV and Va.

6 ship passages lead to transported bed sediment quantities of more than $Q_{\sum,m,bed}(T_0) = 200\,\mathrm{g\,m^{-1}}$. A maximum crosswise wave-induced velocity $u_{Y,W,max} = \pm\,0.3\,\mathrm{m\,s^{-1}}$ tends to indicate a higher suspended sediment transport. The direction of crosswise sediment transport is determined by the ratio between the 'primary' wave-induced displacement flow (during the drawdown Δh, and oriented towards the fairway) and its slope supply flow (during the transversal stern wave H_{stern}, and oriented towards the river bank). 'Secondary' wave-induced velocities rather redistribute the suspended sediments. Over the 3-day measurement campaign, the balance of the bed sediment budget is negative for the shallow water area behind the off-bank timber piling. 800 g of sandy bed sediments are carried away towards the fairway over a unit alongstream length, which amounts to 128 kg over the total length (160 m) of this nature-friendly bank protection (cf Section 3.3).

Dislodged silty bank particles are entrained after 16 ship passages, from which follows their downstream advection (Figure 5.8). The overall amount of dislodged silty bank particles adds up to $1800\,\mathrm{g\,m^{-3}}$ for the 3-day measurement campaign.

Sediment transport towards the fairway is considered as a proxy for bed and bank erosion. Both processes did occur; silty bank particles were dislodged, and the balance of the sandy bed sediment budget was negative. The estimated order

of magnitude values suggest that the off-bank timber piling does not maintain a 'controlled' bed erosion and accretion.
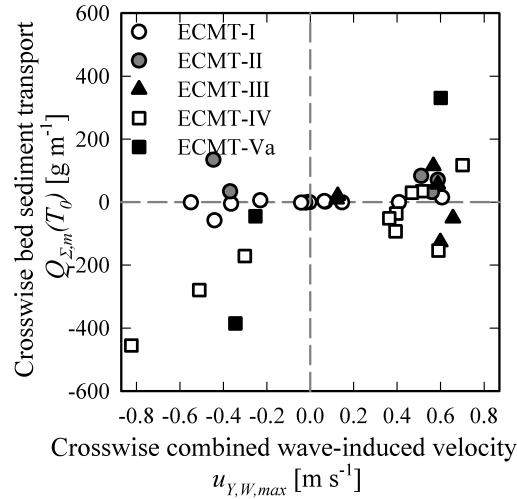

Figure 5.9: Crosswise suspended sediment mass transport $Q_{\sum,m,bed}(T_0)$ due to a ship passage (positive towards the river bank, negative towards the fairway) in relation to the maximum crosswise wave-induced velocity $u_{Y,W,max}$, categorized by ECMT-class. When $u_{Y,W,max} \geq |0.3|\,\mathrm{m\,s^{-1}}$, significant higher suspended sediment transport is observed, resulting in both accretion and erosion of the river bed behind the off-bank timber piling.

5.5 Discussion

Bed sediments are mainly entrained and pumped into the water column during the formation of the drawdown trough. The partly superimposed ship wave patterns cause the (re)suspension of substantial quantities of bed sediments, as reported by Bauer et al. (2002); Houser (2011); Osborne and Boak (1999). Once the sandy bed particles are dislodged and entrained because of critical shear exceedance, bed sediments are instantaneously dispersed through the water column by increased turbulent kinetic energy levels and wave orbital velocities, which both hamper sediment settling (illustrated in Figure 5.2C). The cumulative depth-averaged concentration of suspended bed sediments $C_{\sum,m,bed}(T_0)$ depends however only on the magnitude of combined wave-induced velocities U_W (cf equation 5.12).

Still, the variability in this cumulative depth-averaged concentration $\overline{C}_{\sum,m,bed}(T_0)$ is not entirely described by these parameters. In addition to the natural variability due to the stochastic character of turbulence under wave groups

(Vincent and Hanes, 2002), it is suggested that sediment availability influences the amount of suspended bed sediments as well (Figure 5.10). A prolonged duration of critical shear exceedance $t > \tau_{cr}$ extends the duration of increased suspended sediment concentrations at the location of SSP A. If the duration of critical shear exceedance lasts more than 40 s however, the positive correlation tends to reverse. The duration of increased suspended sediment concentrations drops back for a longer exceedance time of the critical shear threshold. This counterproductive effect took place during the passage of fully loaded and slow sailing ECMT-IV and Va ships. Sediments being suspended and again deposited form a loose top bed layer, more susceptible to resuspension than sediments of the undisturbed bed layer.

This behaviour of reduced sediment suspension is also observed when two ships of similar dimensions follow one another closely, as the latter gives rise to a considerably smaller quantity of suspended bed sediments $\overline{C}_{\sum,m,bed}(T_0)$. Such a reduced or limited sediment supply is also documented by Althage (2010); Houser (2011); Ravens and Thomas (2008); Schoellhamer (1996); Verney et al. (2007).

The maximum ship wave shear stress $\tau_{W,max}$ points out an enlarged availability of bed sediments (Figure 5.11). As from a ship wave shear stress exceeding $1\,\mathrm{N\,m^{-2}}$, substantial higher amounts of suspended sandy bed sediments are noticeable for the heights $z = 0.1\,\mathrm{m}$, $0.2\,\mathrm{m}$ and even, to some extent, $0.3\,\mathrm{m}$ above the river bed. This shear threshold value $\tau_{cr,new} = 1\,\mathrm{N\,m^{-2}}$ describes more accurately the critical shear stress, necessary to initiate motion of the undisturbed bed layer. Lower ship wave shear stresses lead to a rather fixed maximum level of suspended sediments, suggesting that only resuspension of the loose top bed layer takes place. Ships of ECMT-class IV and Va always induce shear stresses τ_W higher than $1\,\mathrm{N\,m^{-2}}$, those of ECMT-class III and II as well on the condition of laden draught.

The shallow water area behind the off-bank timber piling gives rise to non-linear transformations in the ship-generated waves and the confined dimensions of the waterway imply that the 'primary' wave pattern dominates the ship wave signature. On that account, the direction of crosswise sediment transport is determined by the relative importance of the drawdown Δh to the transversal stern wave H_{stern}. The former is accompanied by a return current u_r and displacement flow, the latter is (frequently) accompanied by a significant slope supply flow.

The magnitude of these 'primary' wave-induced velocities shows linear coherency with the ship displacement Δ, sailing speed V_s, relative transversal stern wave height $H_{stern}\,h^{-1}$ and sailing distance from the off-bank timber piling y, of which the first two are the key parameters (cf equation 5.11). They determine the ratio between the ship's sailing resistance (cf blockage coefficient m) and its sailing speed V_s.

This is in line with previous research of Ten Brinke et al. (2004), who con-
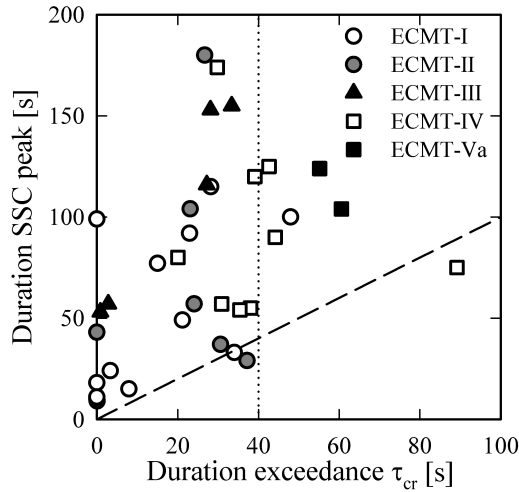
Figure 5.10: Duration of the peak of increased suspended sediment concentration due to a ship passage (at location SSP A) compared to the duration of exceedance of the critical shear stress τ_{cr}. The dotted line indicates $t > \tau_{cr} = 40\,\mathrm{s}$.
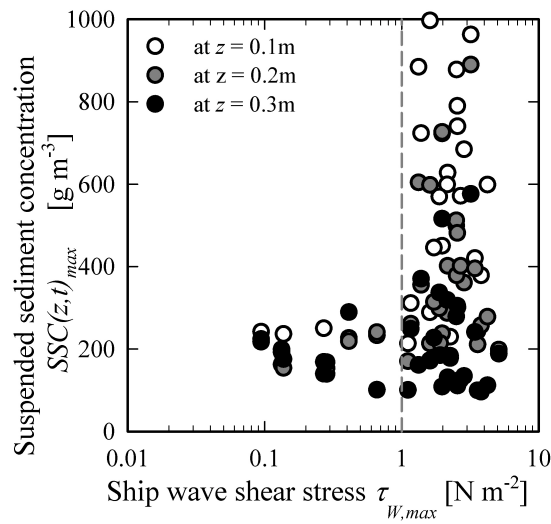

Figure 5.11: Maximum suspended sediment concentration $SSC(z,t)_{max}$, measured on different heights z above the river bed (at location SSP A) compared to the maximum ship wave shear stress $\tau_{W,max}$. The grey dashed line indicates the transition value $\tau_{cr,new} = 1\,\mathrm{N\,m^{-2}}$ to significant suspension of bed sediments.

cluded that the ship displacement Δ and the distance between sailing line and river bank y are the steering parameters for sediment transport. Schoellhamer (1996) too stresses the importance of sailing speed V_s (using the depth-based Froude number Fr_d) and blockage coefficient m, to which Rapaglia et al. (2011) added the ship's length L (thus, taking into account the ship displacement Δ) and the (shallowness of) the water depth h. Although resuspension of bed sediments is caused by nearly all shipping traffic, net crosswise sediment transport is only significant for ECMT-IV and Va ships, which have a length L larger than 80 m, and the largest blockage coefficient m. In the less-confined Rhine, Ten Brinke et al. (2004) found ship-induced erosion mainly for ships longer than 60 m, which indicates once more the sensitivity of these governing ship parameters.

Summarizing, it may be stated that a ship's main variables length L, beam B, draught D, which define its displacement Δ and blockage coefficient m, and its sailing speed V_s, do not vary independently for one another. Their interconnection, reflected by the subdivision of inland navigation in standard ECMT-classes, dictates a ship's hydrodynamic forcing, together with the waterway's boundary conditions.

The contribution of ship-generated waves to sediment transport is found to be significant by a.o. Bauer et al. (2002); Houser (2011); Rapaglia et al. (2011); Verney et al. (2007). Results on the magnitude and direction of sediment transport are however very dependent on the local boundary conditions (confinedness of waterway, bathymetry, ship types, sediment types), which are different for this field study. A direct comparison with these results is therefore not feasible.

5.6   Conclusion

Ship-induced hydro- and sediment dynamics were monitored for 46 ship passages along the measurement transect of the fixed monitoring system during a 3-day measurement campaign from April 13-15, 2011. This short-term field study aimed at quantifying the magnitude of ship-induced hydrodynamic forcing and its relative importance to sediment dynamics in the shallow water area behind the off-bank timber piling.

As elaborately described in Chapter 4, the confined dimensions of the waterway amplify a ship's 'primary' wave pattern, which is reflected in its wave-induced velocity components. The maximum resultant of the 'primary' wave-induced velocity $U_{LP,max}$, which mainly depends on a ship's sailing speed V_s and displacement Δ, is significantly higher than the 'secondary's maximum resultant $U_{SP,max}$. Maximum values for these resultant maxima are about $U_{LP,max} = 1.0\,\mathrm{m\,s^{-1}}$ and $U_{SP,max} = 0.4\,\mathrm{m\,s^{-1}}$ respectively. The enlarged 'primary' wave pattern strongly influences the combined wave-induced velocity U_W, and often dictates the angle of attack of its maximum resultant. Maximum values for the resultant combined

wave-induced velocity amount to $U_{W,max} = 1.1\,\mathrm{m\,s^{-1}}$.

The 'secondary' wave pattern induces however the highest wave shear stresses because of its shorter wave period and correspondingly larger wave friction factor. Maximum values for the maximum 'primary' and 'secondary wave-induced shear stresses are up to $\tau_{LP,max} = 2.5\,\mathrm{N\,m^{-2}}$ and $\tau_{SP,max} = 4.1\,\mathrm{N\,m^{-2}}$ respectively, and the resulting combined ship wave shear stress amounts maximally to $\tau_{W,max} = 5.1\,\mathrm{N\,m^{-2}}$. As from a combined ship wave shear stress $\tau_W \geq 1\,\mathrm{N\,m^{-2}}$, an enlarged sediment availability is observed, i.e. sediments of the undisturbed bed layer become dislodged. This higher shear stress value describes more accurately the actual critical shear stress necessary to initiate motion of the undisturbed bed layer, and is therefore the new critical shear threshold $\tau_{cr,new}$ instead of $\tau_{cr} = 0.16\,\mathrm{N\,m^{-2}}$.

Exceedance of the critical bed shear stress might lead to suspension of bed sediments. The cumulative quantity of suspended sandy bed sediments ranges from a moderate suspension of $\overline{C}_{\sum,m,bed}(T_0) = 1000\,\mathrm{g\,m^{-3}}$ to substantial amounts of $\overline{C}_{\sum,m,bed}(T_0) = 8000\,\mathrm{g\,m^{-3}}$. Large differences in suspended quantities are observed between and within the ECMT-classes, but the occurrence of a maximum resultant combined wave-induced velocity $U_{W,max} \geq 0.4\,\mathrm{m\,s^{-1}}$ is an indicator for substantial suspension. Dislodgement of silty bank particles might take place when the maximum bank-oriented combined wave-induced velocity $U_{W,bank,max}$ exceeds $0.4\,\mathrm{m\,s^{-1}}$. The added suspended silt concentration due to a ship passage amounted to maximum $SSC_{silt} = 270\,\mathrm{g\,m^{-3}}$ (because of the crossing of 2 ECMT-Va ships).

Based on the study area characteristics, dislodgement of silty sediment directly implies their advection downstream. For the sandy bed sediments however, suspension does not necessarily lead to a net sediment transport. Significant (yet in absolute values relatively small) net crosswise sediment transport occurred due to the passage of 6 ECMT-IV and Va ships, which caused a sediment transport of $Q_{\sum,m,bed}(T_0) \geq 200\,\mathrm{g\,m^{-1}}$. The direction of crosswise sediment transport is determined by the ratio between the 'primary' wave-induced displacement flow (during the drawdown, and oriented towards the fairway) and its slope supply flow (during the transversal stern wave, and oriented towards the river bank). 'Secondary' wave-induced velocities rather redistribute the suspended sediments. Over the 3-day measurement campaign, 128 kg sandy bed sediments were carried away over the total length (160 m) of the nature-friendly bank protection.

Sediment transport towards the fairway was considered as a proxy for bed and bank erosion. Both processes did occur; silty bank particles were dislodged, and the balance of the sandy bed sediment budget was negative. Notwithstanding the uncertainties inherent in sediment calculations, and the short duration of the measurement campaign, these estimated order-of-magnitude values for suspended sediment transport suggest that the off-bank timber piling does not maintain a 'con-

trolled' (cyclic) bed erosion and accretion, and does not prevent bank erosion. A reduction of the combined wave-induced velocity to $U_W < 0.4\,\mathrm{m\,s^{-1}}$ behind the off-bank timber piling is required to achieve a significant decrease in sediment dislodgement, (re)suspension and transport for both sediment sources.

6

Effectiveness of the nature-friendly bank protection to obviate bed and bank erosion

6.1 Introduction

Bank erosion and retreat is a point of interest and concern along navigable waterways, being studied in a variety of environmental boundary conditions (Bauer et al., 2002; Houser, 2010; Hughes et al., 2007). It decreases their structural integrity and increases the likelihood of failure (Ellis et al., 2002). Identifying the processes of bank erosion and the key contributing factors is a difficult challenge, particularly in such man-modified environments, where bank response may be triggered by ecological and hydrodynamic forces acting over a wide range of spatial and temporal scales (Houser, 2010).

In non-tidal and restricted fetch waterways, i.e. where wind wave energy is low, failure of revetments, dikes or river banks is known to be the result of forces related to extreme weather events (storms, flooding) and ship wave action (e.g. Bauer et al. (2002); Dorava and Moore (1997)). When shipping traffic is heavy and the sailing line is in the proximity of a shallow water area, ship-generated waves have the potential to erode the river bed and bank (Bauer et al., 2002; Nanson et al., 1994; Parnell et al., 2007; Verney et al., 2007).

The more confined a waterway is in depth and width, the higher the erosive potential of ship-generated waves (Nanson et al., 1994). The admissible ratio of

waterway cross section to ship cross section, i.e. the blockage coefficient m, is then fully exploited and the large frictional resistance results in a correspondingly high bank load (PIANC, 2008). Generally, the rate of bank erosion is linked with the ship wave height and corresponding wave energy or flux (Bauer et al., 2002; Dorava and Moore, 1997; Ellis et al., 2002; Houser, 2010; Hughes et al., 2007; Nanson et al., 1994).

The particular design of the nature-friendly bank protection under study consists of a double wave attenuating configuration: (i) the off-bank timber piling, and (ii) the reed belt before the river bank. To assess the effectiveness of this type of nature-friendly bank protection, the performance of its design must be evaluated against the two main external hydrodynamic forcing parameters, i.e. flooding events and ship wave action. In particular, it is important to evaluate its hydrodynamic performance against ship-induced hydrodynamic forcing.

To this end, the objectives to be met are twofold: (1) is there a difference in bank erosion rate between the nature-friendly protected and the non-protected natural river banks; (2) if progressive bank erosion still takes place, is shipping traffic the system-driving parameter?

This chapter addresses the results of two quantitative field studies. To meet objective (1), a long-term topographic survey was carried out to compare morphological changes of the riverine environment given its nature-friendly protection or naturally eroding bank condition, and to identify controls and triggers of river bank retreat. To meet objective (2), a short-term study was conducted to estimate the importance of an individual ship's wave action on bed and bank erosion in a nature-friendly protected bank area. To conclude, it is verified whether short and long-term morphological changes can be linked with one another.

6.2   Methodology

6.2.1   Long-term topographic survey

Measurement of cumulative bank retreat over long periods is undertaken using standard topographic measurement equipment. Morphological changes are bi-monthly surveyed over one seasonal cycle, from October 2009 to September 2010, with a Total Station (Sokkia SET510k, having an accuracy of $1\text{-}3\cdot10^{-3}$ m). Initially, 3 locations where a nature-friendly bank protection was installed and 3 naturally eroding river bank embayments were selected. Of these locations, one site differed in that the naturally eroding river bank became nature-friendly protected during the survey period (since Dec 2009). Because of this anomaly, it was decided to disregard this site. Table 6.1 gives an overview of the environmental characteristics of the used locations.

At every location, a time series of xyz-coordinates is obtained for the top and

Figure 6.1: Riverine environment along the Lys. A. Nature-friendly bank protection consisting of off-bank timber piling, which separates the fairway from the shallow water area, and a reed belt (white dashed circle), planted at the base of the cut-bank (survey location 3). B. Naturally eroded embayment because of undermining and breaking of the armoured concrete revetment (survey location 5). Dashed line illustrates a surveyed transect on which the markers indicate 1. Top of the cut-bank, 2. Base of the cut-bank and 3. Edge of the foreshore and end of the reed belt.

Table 6.1: Environmental characteristics of the bimonthly surveyed locations during the long-term topographic study

	Initial length of embayment (curved) [m]	Height of cut-bank [m]	Nature-friendly protected?	Vegetation type at water line	Initial coverage by reed at water line [%]	Upper surface of river bank	Transects
Location 1	17.01	3.98	yes	reed	60	grass & woody shrub	R1: reed
							R2: no reed
Location 2	27.34	3.57	yes	reed	60	grass & woody shrub	R3: reed
							R4: no reed
Location 3	47.41	3.68	yes	reed	30	grass	R5: reed
							R6: no reed
Location 4	9.77	3.18	no	weeds and perennials		grass	R7: gradual vegetated slope
							R8: vertical cut-bank
Location 5	12.80	3.35	no	weeds and perennials		grass & woody shrub	R9: gradual vegetated slope
							R10: vertical cut-bank

bottom of the cut-bank and, if present, the edge of the foreshore at its base (composed of slumped bank material) in order to monitor the topographic evolution of the semi-circular embayment. The top was defined as the limit of the stable, vegetated upper area, i.e. overhanging vegetation or grass sods are not taken into account. The bottom of the cut-bank is marked as its intersection with the sandy beach or foreshore, ignoring slump blocks or disjointed reed patches. Measurements were irregularly spaced from one another, with the purpose that linear interpolation between the points closely reproduces the morphological features. The contours of the reed belt and patches were surveyed as well. Undercutting of the cut-bank and the presence of slump blocks are documented with photographs but not measured.

Within every embayment, two different transects, cross sectional to the waterway, were selected to monitor in detail the morphological response of the (unprotected) river bank given varying environmental boundary conditions. As selection criterion in the nature-friendly protected embayments, transects with and without reed belt at the base of the cut-bank are marked, whereas transects in naturally eroding embayments are designated based on difference in slope and vegetation cover of the cut-bank. Figure 6.1 illustrates the survey methodology.

The change in area of a transect is calculated using the trapezoidal integration method. It is attempted to relate these eroded areas to various parameters and to identify thresholds for acting morphological changes.

6.2.2 Short-term assessment of bed and bank erosion caused by an individual ship's wave action

While long-term observation of morphological changes and cumulative bank retreat is easily realized using topographic surveying techniques, it is difficult to measure accurately bed and/or bank erosion due to an individual ship's wave action. Analytical methods are therefore an interesting option to evaluate the importance of an individual ship passage to erosion.

The 3-day measurement campaign, carried out to analyse ship-induced hydro- and sediment dynamics (Chapter 5), took place in the nature-friendly bank protection where transects R1 and R2 of the long-term topographic study are located. Making use of these high-frequency turbidity and velocity data, it is aimed at analytically obtaining an estimation of bed and bank erosion depths due to a single ship event. To this end, data of SSP A is used for the calculation of bed erosion depths and data of SSP B for the calculation of bank erosion depths.

6.2.2.1 Analytical approach for estimation of bed and bank erosion depths

Adapting the analytical approaches of Bauer et al. (2002), an estimation of ship-induced bed and bank erosion rates is acquired using a simplified erosion equation.

A few important assumptions must therefore be taken into account: 1. sediments are uniformly stripped from river bed or bank, 2. upstream sediment contributions as well as from other erosive processes are negligible, 3. local sedimentation does not take place during the time frame under study, 4. measured suspended sediment and velocity data are representative of average conditions in the control volume (for more details regarding these simplifications, see Bauer et al. (2002)). Figure 6.2 provides a schematized overview of the equipment deployment on the cross sectional measurement transect, with indication of the variables used for calculation of river bed and bank erosion depths.

We applied a different methodology for calculation of erosion depths, depending on the sediment grain size ((fine) sand or silt). Bed soil analysis, indicating a sandy top layer of the river bed (cf Section 3.3.2), supports the assumption that, once dislodged, the finer silty fraction of the river bank stays in suspension and will be advected downstream. Entrainment of sandy bank particles results in near-bank settlement and deposition, where they become part of the top bed layer. Their contribution is here indirectly taken into account in the bed erosion depth estimates.

Erosion of silty bank sediments is determined by difference in *pre* and *post* ship passage concentrations of suspended sediments. A ship passage adds silty bank sediments to the suspended load when the *post* ship passage suspended sediment concentration is higher than the *pre* ship passage concentration. This *pre* concentration corresponds to the suspended load averaged over a 15 min time frame before a ship passage, the *post* concentration is determined after turbulence due to ship-induced hydrodynamic forcing settled down. Rather than a time rate of change in bank retreat, an overall value for the depth of the uniform stripped silty layer ED_{bank} [m] after a ship passage is calculated as (Bauer et al., 2002):

$$ED_{\mathrm{bank}} = \frac{SSC_{silt} \cdot V_C}{CA_{\mathrm{bank}} \cdot \rho_{\mathrm{silt}}} \qquad (6.1)$$

where SSC_{silt} is the added suspended sediment concentration [$\mathrm{g\,m^{-3}}$] in the control volume V_C, measured on height $z = 0.10\,\mathrm{m}$ above the river bed (with SSP B), and ρ_{silt} is moist bulk density of silty sediments, here $\rho_{\mathrm{silt}} = 1.5{\cdot}10^6\,\mathrm{g\,m^{-3}}$ (NRCS, 2012). The contributing bank area CA_{bank} consists of a unit alongstream width [m] times the average local daily water depth [m]. The control volume V_C [$\mathrm{m^3}$] encloses the water volume through which the sediments are dispersed, defined by the contributing bank area and perpendicular bed distance between river bank and SSP B (here: 2 m).

The erosive potential of the grouped ship wave structure is analysed by its wave energy E [$\mathrm{J\,m^{-2}}$] towards the river bank. Given that a ship's 'primary' and 'secondary' wave patterns are often superimposed in confined waterways, this widely used parameter grasps tersely their forcing characteristics:
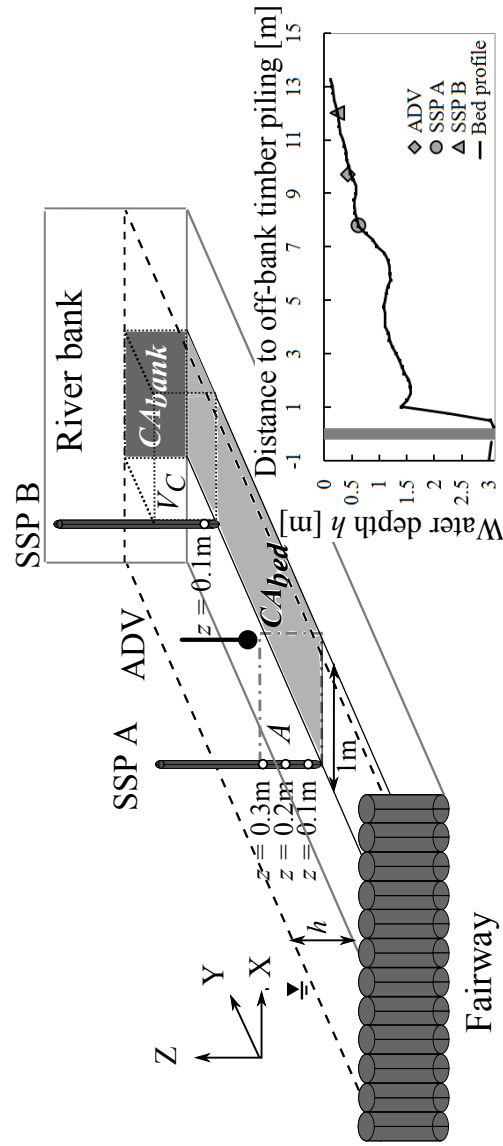
Figure 6.2: Schematized overview of the equipment deployment on the measurement transect of the fixed monitoring system (survey location 1), and the cross sectional bed profile, with indication of the variables used for calculation of river bed and bank erosion depths (cf equation 6.1 and 6.4).

$$E = 1/8\rho g H_{in}^2 \qquad (6.2)$$

where ρ is fluid density, here for water: $\rho = 1 \cdot 10^6 \, \text{g m}^{-3}$ and g is gravitational acceleration [m s^{-2}]. Making use of linear wave theory with a shallow water approximation (similar to Bauer et al. (2002); Houser (2010)), an index wave height H_{in} is calculated for every ship passage:

$$H_{in} = \frac{2U_{\text{W,bank,max}}}{\sqrt{g/h_{ADV}}} \qquad (6.3)$$

where $U_{W,bank,max}$ is the maximum of the combined bank-oriented wave-induced velocity [m s^{-1}] and h_{ADV} is the average daily water depth at the ADV [m].

Bed erosion is linked to the magnitude of bed sediment discharge caused by a ship passage. Within the time frame of ship-induced hydrodynamic disturbance T_0, turbulent water motions are intense because of high kinetic energy levels, and suspended sediment transport is solely driven by ship wave-induced velocities. As a result, an estimate of the total erosion depth ED_{bed} [m] after a ship passage is calculated from the cumulative suspended sediment volume transport $Q_{\sum,s,bed}(T_0)$ [m^3] through a vertical plane A parallel to the river bank and perpendicular to the crosswise wave-induced velocity $u_{Y,W}$ (Bauer et al., 2002):

$$ED_{\text{bed}} = \frac{Q_{\sum,s,bed}(T_0)}{CA_{\text{bed}}} \qquad (6.4)$$

where CA_{bed} is the contributing bed area [m^2], it encompasses the product of perpendicular bed distance between river bank and SSP A (here: 6.5 m) and a unit alongstream width [m]. The cumulative suspended sediment volume transport $Q_{\sum,s,bed}(T_0) = \int_0^{T_0} q_{s,bed}(t)dt$, in which $q_{s,bed}(t)$ is the suspended sediment volume transport at time t [m^3 s^{-1}], calculated as:

$$q_{s,bed}(t) = \frac{q_{m,bed}(t) \cdot A}{\rho_{\text{sand}}} \qquad (6.5)$$

in which $q_{m,bed}(t)$ is the crosswise sediment mass flux [g m^{-2} s^{-1}] through a vertical plane A [m^2], which has a height equal to the water depth at SSP A $h_{SSP\,A}$ [m] and a unit alongstream width [m]; and ρ_{sand} the moist bulk density of sandy sediments, here $\rho_{\text{sand}} = 1.65 \cdot 10^6 \, \text{g m}^{-3}$ (NRCS, 2012).

The time-dependent suspended sediment mass transport $q_{m,bed}(t)$ is the product of back and forth crosswise wave-induced velocities $u_{Y,W}$ (measured with the

ADV) and average suspended sediment concentration over the water column (measured with SSP A) (cf equation 5.8). It accounts for the instantaneaous direction of sediment transport, identifying bed erosion or accretion behind the off-bank timber piling.

Note that the bed distance affected by a ship passage depends on the magnitude of the ship-generated wave patterns. For consistency in the calculation of uniform bed erosion depths, it is in this simplified approach always taken equal to 6.5m (although it might be smaller in reality).

6.3   Results

6.3.1   Rate and mechanisms of river bank retreat

The rate of river bank retreat depends on the processes that act to destabilise and erode the river bank and the processes that remove slump blocks accumulated at the base of the river bank (Nanson et al., 1994). Figure 6.3 shows the total eroded area for all transects over the surveyed seasonal cycle. Except for transect R6, areal loss amounts to maximum 5 m^2. No clear distinction in eroded area between nature-friendly protected and naturally eroding embayments is found. Transects R1, R7, R8 and R10 have comparable absolute areal losses, as do transects R3, R4 and R9. Within site variability in total eroded transect area is only noticeable for locations 3 and 5, despite the marked between-transect differences for every location.

The bimonthly rate of change in eroded area differs between the measurement periods and displays a rather erratic behaviour (Figure 6.5). Again, no distinct dissimilarities in erosion intensity between nature-friendly protected and naturally eroding sites are observed, apart from the singular results for transect R6. Erosion seems to increase during winter months (period December-March) for the transects without reed, giving the highest areal losses for transects R2, R7, R8 and R10. The start of spring (period March-May) initiates a reduction in erosion rates as vegetation regrowth takes place and weather conditions become less severe. No correlation was however found between these periodic erosion rates and seasonal varying climatic parameters (listed in columns 2 - 5 of Table 6.2).

Basically, two distinct retreat mechanisms are observed in the surveyed embayments: 1. sediment wash out of the rhizome layer and destabilisation of the reed fringe for reed belt areas and 2. undermining of the cut-bank and (partial) mass failure for non-reed belt areas, irrespective of installation of a nature-friendly bank protection. The observed rate of bank retreat varies widely within the embayments, where it is linked to the type of erosive process. In addition, spatial heterogeneity in natural properties (e.g. sediment composition, saturation) interferes undoubtedly, adding variability to the location-dependent erosion rate.
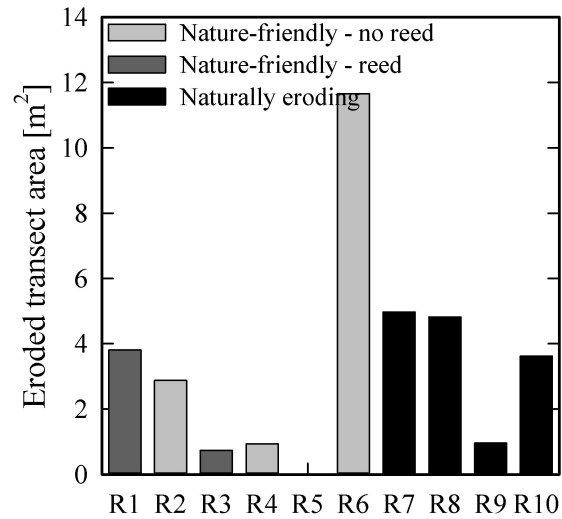
Figure 6.3: Total eroded area of all transects over the surveyed seasonal cycle (Oct 2009 - Sep 2010), with indication of nature-friendly protected or naturally eroding status; subdivision between nature-friendly protected reed and non-reed belt transects.
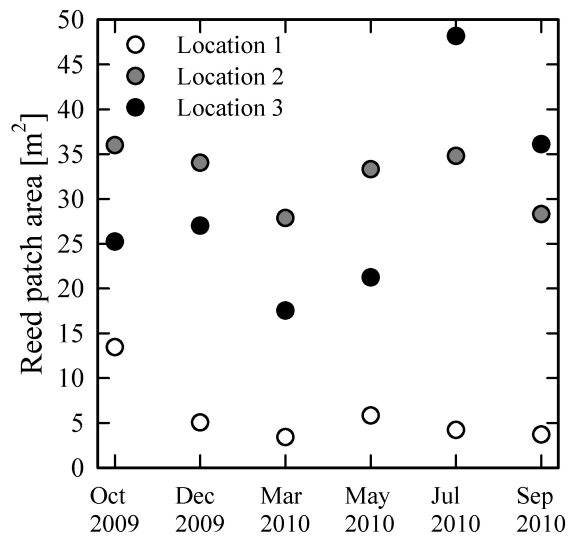

Figure 6.4: Bimonthly evolution of combined reed belt and reed patch area in the surveyed nature-friendly protected locations.
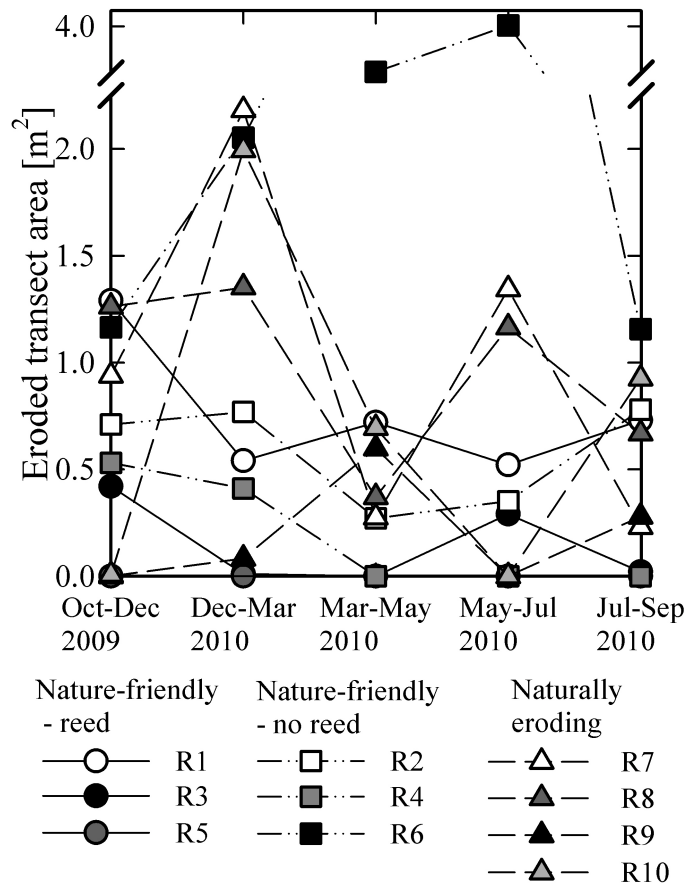
Figure 6.5: Bimonthly rate of change in eroded area of all transects, with indication of nature-friendly protected or naturally eroding status; subdivision between nature-friendly protected reed and non-reed belt transects. No distinct dissimilarities in erosion intensity between nature-friendly protected and naturally eroding sites are observed, apart from the singular high results for transect R6 (location 3).

Table 6.2: Overview of periodic climatic and hydrodynamic parameters over the survey period October 2009 - September 2010

	Average temperature [°C] [*]	Precipitation [mm] [*]	Days of frost [-]	Days of flooding [-]	Number of ship passages [**]
Oct - Dec 2009	10.09	215.73	0.00	4.58	2699
Dec - Mar 2010	2.26	179.20	26.94	9.25	3967
Mar - May 2010	10.75	65.26	1.08	0.08	3205
May - Jul 2010	19.13	73.79	0.00	0.29	4187
Jul - Sep 2010	19.52	292.70	0.00	2.33	2895

[*] source: HIC (1983-2012)
[**] source: W&Z (2009-2011)

Retreat mechanism 1 is linked with the seasonal growth cycle of reed (Figure 6.4). Reed decay and dieback result in reduction of the tensile root strength and the mechanical stem resistance during winter months. In spring, new reed sprouts shoot and regrowth takes place but re-establishment of a dense reed belt only occurs on the condition that areal decrease during winter months was kept within limits (location 2 (R3) and 3 (R5)). In destabilised areas (location 1 (R1), deterioration of the natural reed belt defense continues, reed patches detach and the reed belt fragments. It was not longer situated in transect R1 from July 2010 onward.

Retreat mechanism 2 is a commonly observed phenomenon along natural river banks (e.g. Dorava and Moore (1997); Nanson et al. (1994)). A vertical cut-bank's lower part, subject to wave- and current-induced forcing, is undermined and concavely erodes. Mass or beam failure result from (parts of) the overhanging river bank. A gradual bank slope installs and detached slump blocks form debris at the base of the sloping cut-bank. This slumped material creates an extra protection of the river bank until removal. Next, the sloping river bank steepens again and a vertical cut-bank arises. Its nature implies that this cyclic trend occurs randomized. Certain conditions might favour bank destabilisation but the bimonthly observations pointed out that mass movement of substrate blocks does not directly follow.

Horizontal retreat of the grass covered upper surface of the cut-bank is mainly controlled by the presence of woody shrub, of which the root system largely reinforces the soil. Mass movement of substrate blocks does not directly result in failure of the entire 'overhanging' river bank. First, the rooted area stays intact and forms an (enlarging) overhanging sod, which eventually fails. Horizontal retreat of the top is however greatly put off (Figure 6.6, location 1, 2, 4 and 6). Horizontal retreat of the cut-bank in the bank-water zone is controlled by the retreat mechanism. A cyclic back and forth behaviour takes place in case of undermining and bank collapse whereas a steadily retreat is measured for reed belt areas.
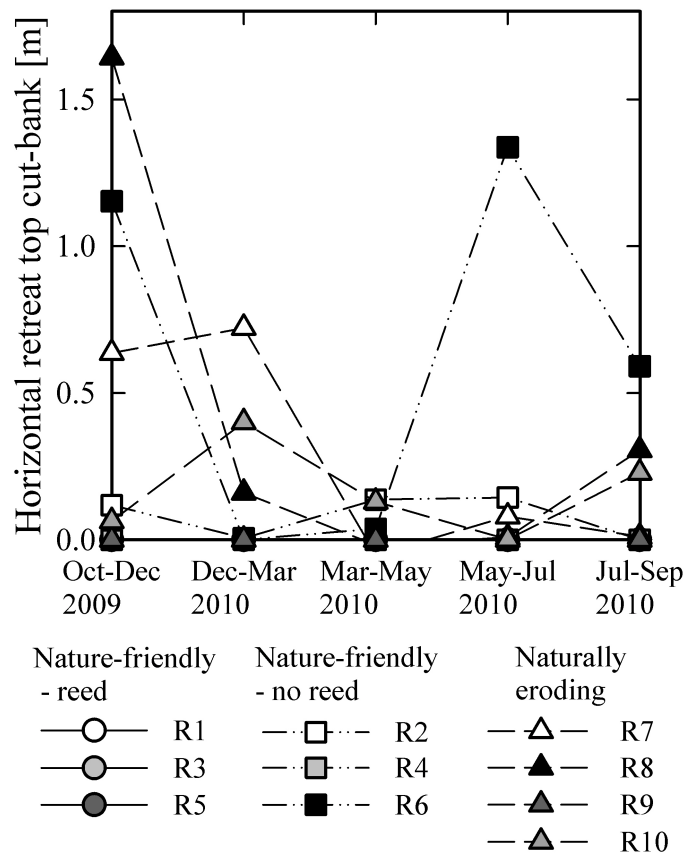
Figure 6.6: Bimonthly horizontal retreat of the top of the cut-bank. Presence of woody shrub (at location 1, 2 and 5) slowed down the retreat of the river bank's upper surface.

6.3.2   Triggers and controls of river bank retreat

River bank retreat might be triggered and controlled by internal and external forces acting over a wide range of spatial and temporal scales (Almeida et al., 2011; Houser, 2010). This hampers any attempt to identify key contributors to bank erosion processes and to define thresholds marking major changes in bank response. Because (in)stability of the upper bank surface contributes to the absolute eroded transect area, horizontal retreat of a transect in the bank-water contact zone is considered as dependent variable to hydrodynamically induced bank erosion. Note that for reed belt transects (R1, R3, R5), the horizontal retreat of the reed fringe is considered.

Given that the Lys is a confined, non-tidal waterway, flooding and ship wave action are considered as external forcing parameters. Flooding events occurred sporadically throughout the surveyed year, i.e. the water level raises to +6.1 m TAW whereby the off-bank timber piling becomes submerged (HIC, 1983-2012), but they are not correlated with the time rate of change in eroded area (Figure 6.7). The punctual disturbance that a ship passage causes locally is taken into account by the number of ship passages over a bimonthly survey period. No correlation is found between the amount of shipping traffic and the bank's response for both nature-friendly protected and naturally eroding locations (Figure 6.8). These external triggers are thus not directly reflected in morphological changes on the transects, and this for both the retreat mechanisms. Short-term changes like the removal of slumped debris can however be attributed to ship-induced hydrodynamic forcing. Significant flooding events only took place in the periods October-December 2009 and December 2009-March 2010 whereas removal of slumped material and horizontal retreat in the bank-water contact zone occurred within every survey period. This infers that ship wave action is able to entrain these sediments.

A controlling parameter for bank erosion and retreat might be the bank's distance to the fairway (Figure 6.9). It is evaluated whether this distance at a certain moment (time i) influences the horizontal retreat of a transect until the following survey (time $i+1$). In general, no distinct correlation between these variables is observed; horizontal retreat persists independent of a distance change. Protection of the cut-bank's base with a reed belt shifted direct ship wave action to this area and prevented hydrodynamic forcing to reach the vertical cut-bank over the surveyed period (transects R1, R3 and R5). However, reed belt deterioration was observed except for location 3 (R5), which remained unaffected throughout the surveyed period. Although a reduced cyclic retreat is noticeable for the nature-friendly protected locations 1 (R2) and 2 (R4) compared to naturally eroding locations 4 (R7 and R8) and 5 (R9 and R10), it appears that off-bank timber piling does not sufficiently attenuate ship wave action.

Incorporating a reed fringe as natural wave dampening barrier is valid only
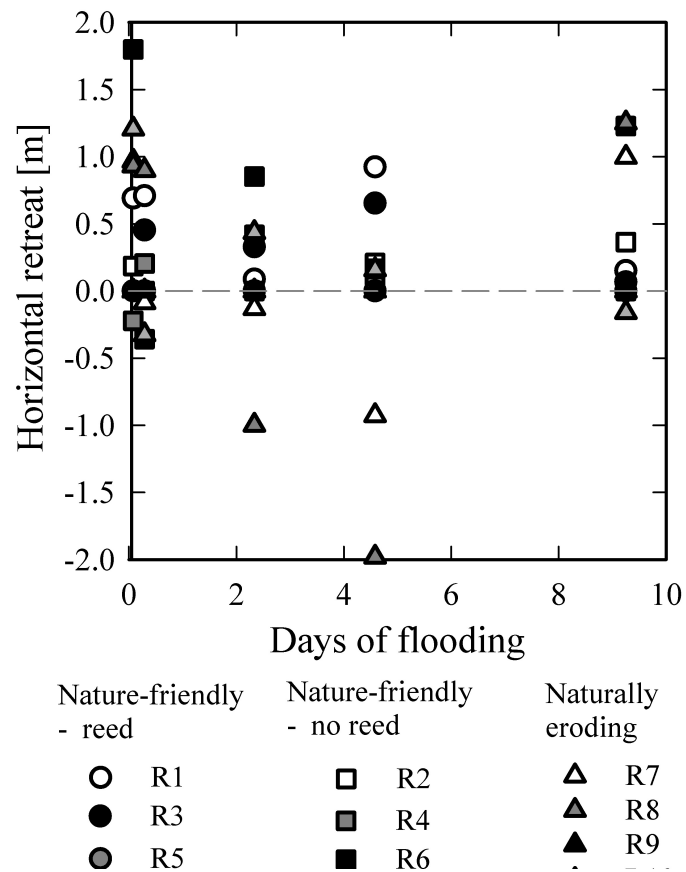
Figure 6.7: Days of flooding (water level > +6.1 m TAW) in relation to the horizontal retreat of a transect in the bank-water contact zone over a bimonthly survey period. Occurrence of flooding events does not demonstrate a direct cause and effect relationship to bank erosion. Positive horizontal retreat indicates a retreat of the transect (and the river bank), negative horizontal retreat indicates an advance of the transect's base towards the fairway.
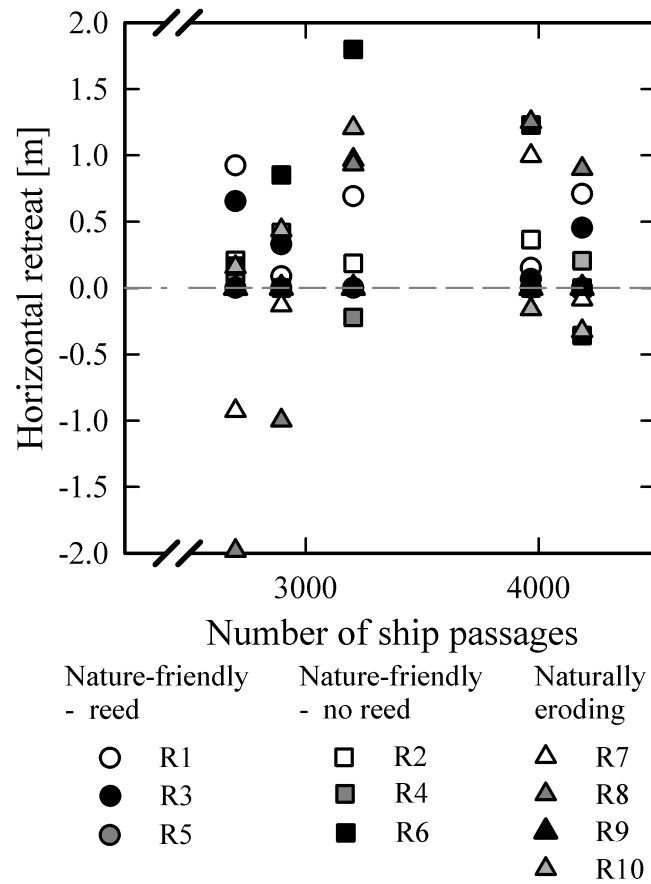
Figure 6.8: Number of ship passages along the Lys in relation to the horizontal retreat of a transect in the bank-water contact zone over a bimonthly survey period. No correlation is found between this external forcing parameter and the bank's response for both the nature-friendly protected and naturally eroding locations. Positive horizontal retreat indicates a retreat of the transect (and the river bank), negative horizontal retreat indicates an advance of the transect's base towards the fairway.
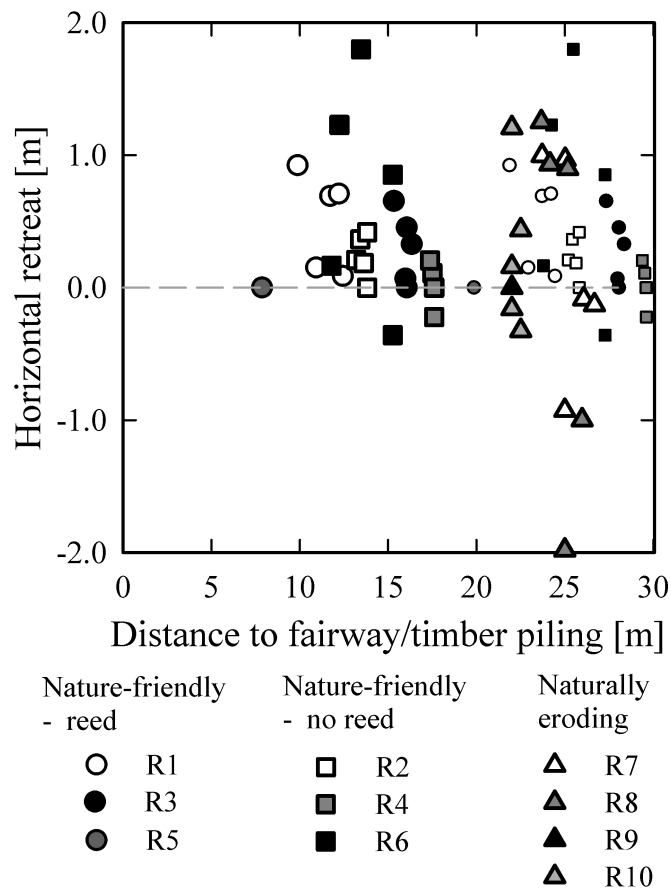
Figure 6.9: Bank distance to off-bank timber piling (large rectangular and circular symbols) and middle of the fairway (large triangular symbols) at survey time i in relation to horizontal retreat of a transect in the bank-water contact zone at survey time $i+1$. The smaller rectangular and circular symbols indicate the bank distance to the middle of the fairway for the nature-friendly protected transects. No controlling function which obviates horizontal retreat is found for this parameter, irrespective of installation of a nature-friendly protection. Note however that for the reed transects, horizontal retreat is shifted to the reed belt area instead of the (vertical) cut-bank. Positive horizontal retreat indicates a retreat of the transect (and the river bank), negative horizontal retreat indicates an advance of the transect's base towards the fairway.

on the condition that ship-induced hydrodynamic forcing is concentrated on the reed stems (location 3). The reed belt is able to withstand mechanical stress on its aboveground vegetation parts, seeing that quasi no stem damage arises and abundant reed regrowth and expansion towards the fairway take place (Figure 6.4). At locations 1 and 2, ship waves mainly act on the rhizome layer, washing out sediments from the root mesh (up to 0.9 m, see Figure 6.9). Uprooting of plants results when the reed belt looses its vital density (location 1).

The well-functioning of the reed belt at location 3 (with transect R5) might to some extent be attributed to the water level on the sloping beach, which hardly reaches the reed fringe. As the beach has a very gentle slope (3°), ship wave energy is greatly dissipated by bottom friction before surging in the reed belt. Contrary, the reed belts at transects R1 and R3 are situated in a water level of 0.5 m and exposed to direct wave attack. This indirect loading mechanism also applies for transect R4, situated at a higher bed level.

A worth noting fact is the singular 'standstill' behaviour of transect R9, located in a naturally eroding embayment. At this location, a gravel layer provides additional protection to the bank-water contact zone and may dissipate the wave energy adequately.

6.3.3   Contribution of an individual ship's wave action to bed and bank erosion

Over the 3-day measurement campaign, 70 ships sailed past the measurement transect at survey location 1. Hydro- and sediment dynamics of 46 ship passages were recorded with adequate quality to be evaluated, of which 5 are pleasure cruising (cf Section 5.4.1). The ship wave signature of the latter did not affect the riverine environment and is further not taken into consideration.

Given the fairway proximity, maximum bank-oriented combined wave-induced velocity, $U_{W,bank,max}$, can be considerably high for ships of all monitored ECMT-classes (Figure 6.10(a), and see also Figure 5.4). Not only a small blockage co-efficient m but also the sailing speed V_s determines the magnitude of the bank-oriented combined wave-induced velocities $U_{W,bank}$. The corresponding index wave height, H_{in}, is mainly situated between 0.15 m and 0.35 m but can amount up to 0.5 m. Energetic impact of this grouped ship wave structure might result in dislodgement of silty bank particles on the condition that its magnitude exceeds $E = 45\,\mathrm{J\,m^{-2}}$ (Figure 6.10(b)). The added suspended silt concentration SSC_{silt} because of this impulse event tends to be linearly correlated with the ship wave energy. The 3 outlying values correspond to a fully loaded and fast sailing ECMT-IV ship and the prolonged ship events due to two closely following ships of EMCT-class III and I and two crossing ECMT-Va ships (encircled symbols).

Relying on these measurements, ship-induced hydrodynamic forcing on the

non-vegetated river bank scoured a uniform silt layer of $ED_{bank} = 0.5$ to $3.6 \cdot 10^{-4}$ m deep into the contributing bank area $CA_{\text{bank}} = 0.3\,\text{m}^2$ (Figure 6.11). 'Compound' ship events have a substantial influence on the scoured depth. Over the 3-day measurement period, ship wave action resulted in a total uniform stripped layer of $ED_{bank} = 26 \cdot 10^{-4}$ m of silty bank particles.

Cumulative suspended sediment volume transport of sandy bed particles $Q_{\sum,s,bed}(T_0)$ is more dependent on the blockage coefficient m (Figure 6.12). The ship's underwater volume in proportion to the confined waterway dimensions determines the magnitude of the 'primary' wave-induced drawdown Δ and transversal stern wave H_{stern} and their wave-induced velocities. Although the majority of monitored ship passages leads to (re)suspension of sandy bed sediments, only fully loaded ships of ECMT-class IV and Va induce a significantly higher (yet in absolute values still relatively small) suspended sediment volume transport of $1.5\text{-}2.5 \cdot 10^{-4}\,\text{m}^3$.

Bed erosion and accretion are balanced in occurrence during the measurement days but not in magnitude (Figure 6.13(a) and 6.13(b)). Because of the prolonged drawdown effects of some larger ships, a very small, uniform layer of $ED_{bed} = 6 \cdot 10^{-5}$ m is eroded from the contributing bed area CA_{bed} of $6.5\,\text{m}^2$ due to the 46 monitored ship passages.

Comparatively translating these 3-day measurement results to the shipping traffic in April 2011 on the Lys, a uniform silt layer of $ED_{bank} = 0.1$ m is eroded from the non-vegetated bank-water contact zone and the river bed is uniformly lowered by $ED_{bed} = 0.2 \cdot 10^{-2}$ m (for a unit alongstream bed and bank width). Further extrapolation under the presumption of steady goods traffic relates these results to a yearly uniform eroded silty bank layer of $ED_{bank} = 1.2$ m and a sandy bed layer of $ED_{bed} = 2.8 \cdot 10^{-2}$ m.

Although these results refer to a simplified description of reality, they indicate that ship-induced hydrodynamic forcing is able to cause bed and bank erosion. Ship wave action brings sandy bed sediments in suspension behind the off-bank timber piling. The magnitude of suspended sediment transport is limited but it is questionable whether a dynamically balanced bed sediment budget, implying a controlled (cyclic) bed erosion and accretion, can be preserved. Bank erosion results from the too strong energetic wave impact of several ships.

6.4   Discussion

Integrating the analytical short-term findings with the surveyed long-term results demonstrates that river bank erosion still progressively takes place despite the installation of a nature-friendly bank protection. These morphological changes of the riverine environment can partly be attributed to ship-induced hydrodynamic forcing. Directly, heavy shipping traffic results in nearly continuous ship wave
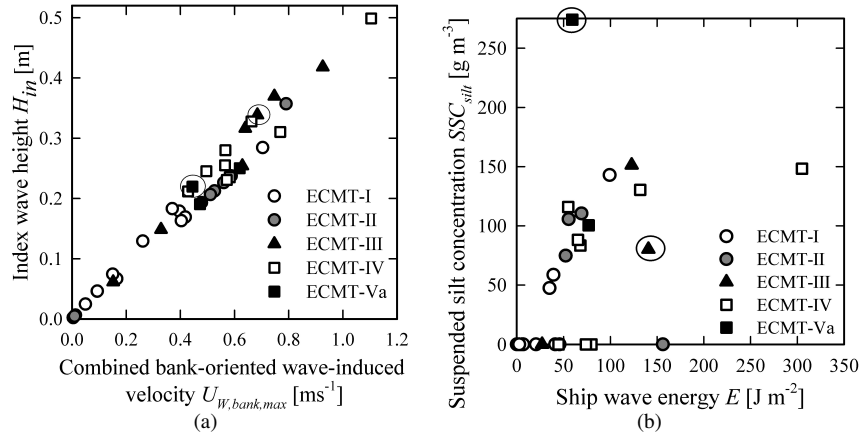
Figure 6.10: Ship wave characteristics, categorized by ECMT-class, and their impact on the river bank (focusing on the silty bank fraction). A. Index wave height H_{in} as a function of maximum bank-oriented combined wave-induced velocity $U_{W,bank,max}$. B. Added suspended silt concentration SSC_{silt}, measured at SSP B, in relation to ship wave energy E. Dislodgement of silty bank particles might result on the condition that the energetic ship wave impact $E \geq 45\,\mathrm{J\,m^{-2}}$. Encircled values correspond to 'compound' ship events, classified in the ECMT-class of the largest ship.
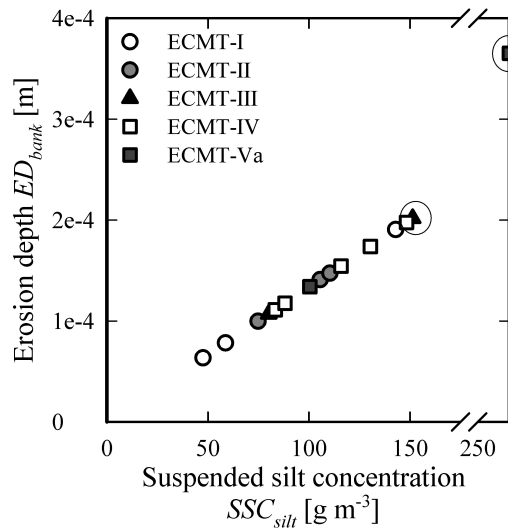

Figure 6.11: Uniform eroded layer of silty bank particles ED_{bank} as a function of the added suspended silt concentration SSC_{silt} in the water column due to ship-induced hydrodynamic forcing, categorized by ECMT-class. Encircled values correspond to 'compound' ship events, classified in the ECMT-class of the largest ship.
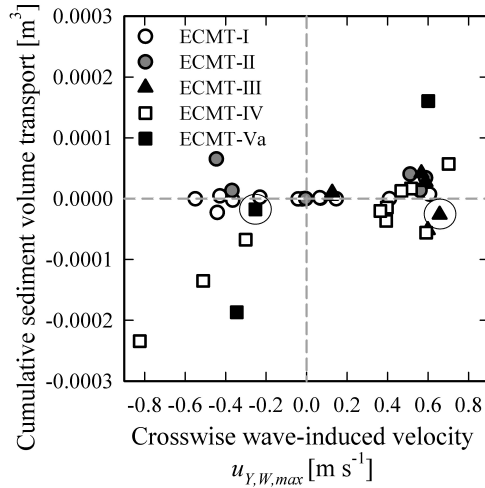
Figure 6.12: Cumulative bed sediment volume transport $Q_{\sum,s,bed}(T_0)$ through vertical plane A as a function of the maximum crosswise combined wave-induced velocity $u_{Y,W,max}$. Negative sediment volume transport indicates net transport towards the fairway (bed erosion), positive sediment volume transport indicates net transport towards the river bank (bed accretion). Encircled values correspond to ship events caused by two closely following or crossing ships, classified in the ECMT-class of the largest ship.
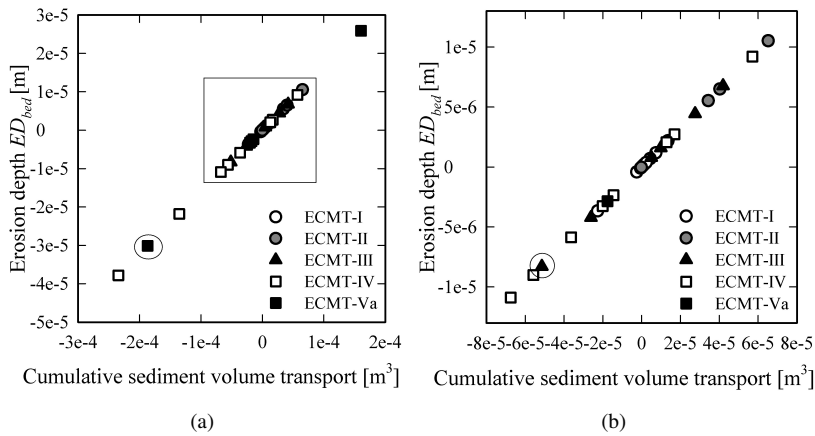

Figure 6.13: Uniform eroded layer of sandy bed particles ED_{bed} as a function of the cumulative bed sediment volume transport $Q_{\sum,s,bed}(T_0)$ due to an individual ship's wave action, categorized by ECMT-class. (a) All erosion depth values (b) Zoom on erosion depth values in square of (a). Negative erosion depth values indicates net bed erosion of the shallow water area behind the off-bank timber piling, positive erosion depth values indicate net bed accretion. Encircled values correspond to 'compound' ship events caused by two closely following or crossing ships, classified in the ECMT-class of the largest ship.

action (during daylight hours), which is able to dislodge and entrain bed and bank sediments. The actual erosion rate depends on the balance between sediment resistance and ship wave energy. Indirectly, ship wave action can accelerate other erosive processes like mass failure by destabilising and undermining the base of the river bank (Castillo et al., 2000; Houser, 2010; Nanson et al., 1994). The latter holds for event-based flooding too, with the annotation that this external force does not regularly recur in the river Lys. Whether the cause of bank erosion is eventually natural or anthropogenic, the latter is at least an additive trigger to bank failure.

The varied nature of environmental boundary conditions impedes a straightforward approach towards decision-making on whether it is good practice to install this type of nature-friendly bank protection in a confined, non-tidal waterway subject to heavy shipping traffic. A single row of closed off-bank timber piling as first ship wave attenuator was not found to alter sufficiently the hydrodynamic regime in the riverine area. Water exchange between fairway and shallow water area is considerably high during a ship passage because of a too strong porosity effect created by gaps between the timber piles (as discussed in Section 4.4 and 4.5). Our results indicate no dynamic balance in the bed sediment budget of the shallow water area (Figure 6.12) and a too strong ship-induced hydrodynamic forcing on the reed rhizome layer (Figure 6.9). To counteract erosion of silty bank particles in non-reed belt areas, ship wave energy E must be reduced below $45\,\mathrm{J\,m^{-2}}$, which corresponds to a wave height of less than $0.2\,\mathrm{m}$. One should however take into account that fine sandy bank lenses are even then preferential erosion sites (Bauer et al., 2002; Nanson et al., 1994). A second wave barrier is thus essential to prevent direct ship-induced hydrodynamic forcing on the natural river bank.

Some hydrodynamic interaction and water exchange between both sections of the waterway is however desirable, allowing a controlled cyclic bed erosion and accretion, in order to preclude silting up of the shallow water area. This would result in a narrowing of the waterway's cross section and hence, hampering shipping traffic. Besides, Coops et al. (1994) found that the positive sheltering effects for reed growth, which are created by a wave attenuating structure, were reversed when accumulation of silt and organic matter took place because of sub-optimal rooting conditions. Physical vitality is imperative for the protective capacity of vegetation. Good root anchoring provides an efficient nutrient uptake and plant stability (Coops et al., 1991) which is essential for the wave attenuating capacities of reed, while soil reinforcement is realized thanks to its rhizome mesh structure.

Ship-induced hydrodynamic forcing must therefore be concentrated on the aboveground reed parts. Reed stems are able to mechanically resist loads of wave heights of 0.2-0.3 m in a 0.5 m water column (Coops et al., 1996), being the general boundary conditions in the river Lys. Its capacity as a wave attenuator will however always depend on its seasonal growth cycle (dieback and regrowth) and

corresponding variations in stem bending stiffness, being lower in February (dead standing reed stalks) and June (young sprouts) compared to a fully developed reed belt in August (Coops and van der Velde, 1996). Consequently, it is critical to reduce ship wave action as shipping traffic stays steadily present throughout the year.

A reduction in exposure to ship-induced hydrodynamic forcing might be additionally obtained by a gently sloping beach fronting the reed belt. Wave energy is then greatly dissipated by bottom friction and the water level is decreased near the reed belt. Reed is most resistant to turbulent water motion in the higher wave breaking or surging zone. Moreover, reed expansion benefits from this reduced water depth gradient because its development towards higher water depths is limited by its physiological plant response (Coops et al., 1994). Transect R5 at location 3 approaches these optimal environmental conditions well.

Due to the rather limited spatial and temporal extent of this experimental study, these results are indicative of the occurring erosive processes and their contributing factors, still subject to validation by longer-term assessments. Longer-term morphological changes in the riverine environment are more complicated, resulting from an interaction of various factors, of which some (e.g. bank saturation, bank weathering) are outside the scope of this study.

6.5   Conclusion

To counteract progressive bank erosion, a nature-friendly bank protection consisting of off-bank timber piling and a reed belt before the river bank was installed in the confined, non-tidal Lys. To evaluate its effectiveness under heavy shipping traffic, a short-term and long-term field study were carried out.

The long-term topographic study did not reveal clear differences in bank erosion rates (total and periodic areal losses) between the surveyed nature-friendly protected and naturally eroding embayments. Although these results did not demonstrate a direct cause and effect relation between hydrodynamic forcing parameters (occasional flooding events and frequent ship wave action) and bank erosion, they qualitatively inferred that ship-induced hydrodynamic forcing is sufficiently high to remove slumped bank material and to affect the bank-water contact zone.

The analytical results from the short-term study indicated that every ship passage is able to transport, to some extent, sandy bed sediments of the shallow water area behind the off-bank timber piling. Ship-induced hydrodynamic forcing on the river bank exceeding $E = 45\,\mathrm{J\,m^{-2}}$, often results in dislodgement of silty bank particles.

This bank protecting configuration would benefit from an improved design to provide sufficient protection against ship wave action as, based on the data analysis, it does not adequately prevent further bank erosion. It is however a valuable

solution to translate a nature-friendly bank protection into a twofold wave attenuating structure, of which the first structure is located in the waterway; especially when limited riverine area is available. Transition between water- and land-based ecosystems is thereby smoothly optimised using the shallow water area, ineffective for economic waterway purposes, as an ecological corridor where a second, natural wave attenuating barrier must be installed to meet the technical requirements of a bank protecting structure.

Planting of a reed belt at the base of the natural river bank is therefore a sustainable option in this waterway (given its ship-induced hydrodynamic forcing conditions) on the condition that environmental growing conditions are more appropriately met. To this end, it is necessary to reduce the transmission of ship-induced hydrodynamic forcing through the first wave attenuator.

Given the predominantly sand-silty river bank conditions along the Lys and the rather high cut-bank, it is questionable whether no additional measures must be taken to prevent non-hydrodynamic erosive bank processes. Besides these studied hydrodynamically induced failure mechanisms, a third process of bank failure is observed at various locations (location 1 and 2). Under the root layer of the grass-woody upper bank surface, large mass failure of the cut-bank was sometimes noted, forming blocks of debris in the excavated cut-bank. This mechanism might contribute also to bank instability.

The important thing is not to stop questioning.
Curiosity has its own reason for existing.
[A. Einstein]

7

Conclusions & Recommendations

7.1   General conclusions

The general objective of this PhD-research was to contribute to a deeper insight into an optimized design for nature-friendly bank protections in non-tidal, confined waterways subject to heavy shipping traffic. The confined waterway dimensions and very frequent hydrodynamic forcing on the one hand, and the ecological needs of a riverine area on the other hand, makes its design a challenging task.

It was therefore aimed at quantifying the (impact of) ship-induced hydrodynamics on a type of nature-friendly bank protection, consisting of off-bank timber piling, which separates the fairway from the shallow water riverine environment, and a reed belt, planted at the base of the vertical cut-bank. This particular type is of interest for installation in confined waterways since it takes up little space in the (generally) limited riverine area available.

To meet this twofold objective, we opted for an experimental approach on a prototype in a 'real' situation. The Lys was selected as study area. The waterway is a (EU) standard scale inland waterway and forms part of the priority TEN-T project 30 'inland waterway Seine-Scheldt' (EU, 2007-2020). This includes a.o. the deepening of the Lys' profile to meet future navigation standards and the installation of nature-friendly bank protection to counteract bank erosion. Hence, the Lys is a nice example of (an attempt to) reconciliation of various 'stakeholder' needs, i.e. the economic EU Trans-European Transport Network and the environmental EU Water Framework Directive.

This experimental approach of prototype monitoring on various locations (and configurations of off-bank timber piling) resulted in 2 deliverables:

■ A fixed monitoring system

An extensive monitoring system was installed at a fixed location. This monitoring system accurately measures the magnitude of ship-induced hydrodynamic forcing on and the response of the nature-friendly bank protection. A variety of physical processes related to ship-generated waves are therefore taken along its design, a.o. incident ship-generated waves, their wave-structure interaction with the off-bank timber piling, related sediment supsension, ... This monitoring system thus provides ample research opportunities to further investigate (and optimize) various configurations of nature-friendly bank protection given these hydraulic boundary conditions for shipping traffic.

■ A mobile monitoring system

A flexible, mobile monitoring system was developed subsequently, in order to enhance the dynamic measurement possibilities for ship-generated waves. In this PhD-research, it was used to assess the hydrodynamic performance of various configurations of off-bank timber piling. Because of its modular and lightweight setup, it could easily be installed at various locations. This monitoring system can however be applied in a variety of environmental boundary conditions for the quantification of both wind- and ship-generated waves.

The acquired knowledge in this PhD-research is to be incorporated by the Advisory Board for the use of nature-friendly bank protection along waterways, a recent initiative of the Flemish government. The department of Civil Engineering, represented by Prof. Troch, is corresponding member of this Advisory Board.

7.2   Answers to the research questions

The results of the experimental study, which were largely obtained through various measurement campaigns, are structured by research question. The answers to the research questions summarize the work done to meet the twofold objective described under 7.1.

1. **What are the characteristics of the ship wave climate in a confined, non-tidal and nature-friendly protected waterway?**

The ship wave climate in the Lys was characterized based on its input and output variables, i.e. the hydraulic boundary conditions for shipping traffic (input), and the magnitude and behaviour of the 'primary' and 'secondary' ship wave patterns in this confined, non-tidal and nature-friendly protected waterway (output).
A sailing ship is bounded to its limit speed V_l, which easily exceeds the imposed speed limit for all light draughted ships. The buoyancy of a ship is generally

balanced to maintain a blockage coefficient $m > 5$. A captain tries to avoid such a high ship resistance in order to be able to sail at considerable speed, which implies a limitation on the utilized carrying capacity for ECMT-III, IV and Va shipping traffic.

The confined dimensions of the waterway amplify the ship's 'primary' wave pattern, which dominates the ship wave signature. The maximum values for its characteristic parameters are: a maximum drawdown $\Delta h_{max} = 0.35$ m, a transversal stern wave $H_{stern} = 0.50$ m, and a maximum return current $u_{r,max} = 1.0\,\mathrm{m\,s^{-1}}$. This highest ship-induced hydrodynamic forcing was caused by light draughted shipping traffic of ECMT-class IV, sailing at a ratio of sailing speed to limit speed $V_s/V_l \geq 1$. The latter aspect is of greatest importance; the higher the ratio V_s/V_l, the higher the ship-induced hydrodynamic forcing. Light draughted shipping traffic is able to sail at $V_s/V_l \geq 1$, where an increase in blockage coefficient m, i.e. an increase in the ship's ECMT-classification, results in a more pronounced 'primary' ship wave pattern. (Fully) loaded shipping traffic of all ECMT-classes (except ECMT-I) caused a similar 'primary' wave pattern (for a similar ratio V_s/V_l).

Ship wave-structure interaction with the off-bank timber piling and the ship waves' shallow water behaviour were examined for various configurations of off-bank timber piling. The magnitude of the 'primary' wave pattern, i.e. the maximum drawdown Δh_{max} and transversal stern wave height H_{stern}, is preserved on the condition that the water level is sufficiently high in the shallow water area. The clear porosity effect of the timber piling yields a significant water exchange between the fairway and the shallow water area, which frequently dries a part of the riverine area. Combination of the large 'primary' wave height transmission and the limited water depth along the river bank might lead to a severe impact of the transversal stern wave H_{stern} on this riverine area.

Relative reduction of maximum 'secondary' wave heights $H_{SP,max}$ ranged from 20% to 55%, but was rather location-dependent than factor-dependent. A varying length of a single or double row of off-bank timber piling did not lead to a higher 'secondary' wave height reduction, nor did the closure of lateral water in- and outflow openings.

The future waterway layout includes an enlarged trapezoidal cross section because of the 1 m deepening of the bed profile. On that account, an increased blockage coefficient m was calculated for all ECMT-classes except for ECMT-class IV and Va (because of the (now vs future) difference in draught restrictions). The shipping traffic's limit speed V_l will increase, which results in a higher potential sailing speed V_s. This will result in a higher amplitude for both ship wave patterns and hence, a larger impact of the ship-induced hydrodynamic forcing. A restriction to the imposed speed limit will therefore be even of bigger importance.

2. **To which extent do ship-induced hydrodynamics contribute to sediment dynamics behind the off-bank timber piling?**

During a 3-day measurement campaign, the contribution of ship-induced hydrodynamics to sediment dynamics behind the off-bank timber piling was quantified for individual ship passages. Morphological changes caused by ship-induced

hydrodynamic forcing were assessed based on their related suspended sediment transport. Sediment transport towards the fairway was considered as a proxy for bed and bank erosion. Note that the role of the reed belt as a second wave attenuating barrier was not considered herein.

Quantification of sediment dynamics for the river bed and bank separately was hampered by the large variability and overlap in bed and bank grain sizes. Relying on the differences in sediment dislodge and transport characteristics for varying grain size, a partial distinction between both sediment sources was made. For the river bed, exceedance of the critical shear stress accounted for incipient bed motion, after which suspension of the sandy bed sediments might take place. For the river bank, the impact of a ship's combined wave-induced velocity determined its suspension of silty bank sediments.

The larger 'primary' wave pattern strongly influences the combined wave-induced velocity, of which the maximum values were up to $U_W = 1.10\,\mathrm{m\,s^{-1}}$. The shorter period 'secondary' wave pattern however, induces the highest wave shear stress. The combined ship wave shear stress amounted maximally to $\tau_W = 5.1\,\mathrm{N\,m^{-2}}$.

The quantity of suspended sandy bed sediments ranged from a moderate suspension of $\overline{C}_{\sum,m,bed}(T_0) = 1000\,\mathrm{g\,m^{-3}}$ to substantial amounts of $\overline{C}_{\sum,m,bed}(T_0)$ $= 8000\,\mathrm{g\,m^{-3}}$. Large differences in suspended quantities are observed between and within the ECMT-classes, but an indicator for substantial suspension was the occurrence of a maximum combined wave-induced velocity $U_{W,max} \geq 0.4\,\mathrm{m\,s^{-1}}$. Dislodgement of silty bank particles might take place when the maximum bank-oriented combined wave-induced velocity $U_{W,bank,max}$ exceeded $0.4\,\mathrm{m\,s^{-1}}$. The added suspended silt concentration due to a ship passage was considerably lower than the suspended quantities of sandy bed sediments, and amounted to maximum $SSC_{silt} = 270\,\mathrm{g\,m^{-3}}$.

Dislodgement of silty sediment directly implies their advection downstream. For the sandy bed sediments however, suspension does not necessarily lead to a net sediment transport. Significant (yet in absolute values relatively small) net crosswise sediment transport occurred due to the passage of 6 ECMT-IV and Va ships, which caused a sediment transport of $\overline{Q}_{\sum,m,bed}(T_0) \geq 200\,\mathrm{g\,m^{-1}}$. The direction of crosswise sediment transport is determined by the ratio between the 'primary' wave-induced displacement flow (during the drawdown, and oriented towards the fairway) and its slope supply flow (during the transversal stern wave, and oriented towards the river bank). 'Secondary' wave-induced velocities rather redistribute the suspended sediments. Hence, dislodgement of bed sediments occurs mainly by the 'secondary' wave pattern, while transport of bed sediments results from the 'primary' wave pattern.

Sediment transport towards the fairway was considered as a proxy for bed and bank erosion. Both processes did occur; silty bank particles were dislodged, and the balance of the sandy bed sediment budget was negative. The monitored order-of-magnitude values for suspended sediment transport suggest that the off-bank timber piling does not maintain a 'controlled' (cyclic) bed erosion and accretion, and does not prevent bank erosion. A reduction of the combined wave-induced ve-

locity to $U_W < 0.4\,\mathrm{m\,s}^{-1}$ behind the off-bank timber piling is required to achieve a significant decrease in sediment dislodgement, (re)suspension and transport for both sediment sources.

3. **Is this type of nature-friendly bank protection effective to obviate river bed and bank erosion?**

The nature-friendly bank protection under study consists of a double wave attenuating configuration: (i) the off-bank timber piling, and (ii) the reed belt before the river bank. In a confined, non-tidal waterway, flood and ship waves are considered to be the external hydrodynamic forcing parameters on the river bank. Its effectiveness to withstand these hydrodynamic forcing parameters was evaluated against the morphological changes that took place in naturally eroding embayments under identical loading conditions. Since this type of nature-friendly bank protection incorporates a natural wave reductor, morphological changes were surveyed over one seasonal vegetation cycle.

The survey did not reveal clear differences in bank erosion rates (total and periodic areal losses) between the nature-friendly protected and naturally eroding embayments. Although these results did not demonstrate a direct cause and effect relation between hydrodynamic forcing parameters (occasional flooding events and frequent ship wave action) and bank erosion, they qualitatively inferred that ship-induced hydrodynamic forcing is sufficiently high to remove slumped bank material and to affect the bank-water contact zone.

Consequently, this bank protecting configuration would benefit from an improved design to provide sufficient protection against ship wave action as, based on the survey, it did not adequately prevent bank erosion. It is however a valuable solution to translate a nature-friendly bank protection into a twofold wave attenuating structure, of which the first structure is located in the waterway. Transition between water- and land-based ecosystems is thereby smoothly optimised using the shallow water area, ineffective for economic waterway purposes, as an ecological corridor where a second, natural wave attenuating barrier must be installed to meet the technical requirements of a bank protecting structure.

Planting of a reed belt at the base of the natural river bank is therefore a sustainable option in this waterway on the condition that environmental growing conditions are more appropriately met. To this end, it is necessary to reduce the transmission of ship-induced hydrodynamic forcing through the first wave attenuator.

7.3   Suggestions for future research

An experimental approach on a prototype in a 'real' situation provides the unique added value to measure and assess the situation 'as is', given all the influencing, sometimes confounding, (and unforeseeable) variables over, preferably, their largest range of occurrence. Its major asset is however also its drawback: the research has a certain site specificness and mutual separation of influencing parameters is less straightforward.

The ship wave climate on the Lys, which is a (EU) standard scale inland waterway with a typical trapezoidal cross section, corresponds to ship-generated waves on other canallike waterways. A further analysis of the large data set of ship events will increase the robustness of the acquired ship wave-related parameters (reduction of the data spread for the different parameter categories). The data set might be useful for e.g. the design of (protecting) structures subject to the impact of heavy shipping traffic. Given its wide range of monitored parameters, it might be used to validate various formulas which predict ship-induced hydrodynamics (e.g. formulas in GBB (2010)).

The importance of ship-induced hydrodynamics to sediment dynamics in the shallow water environment is not yet fully understood. Bed load sediment transport and seepage failure were left out of the PhD-research. An extension on the field study, which takes these processes additionally into account, will gain more insight in the balance between bed erosion and accretion in the shallow water environment, and their controlling and triggering processes.

Furthermore, the extended data set will improve the power of the regression models, which relate various ship characteristics (e.g. ship displacement, sailing speed) to ship-induced hydrodynamics and sediment dynamics. Rather than being a mere explanatory model, the predictive capability of the fitted coefficients, to predict ship wave action in the same study site or at similar shallow water locations, would increase.

The use of off-bank timber piling as a wave attenuating barrier for the ship-generated waves of pleasure cruising is worth investigating. Because of their limited displacement, their 'primary' wave pattern is very small and the 'secondary' wave pattern dominates. Although the measured reduction of the maximum 'secondary' wave height was rather location-dependent than factor-dependent, it deserves a closer look to eliminate possibly confounding factors. Especially the impact of speed boats must be examined, since they can easily operate in the semi-planing range. By sailing with the same speed boat at varying distances and sailing speeds along the measurement transect of the fixed monitoring system, the wave-structure interaction and the waves' shallow water behaviour are quantified in a controlled way. In the same way, various configurations of off-bank timber piling can be monitored using the mobile monitoring system.

The fixed monitoring system provides a valuable, flexible measurement setup to further optimize the design of this type of nature-friendly bank protection. A reduction of ship-induced hydrodynamics behind the off-bank timber piling must be obtained to improve its technical and ecological functionality. Hereto, the use of a second parallel and off-bank wave attenuating barrier is an interesting research path. Installed at the edge of the shallow water environment to preserve the ecologically valuable shallow water area, the porosity of this structure is essential. It must change the impact of, mainly the 'primary', ship wave pattern in such a way that its direct impact on the (temporarily dead) reed belt is limited while silting up of the shallow water area is prevented.

References

Almeida, L. P., Ferreira, O., Pacheco, A., 2011. Thresholds for morphological changes on an exposed sandy beach as a function of wave height. Earth Surface Processes and Landforms 36 (4), 523–532.

Althage, J., 2010. Ship-induced waves and sediment transport in Göta River, Sweden. Master's thesis, Lund University, Sweden.

Bauer, B., Lorang, M., Sherman, D., 2002. Estimating boat-wake-induced levee erosion using sediment suspension measurements. Journal of Waterway, Port, Coastal and Ocean Engineering 128 (4), 152–162.

Bertram, V., 2000. Practical ship hydrodynamics. Chapter 3: Resistance and propulsion. Butterworth-Heinemann, Woburn, UK.

Bhowmik, N. G., Renjie, X., Mazumder, B. S., Soong, T. W., 1995. Return flow in rivers due to navigation traffic. Journal of Hydraulic Engineering 121 (12), 914–918.

Biron, P., Robson, C., Lapointe, M., Gaskin, S., 2004. Comparing different methods of bed shear stress estimates in simple and complex flow fields. Earth Surface Processes and Landforms 29 (11), 1403–1415.

Castillo, J., Luque, C., Castellanos, E., Figueroa, M., 2000. Causes and consequences of salt marsh erosion in an Atlantic estuary in SW Spain. Journal of Coastal Conservation 6, 89–96.

Chanson, H., 2004a. The hydraulics of open channel flow: An introduction. - Part 1: Basic principles of open channel flows. Elsevier Butterworth-Heineman, Oxford, UK. 1-140.

Chanson, H., 2004b. The hydraulics of open channel flow: An introduction - Part 2: Introduction to sediment transport in open channels. Elsevier Butterworth-Heineman, Oxford, UK. 141-246.

Chwang, A., Chen, Y., 2003. Field measurements of ship waves in Victoria Harbour. Journal of Engineering Mechanics, 1138–1148.

Coops, H., Boeters, R., Smit, H., 1991. Direct and indirect effects of wave attack on helophytes. Aquatic Botany 41 (4), 333–352.

Coops, H., Geilen, N., van der Velde, G., 1994. Distribution and growth of the helophyte species *Phragmites Australis* and *Scirpus Lacustris* in water depth gradients in relation to wave exposure. Aquatic Botany 48 (3-4), 273–284.

Coops, H., Geilen, N., Verheij, H., Boeters, R., van der Velde, G., 1996. Interactions between waves, bank erosion and emergent vegetation: An experimental study in a wave tank. Aquatic Botany 53 (3-4), 187–198.

Coops, H., van der Velde, G., 1996. Effects of waves on helophyte stands: Mechanical characteristics of stems of Phragmites australis and Scirpus lacustris. Aquatic Botany 53 (3-4), 175–185.

CUR, 1999. CUR 201: Natuurvriendelijke oevers: Belasting en sterkte. Civieltechnisch Centrum Uitvoering Research en Regelgeving (CUR), Directoraat-Generaal Rijkswaterstaat Dienst Weg- en Waterbouwkunde, Nederland.

Dam, K. T., Tanimoto, K., Fatimah, E., 2008. Investigation of ship waves in a narrow channel. Journal of Marine Science and Technology 13 (3), 223–230.

De Rouck, J., 2008-2009. Rivieren, Kanalen en Sluizen. partim: Rivieren en Kanalen, Hoofdstuk 3: De scheepvaart en de scheepvaartweg. Universiteit Gent, Faculteit Ingenieurswetenschappen en Architectuur.

deWit, P., Kranenburg, C., AUG 1997. The wave-induced liquefaction of cohesive sediment beds. Estuarine, Coastal and Shelf Science 45 (2), 261–271.

Dorava, J. M., Moore, G. W., 1997. Effects of boatwakes on streambank erosion in the Kenai River, Alaska. Water-resources investigations report 97-4105, U. S. Geological Survey, prepared in cooperation with the Alaska Department of Fish and Game.

DOV, 2009. Topografische kaart van een deel van het Leiebekken (Databank Ondergrond Vlaanderen). URL: https://dov.vlaanderen.be, Last visit: December 26th, 2009.

Dyer, K. R., 1986. Coastal and estuarine sediment dynamics. Wiley, Chichester, UK.

ECMT, 1992. Resolution no. 92/2 on new classification of inland waterways. European Conference of Ministers of Transport (ECMT). Athens, June 11-12, 1992, 5.

Ellis, J. T., Sherman, D. J., Bauer, B. O., 2006. Depth compensation for pressure transducer measurements of boat wakes. Journal of Coastal Research 39, 488–492.

Ellis, J. T., Sherman, D. J., Bauer, B. O., Hart, J., 2002. Assessing the impact of an organic restoration structure on boat wake energy. Journal of Coastal Research 36, 256–265.

EU, 2000. The EU Water Framework Directive: Integrated river basin management for Europe. URL: http://ec.europa.eu/environment/water/water-framework/, Last visit: April 5th, 2013.

EU, 2006. Trans-European Transport Network Executive Agency. URL: http://tentea.ec.europa.eu, Last visit: April 5th, 2013.

EU, 2007-2020. Priority Project 30: Inland water-way Seine-Scheldt. URL: http://tentea.ec.europa.eu/en/ten-t_projects/30_priority_projects/priority_project_30/priority_project_30.htm, Last visit: April 5th, 2013.

Garel, E., Lopez Fernandez, L., Collins, M., 2008. Sediment resuspension events induced by the wake wash of deep-draft vessels. Geo Marine Letters 28 (4), 205–211.

GBB, 2010. Grundlagen zur Bemessung von Böschungs- und Sohlensicherungen an Binnenwasserstraßen. Teil 5: Ermittlung der hydraulischen Einwirkungen. Bundesanstalt für Wasserbau, Karlsruhe, Germany.

Georgakaki, A., Sorensen, S., 2004. Report on collected data and resulting methodology for inland shipping. Part of the ARTEMIS EU-project: Assessment and reliability of transport emission models and inventory systems (5th Framework Research Programme), prepared by the Department of Mechanical Engineering, Technical University of Denmark, Denmark.

HIC, 1983-2012. Precipitation, water level and discharge data. Hydrologic Information Centre (HIC), Department of Mobility and Public Works of the Flemish government, Belgium.

Hofmann, H., Lorke, A., Peeters, F., 2008. The relative importance of wind and ship waves in the littoral zone of a large lake. Limnology and Oceanography 53 (1), 368–380.

Houser, C., 2010. Relative importance of vessel-generated and wind waves to salt marsh erosion in a restricted fetch environment. Journal of Coastal Research 26 (2), 230–240.

Houser, C., 2011. Sediment resuspension by vessel-generated waves along the Savannah River, Georgia. Journal of Waterway, Port, Coastal and Ocean Engineering 137 (5), 246–257.

Hughes, Z. J., FitzGerald, D. M., Howes, N. C., Rosen, P. S., 2007. The impact of natural waves and ferry wakes on bluff erosion and beach morphology in Boston harbor, USA. Journal of Coastal Research (50), 497–501.

Kim, S., Friedrichs, C., Maa, J., Wright, L., 2000. Estimating bottom stress in tidal boundary layer from Acoustic Doppler Velocimeter data. Journal of Hydraulic Engineering 126 (6), 399–406.

Lataire, E., Vantorre, M., Eloot, K., 2009. Systematic model tests on ship-bank interaction effects. In: Proceedings of the International Conference on Ship Manoeuvring in Shallow and Confined Water. Antwerp, Belgium. 9-22.

Maes, E., Van Crombrugge, W., Hoekers, C., 2006. Lys river restoration in the Seine-Scheldt connection. In: Proceedings of the 31st PIANC Navigation Congres. Estoril, Portugal.

Mazumder, B. S., Bhowmik, N. G., Soong, T. W., 1993. Turbulence in rivers due to navigation traffic. Journal of Hydraulic Engineering 119 (5), 581–597.

Nanson, G. C., Von Krusenstierna, A., Bryant, E. A., Renilson, M. R., 1994. Experimental measurements of river-bank erosion caused by boat-generated waves on the Gordon River, Tasmania. Regulated Rivers: Research & Management 9 (1), 1–14.

NRCS, 2011. Soil texture calculator. Published by the National Resources Conservation Service (NRCS), United States Department of Agriculture. Last access: May 5th 2011, URL: http://soils.usda.gov/technical/aids/investigations/texture/.

NRCS, 2012. General guide for estimating moist bulk density. Published by the National Resources Conservation Service (NRCS), United States Department of Agriculture. Last access: Dec 11th 2012, URL: http://www.mo10.nrcs.usda.gov/references/guides/properties/moistbulkdensity.-html.

Osborne, P., Boak, E., 1999. Sediment suspension and morphological response under vessel-generated wave groups: Torpedo Bay, Auckland, New Zealand. Journal of Coastal Research 15 (2), 388–398.

Parchure, T., McAnally, W., Teeter, A., 2001. Desktop method for estimating vessel-induced sediment suspension. Journal of Hydraulic Engineering 127 (7), 577–587.

Parnell, K., Kofoed-Hansen, H., 2001. Wakes from large high-speed ferries in confined coastal waters: Management approaches with examples from New Zealand and Denmark. Coastal Management 29 (3), 217–237.

Parnell, K. E., McDonald, S. C., Burke, A. E., 2007. Shoreline effects of vessel wakes, Marlborough Sounds, New Zealand. Journal of Coastal Research (50), 502–506.

PIANC, 2008. Considerations to reduce environmental impacts of vessels. Report 99 of the PIANC Inland Navigation Commission. Brussels, Belgium.

Przedwojski, B., Blazejewski, R., Pilarczyk, K., 1995. River training techniques: Fundamentals, Design and Applications. Balkema, Rotterdam, the Netherlands.

Rapaglia, J., Zaggia, L., Ricklefs, K., Gelinas, M., Bokuniewicz, H., 2011. Characteristics of ships' depression waves and associated sediment resuspension in Venice Lagoon, Italy. Journal of Marine Systems 85 (1-2), 45–56.

Ravens, T. M., Thomas, R. C., 2008. Ship wave-induced sedimentation of a tidal creek in Galveston bay. Journal of Waterway, Port, Coastal and Ocean Engineering 134 (1), 21–29.

Schiereck, G. J., 2001. Introduction to bed, bank and shore protection. Engineering the interface between soil and water. Delft University Press, The Netherlands.

Schijf, J., 1949. Influence on the form and dimensions of the cross section of the canal, of the form, of the speed and the propulsion system of vessels. In: Proceedings of the XVIIth PIANC Navigation Congres, Section I: Inland navigation. Lisbon, Portugal. 61-78.

Schoellhamer, D., 1996. Anthropogenic sediment resuspension mechanisms in a shallow microtidal estuary. Estuarine, Coastal and Shelf Science 43 (5), 533–548.

SNAME, 1988a. Principles of Naval Architecture (Second Revision). Volume I: Stability and Strength. Chapter I: Ship geometry. The Society of Naval Architects and Marine Engineers (SNAME). New Jersey, USA.

SNAME, 1988b. Principles of Naval Architecture (Second Revision). Volume II: Resistance, Propulsion and Vibration. Chapter V: Resistance. The Society of Naval Architects and Marine Engineers (SNAME). New Jersey, USA.

Soomere, T., Rannat, K., Elken, J., Myrberg, K., 2003. Natural and anthropogenic wave forcing in the Tallinn Bay, Baltic Sea. In: Coastal Engineering VI: Computer Modelling and Experimental Measurements of Seas and Coastal Regions. Cadiz, Spain. Vol 9: 273-282.

Soulsby, R. L., 1997. Dynamics of marine sands. A manual for practical applications. Thomas Telford Publications, London, UK.

Stockstill, R., Berger, R., 2001. Simulating barge drawdown and currents in channel and backwater areas. Journal of Waterway, Port, Coastal and Ocean Engineering 127 (5), 290–298.

Taylor, D., Hall, K., MacDonald, N., 2007. Investigations into ship-induced hydrodynamics and scour in confined shipping channels. Journal of Coastal Research (50), 491–496.

Ten Brinke, W., Schulze, F., van der Veer, P., 2004. Sand exchange between groyne-field beaches and the navigation channel of the Dutch Rhine: The impact of navigation versus river flow. River Research and Applications 20 (8), 899–928.

Teschke, U., Peters, K., Baur, T., 2008. Analysis of ship waves in maritime waterways. In: Proceedings of the International Conference on Fluvial Hydraulics (River Flow). Kubaba, Turkey, 2001–2009.

Torsvik, T., Didenkulova, I., Soomere, T., Parnell, K. E., 2009. Variability in spatial patterns of long nonlinear waves from fast ferries in Tallinn Bay. Nonlinear Processes in Geophysics 16 (2), 351–363.

USACE, 2006. Hydraulic design of deep-draft navigation projects. Engineering Manual EM 1110-2-1613. US Army Corps of Engineers (USACE), Washington DC, USA.

Van Rijn, L. C., 1990. Principles of fluid flow and surface waves in rivers, estuaries, seas and oceans. Aqua publications, Amsterdam, The Netherlands.

Van Rijn, L. C., 1993. Principles of sediment transport in rivers, estuaries and coastal seas. Aqua publications, Amsterdam, The Netherlands.

Verney, R., Deloffre, J., Brun-Cottan, J. C., Lafite, R., 2007. The effect of wave-induced turbulence on intertidal mudflats: Impact of boat traffic and wind. Continental Shelf Research 27 (5), 594–612.

Vincent, C., Hanes, D., 2002. The accumulation and decay of near-bed suspended sand concentration due to waves and wave groups. Continental Shelf Research 22 (14), 1987–2000.

Wikipedia, 2013. Picture of the phenomenon of squat of a ship. URL: http://en.wikipedia.org/wiki/File:Squat_hydrodynamic_phenomena-tag.svg, Last visit: April 12, 2013.

W&Z, 2009-2011. Ship characteristic data from navigation locked at Sint-Baafs-Vijve. Waterwegen en Zeekanaal NV (W&Z), Belgium.

A

Particle size distributions of sediment samples

River bed and bank soil samples were taken on various locations in the nature-friendly bank protection where the fixed monitoring system is installed, in order to get a better view on the spatial heterogeneity in river bed and bank sediments. Water samples were also taken in the shallow water riverine area.

Particle size distributions of these samples are determined by Mastersizer 2000 analysis (Malvern Instruments). Soil classification of the river bed and bank samples is according to the USDA classification system (NRCS, 2011).

A.1   Soil samples of the river bed

Undisturbed soil samples were randomly taken in the top layer of the river bed behind the off-bank timber piling using a Kopecki ring. This top layer is classified as 'sand' (Figure A.1).

A.2   Soil samples of the river bank

Undisturbed soil samples were taken on the non-vegetated areas of the eroded river bank, i.e. where no reed belt was present. The river bank was sampled around the still water level using a Kopecki ring. Soil textures are classified as 'silt loam', 'loamy sand', 'sandy loam' or 'sand' (Figure A.2).

(a) Sand

(b) Sand

(c) Sand

(d) Sand

(e) Sand
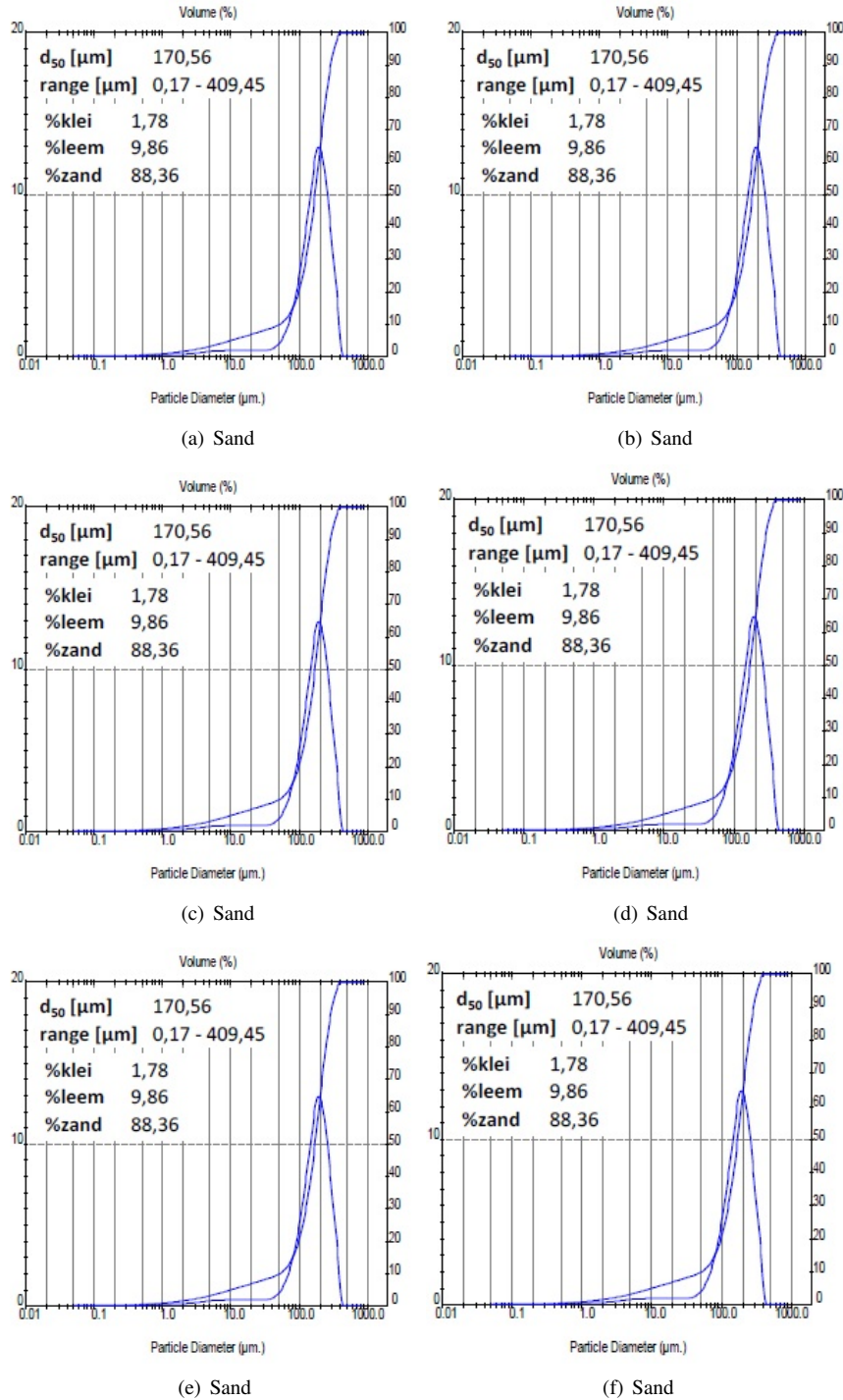
(f) Sand

Figure A.1: Particle size distributions and soil classification for samples of the river bed behind the off-bank timber piling
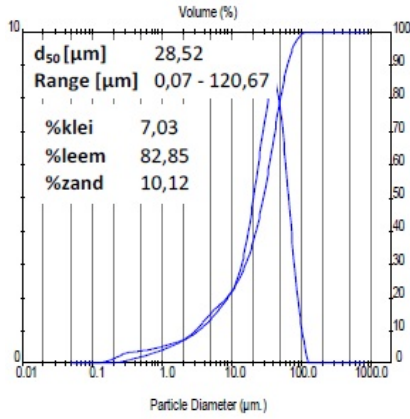
(a) Silt loam
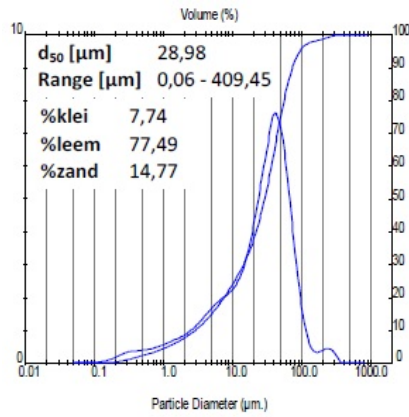
(b) Silt loam
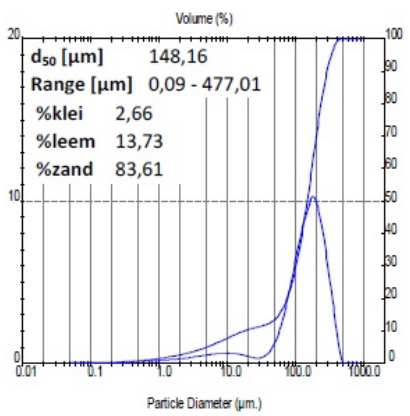
(c) Loamy sand
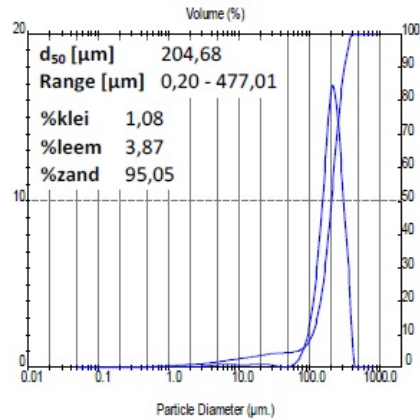
(d) Sand
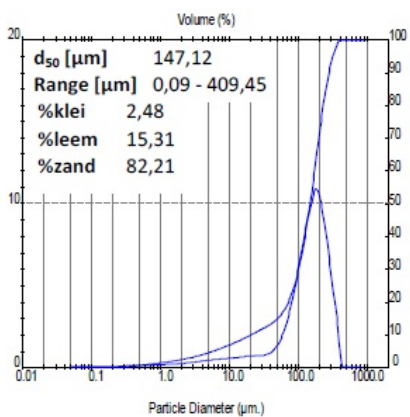
(e) Loamy sand
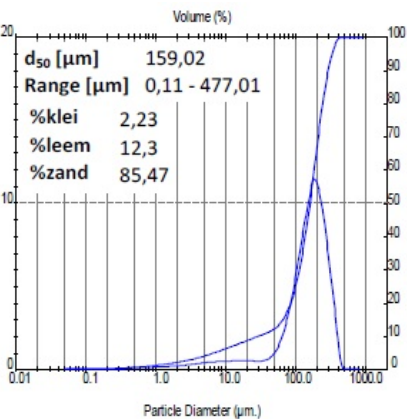
(f) Sand

Figure A.2: Particle size distributions and soil classification for samples of the eroded river bank

A.3 Sediments in the water column

Water samples of suspended sediments were taken manually (Figure A.3a to A.3d) or using an ISCO sampler (Figure A.3e and A.3f). Note that, dependent on the time lag between the water sample and a ship passage and the sampling height z above the river bed, a depth-averaged water sample was used for the determination of the particle size distribution of the sediments in the water column. In this way, a minimum laser obscuration of 10 % was obtained in the Mastersizer, necessary to analyse particle sizes.
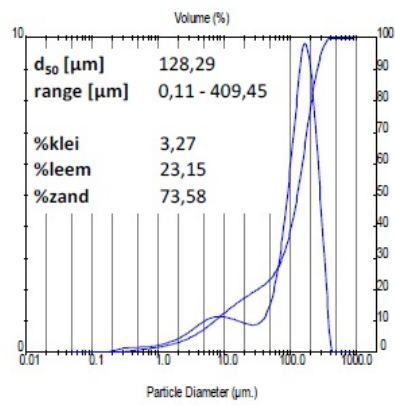
(a) at height $z = 0.05$m, 45 s after ship passage
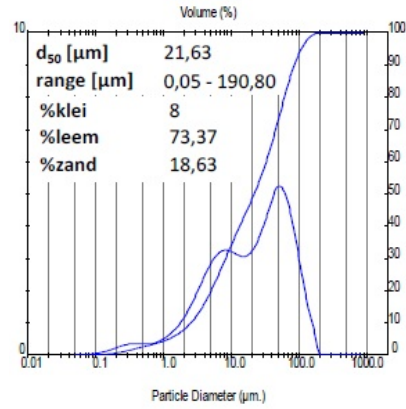
(b) at height $z = 0.1$m, 88 s after ship passage
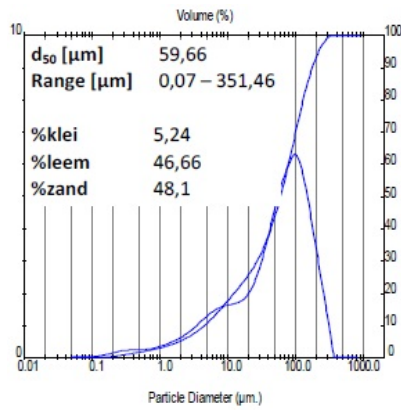
(c) at height $z = 0.05$m, 68 s after ship passage
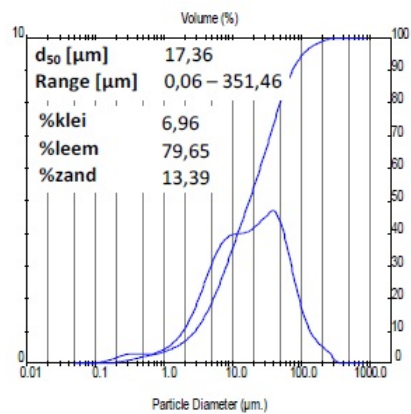
(d) at height $z = 0.05$m, 135 s after ship passage
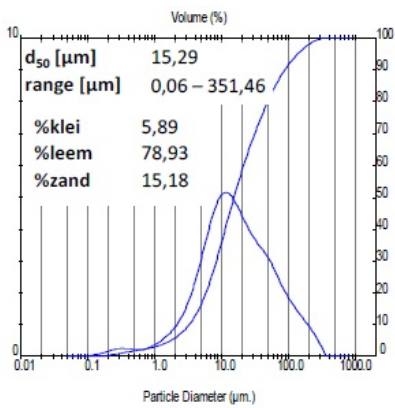
(e) at height $z = 0.2$m, 3 samples
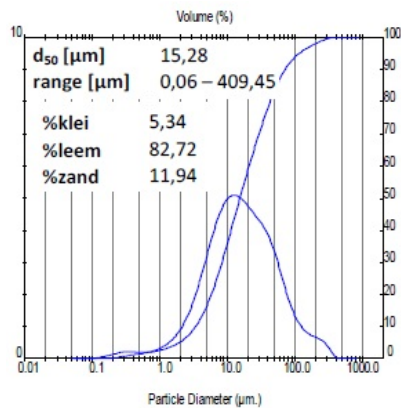
(f) at height $z = 0.3$m, 3 samples

Figure A.3: Particle size distributions for water samples, taken in the shallow water riverine area

B

Various configurations of off-bank timber piling

During the months June - December 2011, several off-bank timber piling configurations were successively investigated on their wave-structure interaction, i.e. ship wave transmission and reduction, making use of the mobile monitoring system. The configurations under study include layouts with a single or double row of off-bank timber piling, of which the bank connection is realized in various ways. These different layouts are monitored at 9 locations (cf Table 4.6 and 4.7). Table B.1 provides a summary of the locations' different layouts.

Figure B.1 shows the plan view of two bank sites which are nature-friendly protected by a single row of off-bank timber piling parallel to the fairway (with and without bank connection). For the monitored location 4, below on the figure, the river bank is additionally protected by a reed belt. This figure illustrates the general position, with respect to the fairway, of nature-friendly bank protections installed along the Lys. Specific plan and side views of the locations are added in Section B.1.

Table B.1: Characteristics of the 9 monitored locations which are nature-friendly protected by off-bank timber piling and, location-dependent, a reed belt.

Location	Bank side	Row of timber piling	Length [m] timber piling *	Bank-connected? - length *[m]	Reed belt planted?
1	Left	Double	79	Yes - 100% closed	no
2	Left	Single	76	Yes - 100% closed	yes
3	Left	Double	51	No	no
4	Right	Single	180	No	yes
5	Right	Single	340	Yes - 5 m	no
6	Left	Single	176	Yes - 5 m	no
7	Right	Single	200	Yes - 5 m	yes
8	Left	Single	165	Yes - Up: 6.2 m & Down: 5.4 m	no
9	Right	Single	253	Yes - 6 m	yes

* source: location and cross section maps of W & Z (drawn up date: April 27, 2011)

Figure B.1: Plan view of the monitored location 4, which consists of a single row of off-bank timber piling, parallel to the fairway and without bank connection. A reed belt additionally protects the eroded river bank. At the opposed bank side, a layout of this nature-friendly bank protection with bank-connected timber piling and without reed belt is shown. (source: Google Earth)

B.1   Plan and side views of the monitored locations

Figure B.2a indicates the layout for the monitored locations 1 and 3. They are nature-friendly protected by a double row of off-bank timber piling parallel to the fairway. In addition, the bank connection at location 1 is entirely closed by timber piling and riprap.

The other 7 locations are piled with a single row parallel to the fairway, which varies significantly in length between the monitored locations. The lateral water in- and outflow to the shallow water riverine area is bounded by the length of the bank-connected timber piling, which determines the variable width of the water in- and outflow openings in locations 5 to 9 (Figure B.2c, B.2d and B.2e respectively). For locations 6 and 9, the bank connection is made by combined use of timber piling and riprap. Location 2 is entirely closed laterally (Figure B.2b), whereas location 4 has no bank-connected piling (Figure B.2c).

Location 2, locations 4 and 7, and location 9 additionally have reed vegetation patches planted at the base of the eroded river bank, as illustrated in Figure B.2b, B.2c and B.2e respectively. This natural wave dampening barrier is not taken into consideration for the characterisation of the wave-structure interaction of the timber piling configurations.

Debarked timber piling is applied for all locations but location 4, where the timber piles are milled.

(a)

Location 1 and 3

(b)

Location 2

(c)

Location 4 and 7

(d)

Location 5, 6 and 8

(e)

NP (+5.61)

Geschilde paal

(6.11)

(+4.3)

Breuksteen bestorting

12/4

Gebroken plaat

Grond afkomstig uit vaargeul

Reed belt

Riprap

Timber piles
(debarked)

2.10 TP (+2,10)

(1,11)

Location 9
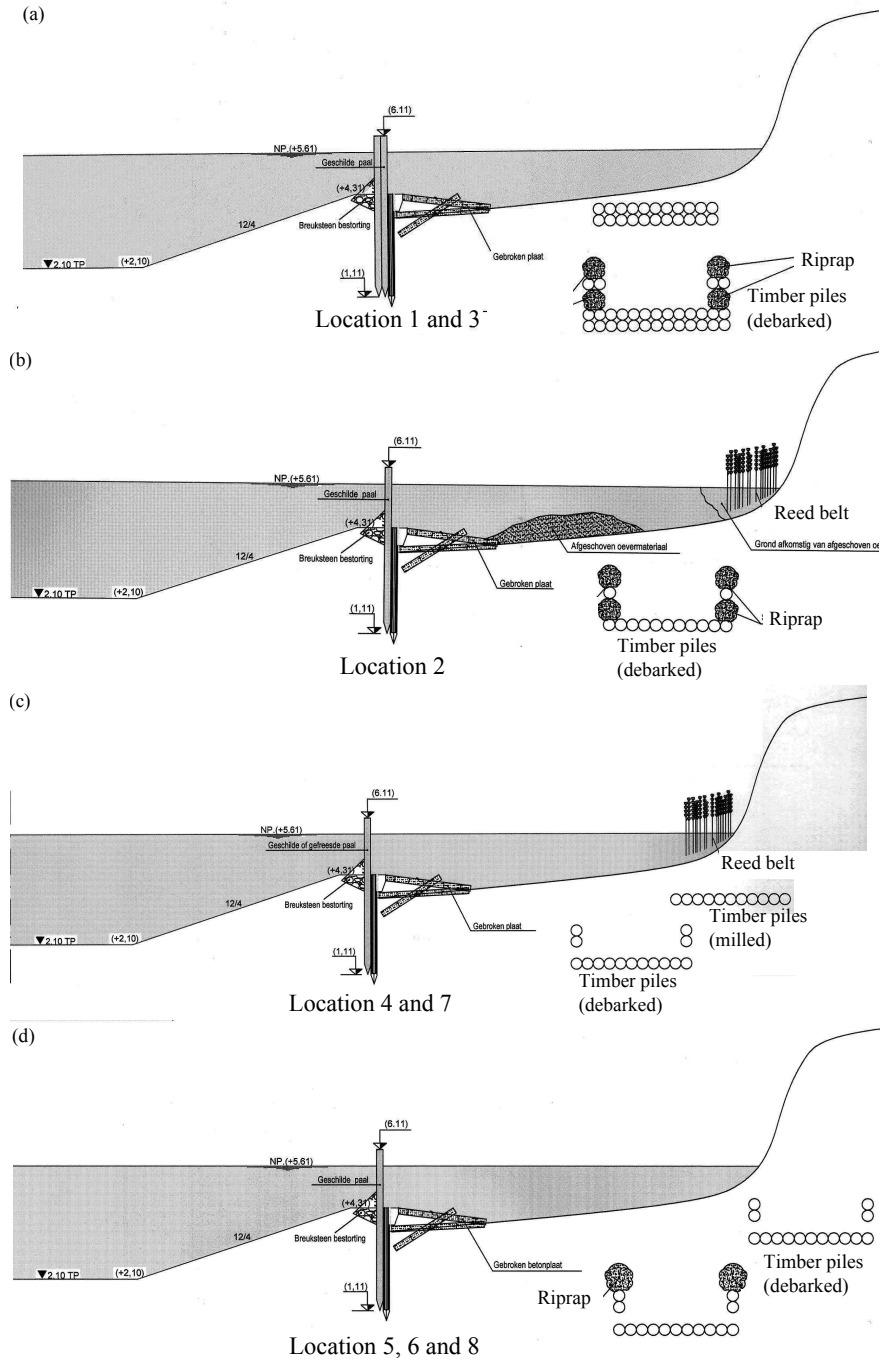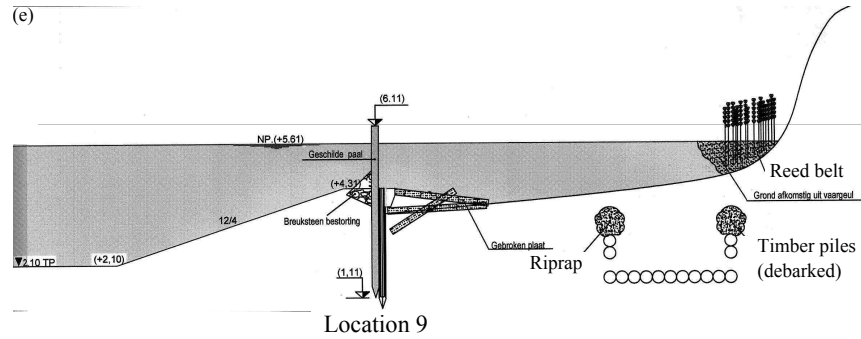
Figure B.2: Various configurations of off-bank timber piling, monitored with the mobile monitoring system to investigate their wave-structure interaction (Adapted from plan and side view maps of W&Z (drawn up date: April, 2011))

C

List of publications

C.1 International journal publications

- De Roo, S. Troch, P. 2013. Field monitoring of ship wave action on an environmentally friendly bank protection in a confined waterway. Journal of Waterway, Port, Coastal, and Ocean Engineering 139(6), xx-xx. (http:dx.doi.org/10.1061(ASCE)WW.1943-5460.0000202)

- De Roo, S. Troch, P. Evaluation of the effectiveness of a nature-friendly bank protection in a confined, non-tidal waterway subject to heavy shipping traffic. Accepted for publication in River Research and Applications, May 2013.

C.2 National journal publication

- De Roo, S. Troch, P. 2009. Experimentele studie van het gedrag van natuurvriendelijke oeververdediging op niet-tijgebonden bevaarbare waterlopen belast door scheepsgolven. Grenzeloze Schelde Nieuws 48(4).

C.3 International conference publications

- De Roo, S. Troch, P. 2010. Analysis of ship-wave loading on alternative bank protection of a non-tidal waterway - first results. In: Proceedings of the 1st European IAHR Congress (digital copy). Edinburgh, UK. May 4-6, 2010.

- De Roo, S. Troch, P. 2010. Field monitoring of ship-induced loads on (alternative) bank protections of non-tidal waterways. In: Proceedings of the 32nd PIANC Congress (digital copy). Liverpool, UK. May 10-14, 2010.

- De Roo, S. Troch, P. 2010. Response of technical-biological bank protection to ship-generated wave actions - first results. In: Proceedings of the 5th International Conference on Fluvial Hydraulics (RiverFlow 2010): Vol 2, 1339-1345. Braunschweig, Germany. September 8-10, 2010.

- De Roo, S., Vanhaute, L., Troch, P. 2012. How ship wave action influences the sediment budget of a nature-friendly bank protection in a confined, non-tidal waterway. In: Proceedings of the General Assembly of the European Geosciences Union (EGU): 10453. Vienna, Austria. April 22-27, 2012.

- De Roo, S., Vanhaute, L., Troch, P. 2012. Impact of ship waves on the sediment transport in a nature-friendly bank protection. In: Proceedings of the 6th International Conference on Fluvial Hydraulics (RiverFlow 2012): Vol 2, 1309-1316. San Jose, Costa Rica. September 5-7, 2012.

- De Roo, S. Troch, P. 2012. Prototype monitoring of ship wave action on a nature-friendly bank protection in a non-tidal, confined waterway. In: Book of Abstracts of the 4th International Conference on the Application of Physical Modelling to Port and Coastal Protection (Coastlab12): 161-162. Gent, Belgium. September 17-20, 2012.

C.4   National conference publication

- De Roo, S. Troch, P. 2010. Design rules for technical-biological bank protection on non-tidal, navigable waterways. In: Proceedings of the 11th UGent FEA PhD symposium: 32. Gent, Belgium. December 1, 2010.